PhD degree in Molecular Medicine

European School of Molecular Medicine (SEMM), University of Milan

Settore disciplinare: BIO/10

ROLE OF THE HISTONE DEMETHYLASE JMJD3

IN CORTICAL DEVELOPMENT AND NEURAL DIFFERENTIATION

Jacopo Sgualdino

European Institute of Oncology (IEO), Milan

Matricola n. R09392

Supervisor: dr. Giuseppe Testa

European Institute of Oncology (IEO), Milan

Anno Accademico 2013-2014

ABSTRACT

Jmjd3 is a H3K27 demethylase that is required for the neural commitment of ESCs and controls the expression of key drivers and markers of neurulation through the demethylation of H3K27me3. Previous work from our lab has demonstrated that loss of Jmjd3 in mouse embryos causes a complex neurodevelopmental phenotype that results in perinatal death. Such lethality is due to a respiratory failure resulting from the lack of a functional pre-Bötzinger complex, a small network of neurons that is responsible for respiratory rhythm generation. Rescue experiments performed with catalytically active or inactive Jmjd3 have demonstrated that its demethylase activity is necessary for developing and maintaining the embryonic respiratory neuronal network. This unanticipated finding claims a broader role in brain development for Jmjd3, whose importance extends from early differentiation choices to the late development of neuronal networks.

To investigate the effect of Jmjd3 loss on neocortical development, we analyzed Jmjd3 KO embryonic brains at different developmental stages using markers for stem cells and differentiated neurons. We found that loss of Jmjd3 causes a late-onset increase in the number of ventricular zone (VZ) neural precursor cells (NPCs) and a reduction in the cortical neuronal production. Jmjd3 KO VZ NPCs display a higher rate of cell cycle re-entry than their WT counterpart, and have an overall longer cell cycle.

In order to pinpoint the mechanism by which Jmjd3 is causally linked to the lengthening of the NPC cell cycle and to the VZ expansion, we investigated the transcriptional effect of Jmjd3 loss by performing RNAseq on mRNA extracted from WT and KO cultured E13.5 primary NPCs. A detailed molecular characterization at the transcriptional level revealed that the phenotype that we observed both *in vivo* and *in vitro* in Jmjd3 KO NPCs is linked to supraphysiological activation of the Wnt/B-

catenin and Notch pathways, two known regulators of the choice between self-renewal and differentiation in the VZ NPCs of the developing brains, whose upregulation has already been shown to correlate with an increased proliferative potential and hampered neuronal differentiation.

Some of the results presented in this thesis appear in the following publication:

Park, D. H., Hong, S. J., Salinas, R. D., Liu, S. J., Sun, S. W., Sgualdino, J., Testa, G., Matzuk, M. M., Iwamori, N., and Lim, D. A. (2014). Activation of Neuronal Gene Expression by the JMJD3 Demethylase Is Required for Postnatal and Adult Brain Neurogenesis. Cell reports.

TABLE OF CONTENTS

ACRONYMS AND ABREVIATIONS

4D cdk4/cyclinD1

5hmC 5-hydroxymethylcytosine

5mC 5-methylcytosine

AP Apical progenitor

BAC Bacterial artificial chromosome

BrdU Bromodeoxyuridine

bFGF Basic fibroblast growth factor

BP Basal progenitor

CdK Cyclin-dependent kinase

Cdkn2a Cyclin-dependent kinase inhibitor 2A

ChIP Chromatin Immunoprecipitation

CNS Central nervous system

CP Cortical plate

DNMT DNA methyltransferase

EdU Ethynyl deoxyuridine

EGF Epidermal growth factor

ES cell Embryonic stem cell

Ezh2 Enhancer of zeste homolog 2

FAD Flavin adenine dinucleotide

FBS Fetal bovine serum

GSK3 glycogen synthase kinase 3

H2AK119 lysine 119 of histone H2A

H3K4 lysine 4 of histone H3

H3K27 lysine 27 of histone H3

HAT Histone acetyl transferase

HBSS Hank's balanced salt solution

HDAC Histone de-acetylase

HDM Histone de-methylase

HE Hematoxylin and eosin

HMT Histone methyltransferase

Hox Homeotic genes

IdU Iododeoxyuridine

INM Interkinetic nuclear migration

IZ Intermediate zone

IP Immunoprecipitation

KDM Lysine de-methylase

LGE Lateral ganglionic eminence

MBD Methyl binding domain

MEF mouse embryonic fibroblast

MLL Mixed lineage leukemia

NPC Neural precursor cell

pA Poly-adenylation

PBC Pre-Bötzinger complex

PBS Phosphate buffered saline

PcG Polycomb group

PCR Polymerase chain reaction

PFA Paraformaldehyde

pH3 Phospho-histone H3

PI Propidium iodide

PLO Poly-L-ornithine

PRC1 Polycomb repressive complex 1

PRC2 Polycomb repressive complex 2

PTM Post-translational modification

RGC Radial glial cell

RNAi RNA interference

RNAPII RNA polymerase II

RT room temperature

RTN/pFRG Retrotrapezoid nucleus/parafacial respiratory group

sA Splice acceptor

SVZ Sub-ventricular zone

SWI/SNF SWItch/Sucrose NonFermentable

TET Ten-eleven translocation

TrxG Trithorax group

VZ Ventricular zone

1 INTRODUCTION

1.1 Epigenetics and chromatin

1.1.1 Definition of epigenetics

The meaning of the term epigenetics has smoothly shifted in shape since its original coinage by Conrad Waddington in 1942 as "the branch of biology which studies the causal interactions between genes and their products, which bring the phenotype into being" (Waddington, 1942).

Recently, more rigorous definitions of epigenetics have been proposed, including that of Berger et al. (Berger et al., 2009), which states that: "an epigenetic trait is a stably heritable phenotype resulting from changes in a chromosome without alterations in the DNA sequence" and that by Riggs et al. (Riggs et al., 1996), which defines epigenetics as "the study of changes in gene function that are mitotically and/or meiotically heritable and that do not entail a change in DNA sequence". A rigorous analysis of the meaning of the term epigenetics and of the history of its development is provided by several review articles (Boniolo and Testa, 2012; Meloni and Testa, 2014).

However, as far as experimental practice and the common use of the word go, a more operative definition would state that epigenetics is essentially "the study of the mechanisms of temporal and spatial control of gene activity during the development of complex organisms", as proposed by Robin Holliday back in 1990 (Holliday, 1990).

Indeed, the study of epigenetics nowadays mainly entails the study of the relationship between chromatin modifications and gene expression, and how chromatin modifiers can influence the expression of target genes upon certain stimuli or during cell state transitions. For the scope of this thesis, I will refer to epigenetics according to the

more practical definition by Holliday, but without forfeiting the concepts of inheritability of a modification and absence of alterations in the DNA sequences, as summarized in the definition by Berger.

1.1.2 Chromatin and histones

In the nucleus of eukaryotic cells, DNA is packaged together with proteins and this complex is called chromatin. There are several levels of DNA compaction that can be achieved during different phases of the cell cycle, up to the hypercondensed state that is represented by metaphase chromosomes. However, the base unit of DNA packaging in eukaryotes is the nucleosome, which is composed by stretch of approximately 147 DNA base pairs wrapped around a globular octameric protein core, formed by 2 copies each of the histone proteins H2A, H2B, H3, H4. The H1 linker histone and its isoforms also participate in chromatin compaction by interacting with the nucleosome near the entry and exit points of the DNA. The N-terminal tail of histones is the substrate of several covalent modifications, which can alter the structural organization of the nucleosome and ultimately influence DNA access and conformation, or function as docking sites for proteins and complexes. More specifically, post-translational modifications of histone tails can contribute to the establishment of global chromatin domains that are functional to the execution of different DNA-based programs, such as genomic imprinting, transcription, DNA repair, DNA replication and chromosome condensation (Kouzarides, 2007).

1.1.3 Covalent modifications affecting chromatin function

The most characterized covalent modifications that can affect chromatin function include DNA methylation and histone post-translational modifications.

In mammals, DNA methylation on the fifth position of cytosine (5mc) is mainly restricted to the CpG dinucleotides, and commonly occurs at centromeres, telomeres, and repeated sequences. CpG-rich DNA stretches, or CpG islands, are usually about 1000-bp long and frequently unmethylated. CpG islands are usually associated with regulatory functions and located at the 5' of genes, and can be identified in about 70% of all mammalian promoters. The methylation of CpG islands plays an important role in transcriptional regulation as it is normally associated with transcriptional silencing (Deaton and Bird, 2011), and it can be performed by three different DNA methyltransferases (DNMTs) in higher eukaryotes (Li et al., 1992; Okano et al., 1999). DNA methylation has been regarded as a stable DNA modification until 5-hydroxymethylcytosine (5hmC) was discovered, suggesting for the first time that 5mC could be further processed (Kriaucionis and Heintz, 2009; Tahiliani et al., 2009). Hydroxylation of 5mC can recruit Methyl Binding Domains (MBDs)-containing "readers", which in turn can exert critical roles in host defense, genome imprinting, and X chromosome inactivation (Suzuki and Bird, 2008). It was subsequently demonstrated that the mammalian ten-eleven translocation (TET 1–3) family of proteins includes the DNA hydroxylases responsible for the catalytic conversion of 5mC to 5hmC.

The N-terminal tails of histones emerge from the octameric core and constitute the main regulatory domain of histones. Several post-translational modifications mainly targeting lysines and arginines have been described, including acetylation, methylation, phosphorylation, ribosylation, ubiquitylation and sumoylation. One of the main consequences of these modifications is to alter the surface charge of histones and change the overall strength of histone-histone and histone-DNA interactions, with a profound effect on the compaction state of chromatin. As an

example, phosphorylation (Wei et al., 1999) or acetylation (Gorisch et al., 2005) can loosen the chromatin fiber by reducing the overall positive charge of the histone tail, making the DNA more accessible to transcription factors and therefore potentially more transcriptionally active.

Histone modifications can also favor or hinder the recruitment of other proteins to the modified histone tails. The concerted action of histone modifications and non-histone proteins contributes to the recruitment of protein complexes that can allow RNA transcription, DNA repair or replication, and chromosome condensation (Kouzarides, 2007) (summarized in fig. 1). Importantly, most modifications are dynamic, and enzymes have been isolated that can add and remove residues. Thus, for example, histone acetylases (HATs) and de-acetylases (HDACs) have been described, as well as histone methyltransferases (HMTs) and demethylases (KDMs).

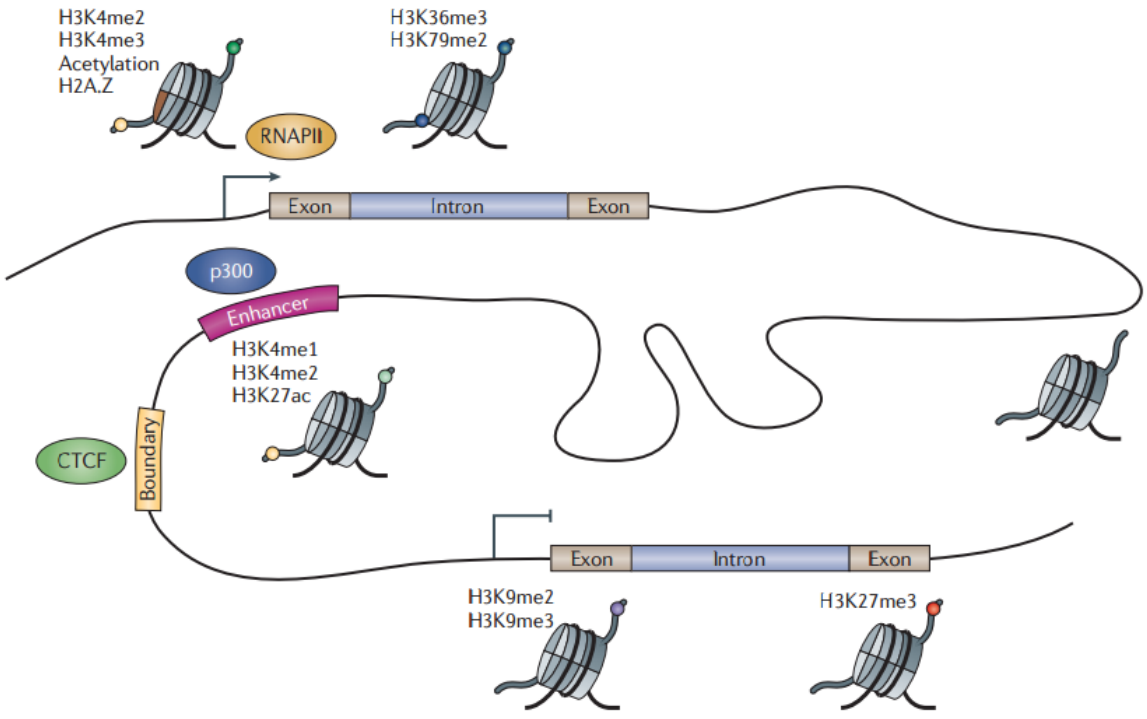

Figure 1. Diagram of the main histone PTMs and their role in transcription (Zhou et al., 2011). Promoters, gene bodies, enhancers and boundary elements are shown. Active promoters are commonly marked by H3K4me2, H3K4me3, acetylation, and H2A.Z histone. Actively transcribed regions are enriched in H3K36me3 and H3K79me2. Repressed genes are usually localized in large domains of H3K9me2/3 or H3K27me3. Enhancers can be enriched in H3K4me1, H3K4me2, H3K27ac and the HAT p300. CTCF is localized at many sites that have been described as boundary elements, insulators or structural scaffolds. RNAPII, RNA polymerase II.

1.1.4 Chromatin and gene transcription

The most widely used technique to investigate the association between proteins and specific DNA sequences is called Chromatin Immunoprecipitation (ChIP) (Shang et al., 2000; Solomon et al., 1988). DNA and its interacting proteins are covalently bound by the use of cross-linking agents such as formaldehyde or disuccinimidyl glutarate, and antibodies specific for the peptide of interest, which can be a histone post-translational modification or a transcription factor are used to precipitate the fragmented, cross-linked chromatin. The interacting DNA is then de-crosslinked and purified, and downstream techniques like qPCR or DNA sequencing are then used to identify the genomic loci that are preferentially bound by the protein of interest.

ChIP has allowed scientists to associate the presence of particular histone tail post-translational modification (PTM) to the transcriptional activity of a target gene. More recently, next-generation sequencing techniques have granted the possibility to highlight genome-wide roles for chromatin structures and elements that were not appreciated in gene-centric studies. The resulting maps and data sets have linked particular modifications with gene activation or repression and with various genomic features, including promoters, transcribed regions and enhancers.

Histone lysine methylation is central to processes of cellular differentiation, since the expression of genes involved in differentiation is dynamically regulated through changes in histone methylation at specific lysine residues, most notably lysine 27 on histone H3 (H3K27), associated with transcriptional repression, and lysine 4 on histone H3 (H3K4), associated with transcriptional activation. Genome-wide analysis showed that tri-methylayion of H3K27 (H3K27me3) labels transcriptionally repressed domains that are present in embryonic stem cells (ES cells) and extend in differentiated cell types, to allow cell type-specific repression (Hawkins et al., 2010). Functionally, these regions might serve for lineage restriction during differentiation

as they cover only approximately 4% of the genome in undifferentiated mouse ES cells, compared to 31% in differentiated ES cells (Wen et al., 2009). "Bivalent domains" were identified at some promoters and deserve special description. These domains are marked by both H3K4me3 and H3K27me3 (Bernstein et al., 2006; Lee et al., 2006; Mikkelsen et al., 2008) and serve a specific function in the context of development. Bivalent genes are indeed transcriptionally silent, but lie in a "poised" state that is resolved either towards activation or definitive repression via the erasure of the H3K27 or H3K4 methylation, respectively. However, the very concept of bivalent domains has been recently challenged (Laugesen and Helin, 2014). It is indeed not entirely certain that the co-occurrence of the two marks, as assessed by ChIP-qPCR or ChIPseq techniques, reflects the presence of methylation on both K4 and K27 of the very same H3 histone tail. Rather, the bivalency might represent an artifact deriving from heterogeneity of the cell population under exam. Alternatively, the two marks might coexist on opposite H3 tails of the same nucleosome, or on neighboring nucleosomes.

1.1.5 Proteins responsible for histone tail modifications

The proteins responsible for transferring the methyl groups onto the histone tail lysins K4 and K27 have been identified by seminal studies performed on Drosophila in virtue of their ability to regulate the expression pattern of homeotic (Hox) genes (Ingham, 1985; Lewis, 1978), but their biochemical activity in catalyzing the addition and removal of methyl groups on lysine residues has been elucidated only later (Schuettengruber et al., 2007; Steffen and Ringrose, 2014)

Some proteins belonging to the Trithorax group (TrxG proteins) are able to catalyze the methylation of lysine H3K4 and confer an active transcriptional status to the

target gene (Byrd and Shearn, 2003), whereas the polycomb group (PcG) proteins repress gene transcription and act via two different complexes.

The Polycomb Repressive Complex 2 (PRC2) act as a holoenzyme composed of four core members and other associated proteins. The catalytic subunit Enhancer of zeste homolog 2 (Ezh2) is responsible for imposing the H3K27me3 mark via its methyltransferase activity (Cao and Zhang, 2004), whereas the Eed subunit is able to recognize the H3K27me3 mark and recruit the PRC2 (Hansen et al., 2008; Margueron et al., 2009). This feed-forward loop between the mark and the enzyme that catalyzes its addition allows H3K27me3 to be maintained upon cell division, making it a *bona fide* epigenetic mark (Morey and Helin, 2010). The polycomb repressive complex 1 (PRC1), on the other hand, can ubiquitinate lysine 119 of histone H2A (H2AK119) via its RING protein subunits, and also recognize H3K27me3 through its chromodomain-containing subunits CBX and HPH. It has thus been proposed that PRC1 can be recruited on chromatin by the activity of PRC2 on H3K27, but there are instances in which this model does not hold true, as it has been shown that the two complexes can target different genes (Schoeftner et al., 2006; Sing et al., 2009). More recently, it has been demonstrated that variant PRC1 complex occupancy can recruit the PRC2 complex and lead to H3K27me3 deposition in an H2AK119ub1-dependent manner (Blackledge et al., 2014), shedding new light on the mechanisms that govern polycomb domain formation and transcriptional repression.

1.1.6 The discovery of histone demethylases

As discussed in the previous paragraph, evidences for the existence of histone methyltransferases date back to the 1970's (Lewis, 1978), but until recently it was thought that histone methylation was a permanent modification that could only be reversed by histone eviction or dilution during DNA replication.

This was until Shi and colleagues discovered the first lysine-specific demethylase (LSD1) in 2004 (Shi et al., 2004). LSD1 can demethylate H3K4 and H3K9 via a flavin adenine dinucleotide (FAD)-dependent amine oxidation reaction and participate in the downregulation of target genes, also in complex with the CoREST silencing transcription factor (Lee et al., 2005). Soon after, proteins belonging to a family of histone demethylases that rely on an entirely different biochemical process for their catalytic activity were identified in several laboratories (Tsukada et al., 2005). This protein family is characterized by the presence of a JmjC domain, which can demethylate lysine in a dioxygenase reaction that depends on Fe(II) and α-ketoglutarate (fig. 2).

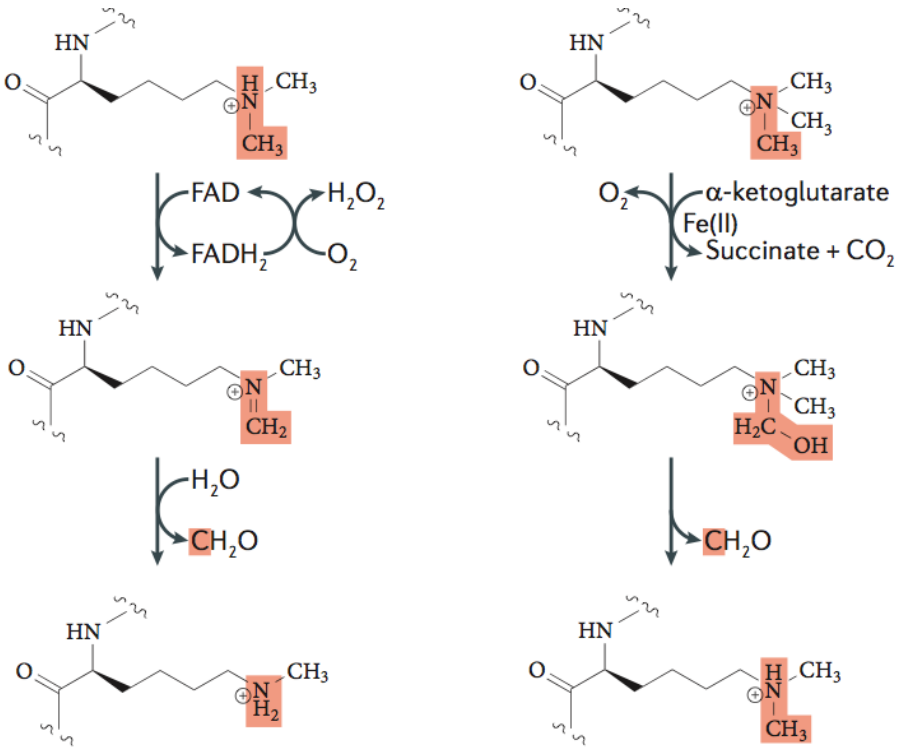

Figure 2. The catalytic mechanisms of histone demethylation. Members of the two different lysine demethylase families have distinct reaction mechanisms. (left) The amine oxidation reaction dependent on FAD is used by KDM1A/LSD1 and KDM1B/LSD2. (right) The dioxygenase reaction is typical of members of the JmjC family, and is dependent on Fe(II) and α-ketoglutarate (Kooistra and Helin, 2012).

1.1.7 Jmjd3

Jmjd3, or Kdm6b, is a member of the JmjC protein family and, together with its paralog Utx, is the only known protein that can mediate demethylation of di- and tri-methylated H3K27 (Hong et al., 2007) (fig. 3). Soon after the discovery of the family of JmjC-domain demethylases, several groups independently published evidences of the function of Jmjd3 as an H3K27-specific demethylase, highlighting a role in Hox gene regulation (Agger et al., 2007; Lan et al., 2007) and inflammation-response programs in macrophages (De Santa et al., 2007).

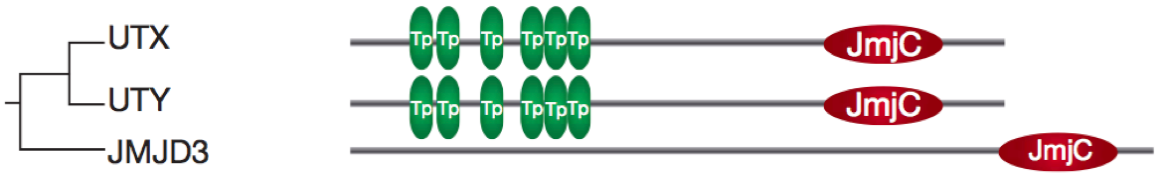

Figure 3. The Kdm6 family of histone demethylases. UTX (KDM6A), JMJD3 (KDM6B) and UTY (KDM6C). Tp, tetratricopeptide repeat; JmjC, jumonji C domain (Kooistra and Helin, 2012).

It was also shown by our lab and others that Jmjd3 is involved in neural differentiation process (Burgold et al., 2008; Jepsen et al., 2007): its demethylase activity was indeed proven necessary for the transcriptional activation of genes that are responsible for the unwinding of neurogenic programs both in embryonic stem cells and in brain-derived neural precursor cells. The observation that genome-wide changes in H3K27me3 accompany the entire process of neural fate acquisition (Mohn et al., 2008) further underscored the importance of a H3K27 demethylase for the proper implementation of the neural development process, and potentially also of other developmental processes that require the activation of inactive genes marked by H3K27me3.

In 2009, two papers proposed that the demethylase activity of Jmjd3 was needed for transcriptional activation of genes involved in tumorigenesis. Specifically, it was shown in mouse embryonic fibroblasts (MEFs) that Jmjd3 counteracts the activity of PcG proteins on the Ink4a/Arf locus and participates in its activation in response to

oncogene-induced senescence, suggesting that Jmjd3 might act as a tumor suppressor in some contexts (Agger et al., 2009; Barradas et al., 2009). A recent report corroborated these findings and extended them by showing that the Jmjd3-mediated activation of the Ink4a/Arf locus constitutes an obstacle to cellular reprogramming (Zhao et al., 2013)

The array of mechanisms of action of Jmjd3 was significantly extended when it was demonstrated that Jmjd3 is able to regulate the transcriptional activity of target genes also in a demethylase-independent manner, and specifically by mediating the interaction of a T-box family member with a Brg1-containing SWI/SNF remodeling complex: this multi-protein functions as a chromatin remodeler to enhance promoter accessibility and activate transcription (Miller et al., 2010).

The activity of several non-histone proteins can be regulated by methylation (Huang et al., 2007), and it has been suggested that histone demethylases might also affect the methylation levels of non-histone targets. Indeed, JmjC proteins are also found in bacteria that do not contain histones, suggesting that these proteins have other functions besides histone demethylation. p53 was one of the first non-histone substrates shown to be post-translationally modified by proteins with demethylase activity. LSD1 is able to repress p53-mediated transcriptional activation and p53-induced apoptosis by demethylating K370me2 on p53, thus inhibiting the interaction between p53 and tumour suppressor p53-binding protein 1 (TP53BP1).

Along the same line, some studies have proposed that Jmjd3 is able to interact with both p53 and TAp63γ and demethylate an unspecified lysine residue, resulting in their nuclear accumulation and affecting their function (Ene et al., 2012; Fonseca et al., 2012; Solá et al., 2011). However, the evidences provided in these works do not amount to a compelling demonstration for the activity of Jmjd3 on p53 or TAp63γ,

and more research ought to be performed to allow considering this result as a credible function of Jmjd3.

1.2 Neocortical development

The mammalian neocortex develops from the embryonic ectoderm, in and particular from the neural plate, which folds and coalesces forming the neural tube. From the most anterior part of the neural tube develops the telencephalon, which will give rise to the cerebral hemispheres and hence to the neocortex, while from the cavity inside the neural tube derives the ventricular system. In the mouse, neurogenesis takes place between embryonic days (E) E11 and E19, and starts with a single layer of epithelial founder cells constituting the walls of the neural tube, the neuroepithelial cells. Neuroepithelial cells display an apico-basal polarity and divide symmetrically in a self-renewing fashion in order to increase their pool. When neurogenesis is initiated, neuroepithelial cells downregulate epithelial features (Aaku-Saraste et al., 1997) and start displaying astroglial markers, transitioning into a distinct cell state known as radial glial cells (RGCs), which essentially represent a more fate-restricted counterpart of neuroepithelial cells, and constituting the so-called ventricular zone (VZ).

1.2.1 Radial glial cells dynamics and differentiation

The neocortex is formed by six layers of projection neurons, which are generated during corticogenesis by the radial glial cells (RGCs) following an inside-out pattern, such that the first-born neurons occupy the deepest layer and are closest do the VZ, whereas the late-born neurons occupy the most superficial layer and are close to the meninges. RGCs can divide symmetrically or asymmetrically in the cortical VZ to self-

renew and generate neurons directly or, more frequently, indirectly via intermediate progenitor cells (Kriegstein and Álvarez-Buylla, 2009) (fig. 4).

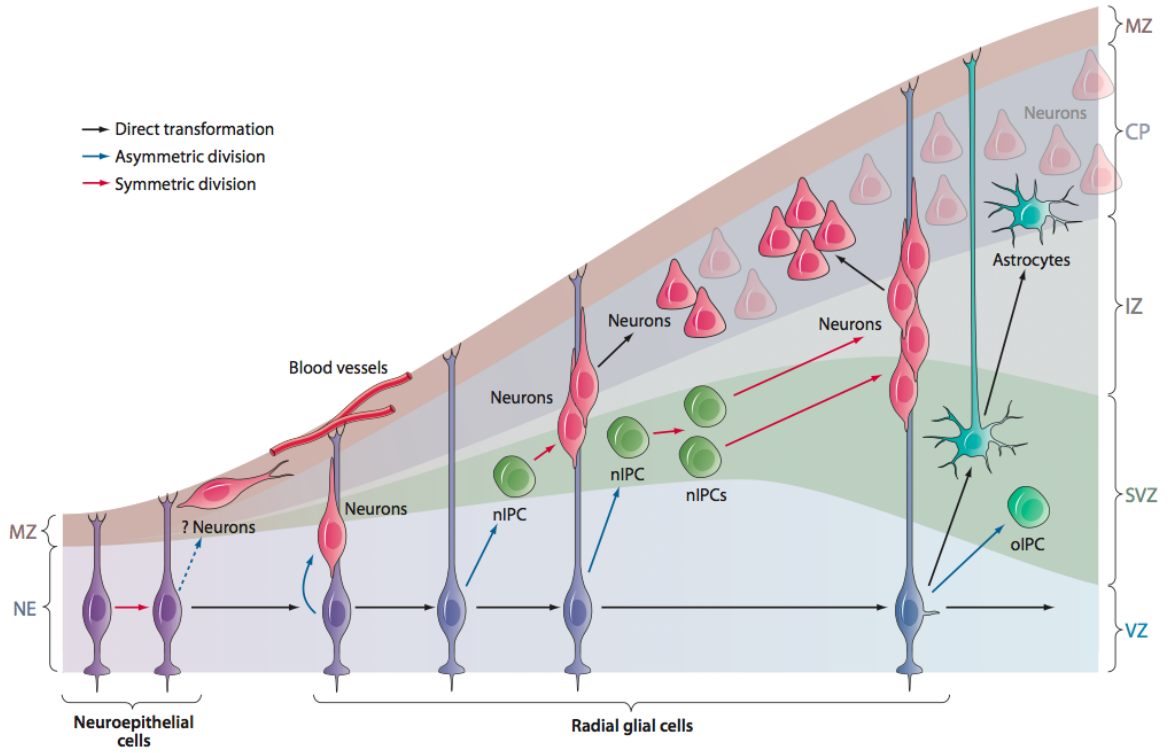

Figure 4. Model of neurogenesis in the developing mammalian neocortex. Neuroepithelial cells in early neocortical development divide symmetrically to expand their pool, and also likely produce early neurons. As development proceeds, neuroepithelial cells elongate and convert into radial glial (RG) cells. RG cells then start dividing asymmetrically to generate neurons directly or indirectly through intermediate progenitor cells (nIPCs). Oligodendrocytes are also produced by RG cells through intermediate progenitor cells that generate oligodendrocytes (oIPCs). RG cells have apical-basal polarity: apically (down), RG cells contact the ventricle, where they project a single primary cilium; basally (up), RG cells contact the meninges, basal lamina, and blood vessels (Kriegstein and Álvarez-Buylla, 2009).

The exact mechanisms that establish cellular diversity in the neocortex starting from a single founder cell population are not still completely elucidated, and two main paradigms have been proposed in the past years. The classic hypothesis maintains that a single RGC is able to generate all the neuronal subtypes through progressive lineage restriction, and following a temporal order that is largely cell-autonomously determined (Desai and McConnell, 2000; Hirabayashi et al., 2009; Mcconnell and Kaznowski, 1991; Shen et al., 2006). Another hypothesis claims the presence of heterogeneous lineage-restricted progenitors that are able to contribute specifically to subsets of projection neurons (Schuurmans et al., 2004), identifiable by molecular

markers and belonging to a specific layer. A recent paper published on Science provided compelling evidence that a subpopulation of Cux2+ RGCs, detectable since the beginning of neurogenesis, was indeed intrinsically specified to generate only late-born, upper layer neurons (Franco et al., 2012). However, a research paper published in 2013 (Guo et al., 2013) challenged quite directly the findings of Franco and co-workers, by demonstrating that Fezf2+ RGCs can sequentially generate all the neuronal subtypes, including Cux2+ neurons, and that the lineage tracing approach used in the Science 2012 paper suffered some flaws that made its conclusions unwarranted.

Though these and other findings do not exclude that subsets of RGCs intrinsically restricted in their lineage potential may actually exist, the model entailing progressive lineage restriction of a single RGC seems to be more supported by the current literature. Along these lines, it has been proposed that the cell-autonomous mechanisms that govern the production of different neuronal subtypes might be regulated by the progressive downregulation of epigenetic repressor (Testa, 2011). This hypothesis is consistent with published data that report a progressive downregulation of the H3K27 methyltransferase Ezh2 as neurogenesis proceeds *in vivo* (Pereira et al., 2010).

1.2.2 Cell cycle regulation in mammalian neocortical development

Seminal experiments that date back almost 50 years have demonstrated that the cell cycle of VZ neural progenitors lengthens as neurogenesis proceeds (Fujita, 1962), from 12 hours at day 11 to 18 hours at day 18. With the advent of more refined reagents and techniques such as differentially labelled thymidine analogues (Martynoga et al., 2005; Takahashi et al., 1995) and live imaging (Betizeau et al., 2013; Pilz et al., 2013), this notion has been extensively corroborated and more

details on the cell cycle dynamics of RGCs have been gained. In particular, it has been demonstrated that the progressive lengthening on the cell cycle during the unwinding of neurogenesis is mainly due to a specific lengthening of the G1 phase (Caviness et al., 1995; Dehay and Kennedy, 2007; Salomoni and Calegari, 2010).

In tissues, the balance between self-renewal and differentiation of the stem compartment determines the final composition of the tissues. In the case of the brain, if the VZ RGCs would exhaust their pool soon in neurogenesis through symmetric, differentiative divisions, the final thickness of the cortex would be reduced, and likely the complexity of neuronal subpopulations as well. The fine-tuning of the mitotic choices in the VZ is hence of capital importance for a proper neocortical development. Several studies have found that cortical progenitor cells undergoing differentiative divisions tend to have a longer cell cycle than the ones that self-renew, and that this lengthening is mainly due to a longer G1 phase.

Federico Calegari and coworkers established a causal link between G1 phase lengthening and increased differentiation (Calegari et al., 2005; Lange et al., 2009), by modulating cdk4/cyclinD1 (shortened in "4D") *in vivo* via *in utero* electroporation. 4D overexpression led to a shortening of both G1 phase and total cell cycle length, and was associated to lower numbers of differentiative cell divisions, as assessed by positivity for Tis21, and increased numbers of Tbr2+ basal progenitors; consistently, 4D downregulation through an RNA interference (RNAi) approach induced opposite effects. Interestingly, the authors report that 4D overexpression led to an overall shortening of the cell cycle despite a relative increase in S and G2+M phases: the G1 shortening was indeed long enough to overcome the lengthening of the other phases, yielding a net shortening of the cell cycle. It is anyway worth noting that the shift of the balance towards self-renewal at the expense of differentiation in VZ neural

progenitors was associated not only to a G1-phase shortening but also to a S-phase increase.

A follow up paper from the Huttner lab (Arai et al., 2011) reported a detailed analysis of the cell cycle parameters of differentiating versus self-renewing neural progenitors, further breaking down the VZ neural progenitor population based on their positivity for Pax6 (true RGCs) or Tbr2 (intermediate progenitors). According to their analysis, expanding apical (Pax6+) (AP) and basal (Tbr2+) progenitors (BP) exhibited a two- to three-fold longer S-phase than their neurogenic counterpart, and an overall longer cell cycle. It was also demonstrated that BP have an overall longer cell cycle (BP 26.5 hrs, AP 19.1 hrs) and a shorter S-phase (BP 3.2 hrs, AP 5.0 hrs) than AP, and that the lengthening is due to a 2-fold increase of G1 phase (AP 11.6 hrs, BP 21.2 hrs).

Weaving together these and other experimental evidences, a unifying theory has been proposed under the name of "cell cycle hypothesis" (Arai and Pierani, 2014; Calegari et al., 2005; Götz and Huttner, 2005), aimed at explaining the relationship between cell cycle length and mitotic choice of neocortical progenitors. According to this hypothesis, "the ability of a cell fate determinant(s) to trigger a biologic effect depends on the amount of time given to such determinant(s) to act" (Salomoni and Calegari, 2010), implying that the length of a specific cell cycle phase might influence the overall availability and hence activity of a cell fate determinant that is typically present during that phase, such as proteins belonging to the Wnt or Notch pathways, influencing the final choice between self renewal and differentiation.

The experiments causally linking G1 length to fate choice indeed strongly support this theory, at least as far as G1 lengthening is concerned, although mechanistic insights are still lacking. Of course the big picture is likely a rather complex one, and the importance of the absolute and relative length of other phases to neural progenitor

fate choice is yet to be determined. However, as outlined above, several evidences seem to link a self-renewing behavior in neural precursor cells (NPCs) to a longer S phase, although the question whether the two events are causatively linked or simply correlated has not be addressed.

1.2.3 Epigenetic regulation of transcription in neocortical development

A tight control on the regulation of the chromatin state of developmental genes, and hence of their transcriptional activity, is critical to ensure that neurogenesis proceeds correctly, and that all the neuronal subtypes are generated with the right timing, sequence, and abundance. Given the necessity, in a developmental process that involves a sequence of cell fate switches, of a sequential activation of genes, it would be expected that the level of a transcriptional repressor goes down with time, allowing for the activation of genes that regulate the subsequent phases. This has been demonstrated to be the case for Ezh2 in cortical development: its expression pattern has indeed been shown to decrease both in NPCs during time and in differentiating cells (Pereira et al., 2010). The role of H3K27 modulation in corticogenesis has been investigated via conditional deletion of the catalytic subunit Ezh2, using two different deletion approaches that led to diverging conclusions. Deletion using the Emx1-Cre driver, which expresses Cre from E9.5, caused acceleration of neuron production, due to the precocious de-repression of transcription factors, eventually leading to exhaustion of the proliferative potential of NPCs and to a thinner cortical plate at birth (Pereira et al., 2010). In an opposing fashion, Ezh2 deletion in an in vitro NPC culture mimicking the late phases (E14-17) of cortical development led to a delay in the progression of neural development, due to a failure in repressing the Ngn1 factor (Hirabayashi et al., 2009).

These two apparently diverging lines of evidence can be weaved together in a unifying model that entails a redistribution of PRC2 to new targets during the late phases of corticogenesis, despite the global reduction of Ezh2 levels, and corroborate the idea that a fine-tuning of H3K27 methylation is required for the proper sequence of neuron and astrocyte production, which are produced following a precise temporal sequence that is mostly encoded cell-autonomously (Testa, 2011) (fig. 5).

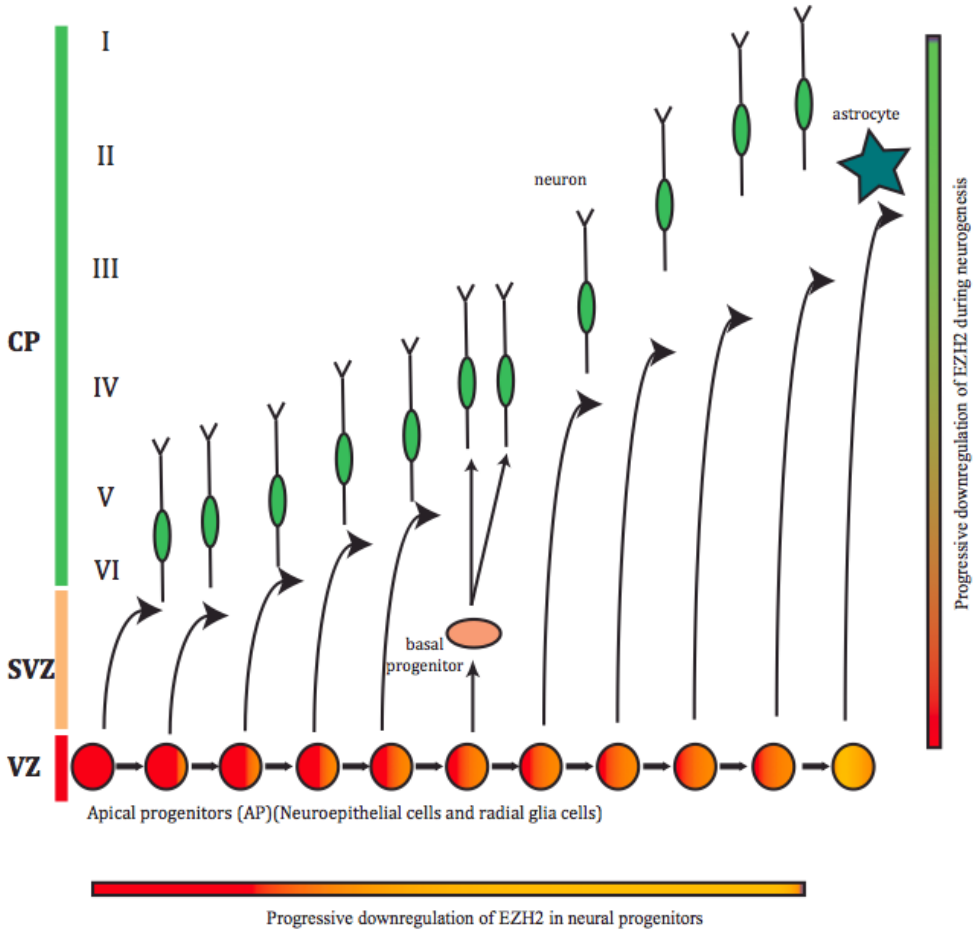

Figure 5. Diagram of mouse neocortical development with expression gradients of the PRC2 protein Ezh2. As neurogenesis proceeds (X-axis), apical progenitors (AP) in the VZ generate, by asymmetric division, neurons (green) or intermediate progenitors, known also as basal progenitors (BP, pink) that occupy the SVZ. Neurons progressively constitute the six layers of the cortical plate (CP). A neurogenic-to-astrogenic switch at the end of neurogenesis enables the production of astrocytes (blue). The expression of the PRC2 member Ezh2 decreases progressively in neural progenitors as neurogenesis proceeds (X-axis), as well as during the generation of neurons (Y-axis). CP, cortical plate; SVZ, subventricular zone; VZ, ventricular zone.

In such context, the evidence suggests that a H3K27 demethylase might play a fundamental role in activating key genes that instruct cell fate decisions in neural differentiation.

1.3 Jmjd3 and neural differentiation

As outlined above, our lab has demonstrated that Jmjd3 is a H3K27 demethylase that is required for the neural commitment of ES cells and controls the expression of key drivers and markers of neurulation through the demethylation of H3K27me3 (Burgold et al., 2008). Moreover, Jmjd3 expression is induced by retinoic acid (Jepsen et al., 2007), which is secreted from the meninges in the developing brain and regulates cortical neurogenesis (Siegenthaler et al., 2009). These lines of evidence prompted us to investigate the role of Jmjd3 in embryonic cortical development and neural differentiation. To do so, we generated a loss-of-function hypomorphic mouse strain (XB814), which displays a reduction of the Jmjd3 mRNA of more than 90% during central nervous system (CNS) development, (Burgold et al., 2008). This mouse shows a complex neurodevelopmental phenotype that results in perinatal death. Previous work from our lab demonstrated that lethality is due to a respiratory failure resulting from the lack of a functional pre-Bötzinger complex, a small network of neurons that is responsible for respiratory rhythm generation (Burgold et al., 2012). In KO mice, the pre-Bötzinger complex is initially formed and functional, but Jmjd3 loss leads to a selective failure to maintain it. Rescue experiments performed with catalytically active or inactive Jmjd3 have demonstrated that its demethylase activity is necessary for developing and maintaining the embryonic respiratory neuronal network. This unanticipated finding claims a broader role in brain development for Jmjd3, whose importance extends from early differentiation choices to the late development of neuronal networks.

1.4 Aim of the thesis

The work presented in this thesis stems from the characterization of the function of Jmjd3 in the development of the pre-Bötzinger complex that has previously published by our lab (Burgold et al., 2008; Burgold et al., 2012). As outlined in the thesis introduction, the work of our lab and several others has highlighted a role for Jmjd3 in neural development and cell state transitions, mainly via its demethylase activity on the H3K27 substrate, and hence on the transcriptional activation of neural-specific genes. Furthermore, Jmjd3 expression is induced by retinoic acid, which is secreted from the meninges in the developing brain and regulates cortical neurogenesis (Jepsen et al., 2007). These lines of evidence prompted us to investigate the role of Jmjd3 in embryonic neocortical development and neural differentiation *in vivo*.

2 MATERIALS AND METHODS

2.1 Cell culture

2.1.1 Mouse embryonic stem cells (ES cells)

Jmjd3.fl ESCs were maintained in culture under defined culture conditions with small molecule inhibitors that block extrinsic differentiation-inducing signals, the mitogen-activated protein kinase (MAPK/ERK1/2) and glycogen synthase kinase 3 (GSK3), in the presence of LIF (Ying et al., 2008). This medium is named 2i/LIF culture medium and comprises N2B27 medium [DMEM/F-12 (with GlutaMax™; Gibco) and Neurobasal™ medium (Gibco) in a 1:1 mixture, with N2 (Gibco), B27 (Gibco), 2 mM L-glutamine (Gibco), 15 mM HEPES and 0.1 mM 2-mercaptoethanol (Gibco)] supplemented with 1 μM of MEK inhibitor PD0325901 (ABCR), 3 μM of GSK3 inhibitor CT99021 (ABCR) and LIF. Under these culture conditions cells were passaged every three days by detaching them with Accutase® (Sigma) and replating on gelatinized plates at a density of 2×10^4 cells/cm^2. Jmjd3.Venus ES cells were cultured under the same conditions, but were routinely passaged on uncoated 10cm culture dishes.

For cryoconservation, ES cells cultured in 2i/LIF medium were resuspended in 2i/LIF medium with 20% Knockout™ Serum Replacement (KSR; Gibco) and 10% DMSO. Cells were distributed into cryovials at a density of $5x10^6$ cells/ml freezing medium and frozen at -80 °C. The next day tubes were transferred to liquid nitrogen for long-term storage.

2.1.2 Derivation and culture conditions of cortical neural precursor cells (NPCs)

Pregnant mice were sacrificed at day E13.5 according to standard procedures and in accordance to the Italian law. The protocol for the derivation of embryonic cortical NPC has ben adapted from (Ravin et al., 2008).

The intact uterus was carefully extracted and transferred to a 10 cm dish containing sterile phosphate buffered saline (PBS). The embryos were extracted and kept in sterile Hank's Balanced Salt Solution (HBSS), and the heads were separated using dissection scissors. Using Dumont no.5 jeweler's forcipes, the cortices were separated from the rest of the brain and form the basal ganglionic eminences, and kept in 1.5 tubes containing sterile HBSS. The cortices were mechanically triturated using a p1000 until a single cell suspension was obtained. The cells were then pelleted using a tabletop microcentrifuge, and resuspended in DMEM/F12 (MediaTech) with N2 supplement using human apo-transferrin (Sigma), basic fibroblast growth factor (bFGF) (Peprotech, 30 ng/ml), and insulin (Sigma, 25 ng/ml). The cells were then plated at a density of 10,000-20,000 cells/cm^2 in poly-L-ornithine/fibronectin-coated 10 cm tissue culture plates and grown for 5-6 days prior to cryoconservation in N2 medium with 10% DMSO or further passaging. bFGF was added on a daily basis with complete medium replacement every second day.

Upon reaching 70-80% confluence, plates were washed once with HBSS and the cells were mechanically detached prior to centrifugation and passaging into fresh N2+bFGF.

2.1.3 Growth curves

Growth curves were performed over serial re-passaging of individual NPC lines. At each passage, $1x10^6$ cells were plated onto in poly-L-ornithine/fibronectin-coated 10 cm tissue culture plates. Three days later, cells were mechanically detached and

counted, and $1x10^6$ cells were re-plated onto coated dishes. Cumulative cell numbers were obtained by multiplying the number of cells obtained at each passage by the cumulative number of cells counted at the end of the previous passage.

2.1.4 EdU/PI staining for the determination of cell cycle distribution

Ethynyl deoxyuridine (EdU) (Life Technologies) incorporation and detection was performed according to the manufacturer's instructions. EdU powder was resuspended in DMSO and was added to the cultured cells at a final concentration of 10 uM. After 30' of incorporation, cells were washed and fixed with PBS containing 4% paraformaldehyde (PFA). The cells were harvested and EdU was detected according to the manufacturer's instructions using an alexa 488 azide. After EdU detection, Propidium Iodide (PI) DNA staining was performed by overnight incubation at 4°C in PBS with a final concentration of PI 2.5 µg/mL plus RNase 8 µg/mL. Flow cytometry analysis was performed on a BD FACSCALIBUR (BD Biosciences) machine, using low or medium pressure to enable reliable recording of the events. At least 20,000 events per sample were acquired, and the data were analyzed using FlowJo software.

2.1.5 Double thymidine block and release

The block in G1/S and release were performed by double thymidine administration. $1x10^6$ NPCs were plated and grown for 24 hours in N2+bFGF, after which a first block was performed by adding thymidine to the culture medium to a final concentration of 2 uM for 13 hours. Cells were released by complete medium change and wash for 10 hours, and then a second block of 13 hours was performed. The cells were then released and time course samples were taken every hour by fixing with PBS 4% PFA. EdU detection and PI staining were performed as described above.

2.1.6 Time-lapse videomicroscopy of NPCs

Frozen E13.5 brain-derived NPCs were thawed on poly-L-ornithine (PLO)/fibronectin-coated 10cm dishes in N2 medium, as described above. Cells were grown to 70% confluence at 37°C, 5% CO2, 5%O2 and then passaged onto coverslip-bottom, PLO/fibronectin-coated, dishes (Advanced TC 35 mm, Greiner Bio-one, cat# 627965) for imaging. 20,000 cells for each genotype were seeded in the N2 medium described above (10 ng/ml bFGF, 25 µg/ml Insulin) and 10-12 hours after plating, plates were etched with a custom etching device to create restricted growth areas of 300 x 300 um. Then, imaging was performed at 37°C, 5% CO2 and 5% O2. Four restricted growth area both for wild type and mutant cells were captured every 2 minutes for 48 hours. Lineage data was derived using BioCell (SIMI Reality Motion Systems), and the cell cycle length was measured as difference in time (ΔT) of two subsequent mitoses occurring in the recorded time frame. Statistics were performed with GraphPad (Prism) and mean and standard deviation were calculated. The p-value was calculated using Mann-Whitney U test.

2.1.7 Derivation and culture of post-natal SVZ radial glial cells (RGCs)

Mouse SVZ monolayer cultures were derived as previously described (scheffler 2005). Postnatal SVZ were isolated from P7 mouse brains, and were dissociated via mechanical trituration in presence of 0.25% trypsin. Cells were plated at 30,000 cells/cm^2 in 10cm culture dishes in N5 proliferation medium (DMEM/F12, N2 supplement (Life Technologies), 5% FCS (Gibco), 20 ng/ml EGF (Peprotech), 20 ng/ml bFGF (Peprotech), 35 µg/ml bovine pituitary extract (BPE) (Life Technologies). Non-attached cells were collected after 1 day and replated into 10cm dishes. After 7 days, the cells were confluent and could be passaged 1:2, after

detachment with 0.25% trypsin. Cells were passaged 4–6 times before use in experiments. Neural differentiation was induced by removal of epidermal growth factor (EGF), bFGF and fetal bovine serum (FBS) from the medium (N6 medium).

For cryopreservation, cells were resuspended in cryoconservation medium (N5, 10% DMSO, 10% FCS), stored in cryovials and kept at -80°C for three days in a cryobox prior to storage in liquid nitrogen.

2.2 Molecular biology techniques

2.2.1 Isolation of genomic DNA from cells and tails

Cells or tails were lysed in lysis buffer consisting of 100 mM Tris-HCl pH 8.5, 5 mM EDTA, 0.2% sodium dodecyl sulphate (SDS), 200 mM NaCl and 100 µg/ml proteinase K. The lysate was incubated overnight at 55°C. The DNA was then precipitated with isopropanol according to a previously published protocol (laird 1991) and then centrifugated at 16000 × g for 20'. The DNA pellet was washed with 70% ethanol and centrifuged again. The DNA was finally resuspended in TE (10 mM Tris-HCl pH 8.0, 1 mM EDTA) or water. Lysates from tails can be used directly for genotyping, after one step of proteinase k heat inactivation, performed at 94°C for 10 minutes. Before use, the crude extract was diluted 1:5 in water in order to reduce interference by SDS in the polymerase chain reaction (PCR). For specific purposes, like copy number assay, DNA was also purified using Qiagen DNeasy® blood and tissue kit according to manufacturer instructions.

2.2.2 Polymerase Chain Reaction (PCR)

PCR reactions were carried out in a total volume of 20 µl with 0.2 mM dNTPs (each dNTP), 0.5 mM primers, DNA template (in various amounts depending on the source),

0.01 U/µl Phusion® DNA polymerase (Finnzymes) or GoTaq (Promega) and the appropriate buffer provided by the supplier. The reaction protocol varies between experiments but follows this general scheme: 30'' initial denaturation at 98°C, 35 cycles consisting of 10'' denaturation at 98°C, 15'' of annealing at the for each primer combination optimized temperature and variable times of extension depending on amplicon length and complexity at 72°C. The last cycle was followed by a final extension step for 10' at 72 °C.

PCR reactions were separated by electrophoresis in agarose gels at different concentrations based on the band size (1-3%) in Tris-acetate-EDTA buffer with 0.5 µg/ml ethidium bromide. For downstream applications the PCR products were purified using the QIAquick PCR purification kit or QIAquick Gel Extraction kit (Qiagen).

2.2.3 RNA Extraction

Total RNA was extracted from cells using Qiagen RNeasy® Plus Mini kit according to the instructions of the manufacturer. The procedure comprises a step of DNA removal via gDNA eliminator column. Low-density agarose gel electrophoresis was performed to exclude gDNA contamination. Finally RNA was resuspended in RNAse-free water and quantified using a NanoDrop ND-1000 Spectrophotometer (Thermo Fisher Scientific).

2.2.4 cDNA synthesis

cDNA synthesis was performed using SuperScript® VILO™ cDNA Syntesis kit according to the manufacturer's instructions. Briefly, the reaction takes place in 20 µl with: 4 µl of 5X VILO™ reaction mix (which includes random primers, MgCl2 and dNTPs) 2 µl of 10X SuperScript® enzyme mix (which includes SuperScript® III

reverse transcriptase, RNaseOUT™ recombinant ribonuclease inhibitor and an helper protein), 300ng-1μg of RNA and water. The reaction is incubated at 25°C for 10', at 42°C for 60' and finally at 85°C for 5' to terminate the reaction. The resulting cDNA can be used diluted or undiluted in qPCR analysis.

2.2.5 Real Time Quantitative PCR (qRT-PCR)

qRT-PCR was performed on 7900HT Fast Real-Time PCR system (Applied Biosystems) using TaqMan® Gene expression assays (Applied Biosystems). Each sample was analyzed in triplicates and normalized to TATA-Binding Protein (TBP). Normalization was used to correct variations in RNA concentration and integrity among samples. Relative mRNA amounts were calculated by the comparative cycle threshold (Ct) method using the formula $2^{-\Delta Ct}$. In the case of Taqman Assays 5 ng of cDNA was amplified (in triplicate) in a reaction volume of 15 μl containing the following reagents: 7.5 μl of TaqMan® PCR Mastermix 2x No UNG (Applied Biosystems), 0.75 μl of TaqMan® Gene Expression Assay 20x (Applied Biosystems). The cycling steps are: 10' at 95°C, followed by 40 cycles of 15'' at 95°C and 60'' at 60°C. A control for DNA contamination was prepared using samples that were not subjected to the reverse transcription step and therefore would not produce any amplification.

2.2.6 RNAseq library preparation

RNAseq libraries were prepared with the TruSeq Stranded Total RNA with Ribo-Zero Human/Mouse/Rat kit, according to the manufacturer's instructions. 1 μg of total RNA was used as starting material for the library preparation procedure. The final library product was quantified using the NanoDrop ND-1000 Spectrophotomer (Thermo Fisher Scientific) and the Qubit® 2.0 Fluorometer (Life Technologies). The

size of the resulting fragments was assessed using the 2100 Bioanalyzer and the DNA HS Kit (Agilent).

2.3 Bionformatic analysis

2.3.1 RNAseq analysis

RNAseq sequence reads were aligned to the mm9 transcriptome using TopHat 2.0.10, disabling coverage search. The alignment was first performed on the RefSeq transcriptome to prioritize alignment to know transcripts. Then, all reads that had an edit distance above 1 (e.g. more than one mismatch/indel/break with respect to alignment location) were realigned on the whole genome. For the telencephali data (100bp unstranded paired-end reads), only alignments with read edit distance and mismatches below or equal to 3 were retained. Because the data from *in vitro*-cultured neural progenitors had a shorter read length (50bp stranded paired-end reads), we tolerated only 2 mismatches/edit per read for this analysis (and used the fr-firststrand library type).

Quantification of reads over the RefSeq transcriptome (masking ribosomal RNAs) was performed with Cufflinks 2.2.1 using sequence-bias, multi-read, and length corrections. Differential gene expression was estimated with Cufflinks 2.2.1 using pooled dispersion models and geometric normalization.

2.3.2 ChIPseq analysis

ChIPseq reads were trimmed for adapter contamination using Scythe 0.981 (requiring a minimum match of 3 for the sequence to be trimmed, and discarding trimmed sequences shorter than 20bp), before being aligned to the mm9 genome using Bowtie 1.0 (allowing 2 mismatches and discarding multiply aligning reads).

Peaks were called using Macs 1.4.2 with default settings and discarding duplicated reads. Genes with a peak in a −2.5kb/+1kb region around (any of) their transcription start sites were considered target genes.

2.4 Biochemistry Techniques

2.4.1 Protein extraction

In order to avoid degradation of proteins and loss of information, proteins were always extracted from freshly pelleted cells. RIPA buffer (10 mM Tris-Cl (pH 8.0), 1 mM EDTA, 0.5 mM EGTA, 1% Triton X-100, 0.1% sodium deoxycholate, 0.1% SDS, 140 mM NaCl), freshly supplemented with a protease inhibitor cocktail (Roche) was used to prepare total cell lysates. Lysed pellets were put for 30' on a rotary wheel at +4°C and subsequently pelleted by 25' centrifugation at +4°C and 13000 rpm on a refrigerated tabletop microcentrifuge to clear the lysate.

2.4.2 CSK fractionation

Triton X-100 extraction and release of chromatin-bound material was performed as in (Groth et al., 2007) in multiwell plates. In brief, soluble proteins were extracted by CSK (10 mM PIPES (Sigma) pH 7, 100 mM NaCl (Sigma), 300 mM sucrose (Sigma), 3 mM MgCl2 (Sigma)) for 5 minutes on ice. The chromatin pellet was washed once in 0.1%T CSK and resuspended in Laemmli sample buffer + 100mM DTT for Western blotting. This insoluble fraction was called CSK fraction. All buffers were supplemented with protease inhibitor cocktail (Roche). Similarly to pre-extracted, the respective total extracts were prepared for Western blotting by resuspension in Laemmli sample buffer 1X + 100 mM DTT.

2.4.3 Chromatin immunoprecipitation (ChIP)

Adherent cells were cross-linked by adding formaldehyde to the culture medium at a final concentration of 1%. After 5 min fixation the reaction was quenched by adding Glycine to a final concentration of 125 mM, cells were thoroughly washed in PBS and harvested by scraping. Cell membranes were disrupted in L1 swelling buffer (50 mM Tris-HCl pH 8.0, 2 mM EDTA, 0,1% NP-40, 10% Glycerol, 1× protease inhibitor cocktail (Roche)), 900 µl for a 10 cm dish. Nuclei were precipitated and resuspended in 600 µl of nuclear lysis buffer (50 mM Tris-HCl pH 8.0, 5 mM EDTA, 1% SDS, 1× protease inhibitor cocktail). Shearing of genomic chromatin was performed with a Diagenode Bioruptor® sonicator (high power, four cycles of 30'' pulse and 30'' pause each) yielding DNA with an average fragment size from 200 to 1000 bp. DNA concentration was measured with NanoDrop ND-1000 Spectrophotomer (Thermo Fisher Scientific) and DNA of different samples was employed in equal quantities for the immunoprecipitation. Salt and detergent concentrations in the immunoprecipitation were adjusted for an optimal antibody performance by diluting the sonicated lysate with nine volumes of dilution buffer (50 mM Tris-HCl pH 8.0, 5 mM EDTA, 200 mM NaCl, 0.5% NP-40) for ChIP assays on Jmjd3 and total histone H3 or by adding 1/10 volume of 10% Triton X-100 for the immunoprecipitation of histone H3 trimethyl-lysine 27 (H3K24me3). Lysate was precleared with 50 µl slurry of salmon sperm DNA saturated protein A sepharose beads (GE Healthcare), rotating for 1 h at 4 °C. Beads were pelleted by centrifugation and antibody was added to precleared extract (Table 5). Immunoprecipitation was carried out a 4 °C overnight. ChIP complexes were collected by incubating with 20 µl of salmon sperm DNA/protein A sepharose beads for 30' at 4°C. ChIP-beads complexes were washed four times in washing buffer (20 mM Tris-HCl pH 8.0, 2 mM EDTA, 0.1% SDS, 1% NP-40, 500 mM NaCl) and three times in 1× TE. ChIP complexes were eluted in 120 µl of

1× TE containing 2% SDS at 65 °C for 15 min and the crosslink of proteins to DNA was reversed at 65 °C overnight. DNA was purified with the QIAquick PCR Purification Kit (Qiagen), following the manufacturer's instructions and eluted in 100 µl of provided buffer EB. 5 µl of DNA were used in a 25 µl qRT-PCR reaction using the primers listed in Table 1. The abundance of target genome DNA was normalized relative to that of input.

Table 1. *List of primers used for ChIP-qPCR*

Primer	Sequence
Dlx2_60_F	TTGGCTAAGGAAGGCCTAGA
Dlx2_60_R	CACCAGGGAGCGTTTCTAAT
Dlx2_82_F	CGGGACAGGAAAGAGCAC
Dlx2_82_R	GAAGGGACCCGGAGAGATA
Olig2_89_F	ACTAATGACTGCCTGGGTGTCT
Olig2_89_R	TCGCAACAGGAGTTATTGGA
Mash1_3_F	CCCTGGCCAGAAGTGAGA
Mash1_3_R	CTGGGTGTCCCATTGAAAAG

2.4.4 Immunoblotting

Proteins were separated by sodium dodecyl sulfate polyacrylamide gel electrophoresis (SDS-PAGE). NuPage system (Invitrogen) was used to perform Western Blot, therefore the lysate was mixed with the loading buffer (4X LDS) supplied by the company. According to the size of the target protein, 4-12% Bis-Tris or 3-8% Tris-Acetate polyacrylamide gel were used to achieve protein separation. The gels were run using buffers supplied by the manufacturers according to the type

of gel (MOPS or TA, Life Technologies), at constant 170V for 1-3 hours depending on the degree of separation needed.

Proteins were transferred to a nitrocellulose membrane using the standard Towbin Buffer (25 mM Tris base, 190 mM glycine, 20% methanol) and the Mini Trans-Blot equipment (BioRad). Efficiency of the transfer was assessed by Ponceau staining (VWR). The nitrocellulose membrane was blocked in 5% (w/v) skimmed milk powder in TBS-T buffer (25 mM Tris, 150 mM NaCl, 2 mM KCl) for 1 hour at room temperature. All antibodies were then diluited in 5% milk in TBS-T.

Primary antibodies were incubated overnight at 4°C while species-specific secondary antibodies, conjugated with horseradish peroxidase (BioRad) or with fluorochromes (LI-COR Biosciences), were incubated for 2 hours at room temperature (RT). According to the type of secondary antibody used (HRP or fluorescent), the signal was acquired using the ECL plus reagent and chemiluminescent detection (HRP), or digitally processed using the LI-COR Odissey platform (LI-COR biosciences). ImageJ was used to process the raw images acquired with the LI-COR Odissey platform.

2.5 Histology techniques

2.5.1 Brain dissection

Brains (E16.5, E18.5) or intact heads (E13.5) were dissected in PBS, fixed overnight in PBS, 4% PFA at 4°C, cryoprotected in PBS, 30% sucrose overnight at 4°C and embedded in cryostat freezing medium (Bio-Optica). Brains were coronally sectioned in 10 um-thick slices and placed serially onto SuperFrost Ultra Plus glass slides (Thermo Fisher Scientific). Sections were post-fixed for 10' with 4% PFA. For the detection of nuclear antigens an antigen enhancement step was performed by briefly boiling the slides in 10 mM sodium citrate pH 6.0 using a microwave. Sections were

incubated in permeabilization/blocking solution (0.2% Triton X-100, 10% goat serum in PBS) for 30 min at RT and incubated with primary antibodies diluted in PBS plus 2.5% goat serum, 0.05% Triton X-100 at 4 C overnight. The antibodies and their dilutions used in this study are listed in Table 2. Specimens were incubated with the appropriate species-specific secondary antibodies conjugated to Alexa488, Alexa568, Alexa647 (Life Technologies) at 1:200 dilution for 3 hr at RT, then incubated with DAPI (Sigma-Aldrich) nuclear counterstain, and coverslipped with VectaMount AQ aqueous mounting medium (Vector Laboratories). Widefield microscope images were acquired with an Olympus fluorescence microscope equipped with a CoolSNAP EZ CCD camera (Photometrics) using MetaVue software (Molecular Devices). Confocal microscope images were acquired on a Leica SP5 system, using a motorized stage and automated stitching for high-content images.

For clarity, images were adjusted for contrast and brightness using ImageJ software. Cell counts were manually performed using ImageJ softeware and CellCounter plugin.

Table 2. *List of primary antibodies used for immunofluorescence*

Antigen	*cat. no*	*Company*	*Dilution*
Ki67	ab15580	Abcam	1:500
Ctip2	ab18465	Abcam	1:300
Tbr1	ab31940	Abcam	1:500
Brn2	sc-6029	SantaCruz	1:200
Pax6	PAX-6 (b)	Hybridoma Bank	1:1000
Pax6 (Alexa 488)	561664	BD Biosciences	1:200
Tbr2	ab23345	Abcam	1:200
BrdU	OBT0030G	Serotec	1:100
IdU-BrdU	347580	BD Biosciences	1:50
Sox2	MAB2018	R&D Systems	1:100

2.5.2 Determination of cell cycle parameters in vivo

In order to assess the length of S phase (T_s) and the total cell cycle length (T_c) *in vivo*, we performed the double thymidine analogue incorporation assay, as first described in (Martynoga et al., 2005).

E13.5 pregnant mice were intraperitoneally administered Iododeoxyuridine (IdU) at t=0h, followed by Bromodeoxyuridine (BrdU) at t=1.5h, and the mice were sacrificed at t=2h. For both thymidine analogues 150 ul of a solution at a concentration of 10 mg/ml were administered (approx. 50 mg IdU/BrdU per kg of body mass). The fraction of cells that are in S phase at both t=0h and t=1.5h, and thus incorporate both analogues, constitutes the S_{cells}, whereas the fraction of cells that incorporate IdU but not BrdU constitutes the leaving fraction, or L_{cells}. The time interval between the administration of IdU and BrdU (=1.5 h) is called T_i.

The ratio of the length of any fraction of the cell cycle to that of another fraction is equal to the ratio of the number of cells in the first fraction to the number of cells in the second fraction. Hence, the ratio of the number of cells in the L_{cells} to the S_{cells} fractions is equal to the ratio between T_i (which equals 1.5 h) and T_s.

$$(1)\ T_i / T_s = L_{cells}/S_{cells} \therefore T_s = T_i/(L_{cells}/S_{cells})$$

The calculated T_s in (1) can then be used to estimate T_c:

$$(2)\ T_s/T_c = S_{cells}/P_{cells} \therefore T_c = T_s/(S_{cells}/P_{cells})$$

In (2), P_{cells} represents the number of actively proliferating cells in the analyzed area. The number of P_{cells} is estimated by counting the total cell number in the ventricular

zone (VZ), and is based on the assumption that 98-100% of the cells in the VZ are actively proliferating, as previously assessed (Caviness et al., 1995; Estivill-Torrus et al., 2002; Takahashi et al., 1993; Takahashi et al., 1995). The cell numbers were counted in areas of constant width (200 μm), and height determined by the thickness of the ventricular zone.

Immunofluorescence staining was performed as previously described, with the exception of a shorter incubation time for the primary (2 hours at RT instead of overnight at 4°C), and the specific primary and secondary antibodies are listed below in Table 3.

Table 3. *List of primary and secondary antibodies used for in vivo cell cycle analysis*

Antigen	*Cat no.*	*Company*	*Dilution*
Primary Abs			
BrdU	OBT0030G	Serotec	1:100
IdU-BrdU	347580	BD Biosciences	1:50
Secondary Abs			
Gt anti-Ms, Alexa 488	A11029	Life technologies	1:200
Gt anti-Rt, Alexa 568	A11077	Life Technolgies	1:200

2.6 Mouse strains

All strains used in this study were bred into C57BL/6 background. The day of vaginal plug was considered to be E0.5. Analysis of the phenotype and genotype were performed independently in blind experiments and compared afterward.

The XB814, R26.Jmjd3.fl.stop and BAC.Jmjd3mut mouse strains were previously generated by our lab and have been described in (Burgold et al., 2012). For completeness, the detailed procedures used for their generation are reported below,

together with the unpublished procedures for the generation of the Jmjd3.fl and Jmjd3.Venus mouse strains.

2.6.1 PGK-Cre deleter strain

The PGK-Cre mouse strain has been previously published (Lallemand et al., 1998). Genotypes were assessed by PCR on genomic DNA extracted from tail biopsies using the primers P19 and P20 (Table 4).

2.6.2 Rosa26-Cre inducible deleter strain

The Rosa26-Cre inducible has been previously published (Seibler et al., 2003). Genotypes were assessed by PCR on genomic DNA extracted from tail biopsies using the primers R26_WTF, R26_WTR and R26_MUTR (Table 4).

2.6.3 Generation of the XB814 Jmjd3 KO mouse strain

The mouse ESC line XB814 harboring a gene trap insertion in Jmjd3 was obtained from BayGenomics (http://www.mmrrc.org/catalog/overview_BG.php) (Stryke et al., 2003) and the insertion site of the trap cassette was mapped to Jmjd3 intron 1 by sequence analysis. ES cells were injected into C57BL/6 blastocysts to generate chimeras following standard procedures (Nagy et al., 2003). Germline transmission was confirmed by PCR on genomic DNA extracted from tail biopsies using the primers JBaygD2, JBaygR2, and GT3_rev (Table 4).

2.6.4 Generation of the R26.Jmjd3.fl.stop mouse strain

To generate tissue-specific conditional *Jmjd3* transgenic mice, we cloned full-length mouse *Jmjd3* cDNA into the pR26 loxP2STOP frt2 IRES eGFP targeting vector (Sasaki et al., 2006). C57BL/6-derived ES cells were transfected, cultured and selected as

previously described (Casola, 2004). Correctly targeted ESCs were injected into C57BL/6 albino blastocysts to generate chimeras and germline transmission was confirmed by Southern blot. Expression of the *Jmjd3* transgene was induced upon breeding to the ubiquitous Cre-deleter strain PGK-Cre (Lallemand et al., 1998).

For PCR genotyping of genomic DNA extracted from tail biopsies the primers R26.SA_Fw, Jmjd3.1_Rev and Neo_Fw were used (Table 4).

2.6.5 Generation of the BAC Transgenic Jmjd3mut mouse strain

A mouse BAC (RP23-107C10) containing the *Jmjd3* gene locus was engineered to insert a point mutation resulting in the Histidine to Alanine substitution at position 1388 (H1388A). Microinjection into fertilized oocytes and generation of transgenic mice was performed by standard techniques using oocytes derived from FVB mice (Muyrers et al., 2004; Testa et al., 2004b; Vintersten et al., 2004). Transgenic founder animals were selected by PCR of tail biopsies using primer pair 8_F and 8_R (Table 4). Two transgenic founders (*Jmjd3mut21* and *Jmjd3mut65)* were selected for further characterization and the number of BAC integrations was assessed by Southern blot and real-time PCR using a TaqMan copy number assay. In order to confirm the expression of the mutant *Jmjd3* allele brain cDNA of *Jmjd3mut21* and *Jmjd3mut65* transgenic mice was amplified by PCR using the primers F_{RTseq} and R_{RTseq} (Table 4). PCR products were subcloned into pCR2.1-TOPO vector (Invitrogen) and sequenced. In order to distinguish the *Jmjd3* trap allele from the *Jmjd3mut* BAC transgene in compound heterozygous crosses, a TaqMan copy number assay was designed based on a probe spanning the junction between intron 1 and the gene trap cassette ($Probe_{cnTrap}$ CACTTTCGCCCCCTCAGCCAG) along with the amplification with primers F_{cnTrap} and R_{cnTrap} (Table 4).

2.6.6 Generation of the Jmjd3.fl mouse strain

In order to generate a conditional strain for Jmjd3, a targeting vector (pACYC177-Jmjd3-FRTbgeok-flox) has been generated in our lab to target ES cells by homologous recombination. This vector is based on the 'knockout-first' design (Testa et al., 2004a) and allows in a single ES cell targeting step to generate both a constitutive and a conditional knockout (fig. 6), thanks to the presence of FRT sites surrounding a βgeok selection cassette placed in an intronic region, followed by loxP sites flanking one or more exons. The βgeok cassette generates a constitutive knockout based on the presence of a splice acceptor (sA) site and a poly-adenylation (pA) signal, which cause a capture and truncation of the endogenous RNA transcript. As illustrated in fig. 6, upon removal of the βgeok cassette by Flp recombinase, the constitutive knockout allele is converted into a conditional allele, which allows studying the loss-of-function phenotype in a spatially- and temporally-controlled manner.

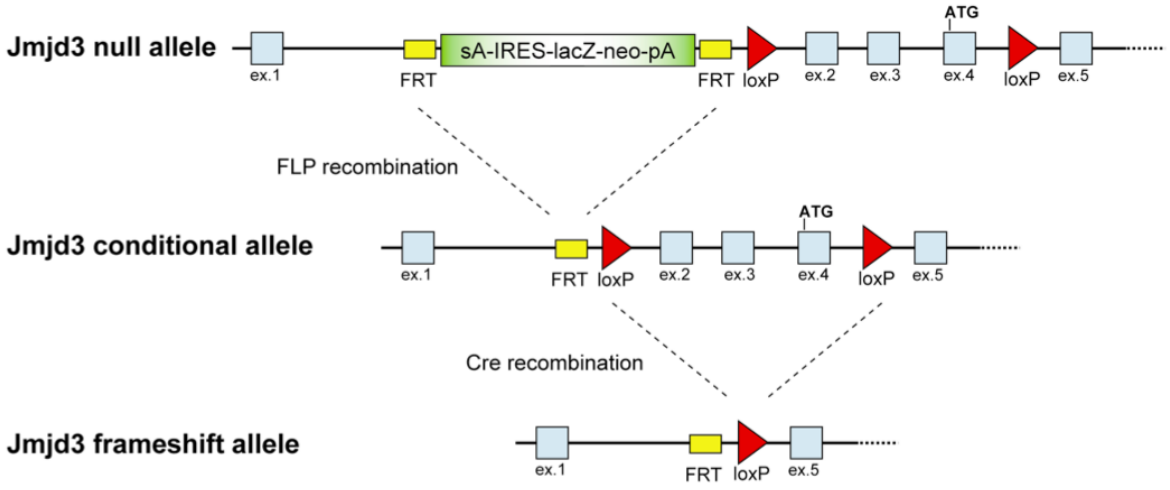

Figure 6. The Jmjd3 multipurpose allele, and the 'knockout-first' design. The strategy entails insertion of a FRT-flanked reporter cassette, comprising a splice acceptor (sA), an internal ribosomal entry site (IRES), a lacZ-neo fusion and a polyadenylation (pA) signal into the first intron of Jmjd3 and the additional insertion of two loxP sites to flank exons two to four.

C57BL/6 ES cells were electroporated with the targeting construct and selected by addition of G418. Following G418 selection the ESC clones were screened by Southern Blot, and two ES cell clones that displayed the correct integration of the targeting vector were injected into C57BL/6 mouse blastocysts. 11 male chimeras

were obtained, and have been bred to C57BL/6 females to transmit the targeted Jmjd3.fl allele through the germline. Mice positive for the targeted allele were selected by PCR of tail biopsies using primers JBaygD2, JBaygR2 and LoxP_R2 (Table 4).

2.6.7 Generation of the Jmjd3.Venus mouse strain

Based on a collaboration with the laboratory of Francis Stewart, we obtained the lab of a mouse BAC (RP24-244F21) containing the whole Jmjd3 locus, which has been engineered with a Venus fluorescent protein in-frame at the C-terminal end of the Jmjd3 coding sequence. The resulting product is a fusion protein constituted by the WT protein sequence of Jmjd3, tagged at the C-terminus by a Venus fluorescent protein. The Venus fluorescent protein is a derivative of YFP with faster folding time, allowing for immediate detection of the fusion product by direct or indirect immunofluorescence. The Venus tag has been successfully used for both live and fixed-sample imaging, and for immunoprecipitation applications (Ciotta et al., 2011; Hofemeister et al., 2011).

Microinjection into fertilized oocytes and generation of transgenic mice was performed by standard techniques by the Transgenics Facility at the IFOM-IEO Campus using oocytes derived from C57BL/6 mice (Van Keuren et al., 2009; Vintersten et al., 2008). Transgenic founder animals were selected by PCR of tail biopsies using primer pair VENfw01 e VENrv01. One transgenic founder female (#889) was selected for further characterization and colony expansion.

Table 4. *List of primers used for genotyping*

Strain	*Primer*	*Sequence*
XB814	JBaygD2	AGGATACAGGAGCCACGCG
	JBaygR2	TGACTCTCCACTCGATCACCC
	GT3_rev	TCCGGAGCGGATCTCAAAC
R26 WT/Cre	R26_WT F	AAAGTCGCTCTGAGTTGTTAT
	R26_WT R	GGAGCGGGAGAAATGGATATG
	R26_MUT R	CCTGATCCTGGCAATTTCG
R26.Jmjd3.fl-stop	R26.SA_Fw	CTCGCGGTTGAGGACAAACTCTTCGCGGTC
	Jmjd3.1_Rev	GGTCCCAGCTCGGCGAAGCT
	Neo_Fw	CCATCATGGCTGATGCAATGCG
Cre	P19	GCCTGCATTACCGGTCGATGCAACGA
	P20	GTGGCAGATGGCGCGGCAACACCATT
Jmjd3.fl	JBaygD2	AGGATACAGGAGCCACGCG
	JBaygR2	TGACTCTCCACTCGATCACCC
	LoxP_R2	GGAGCTACTGCCATGAGATG
BAC.Jmjd3	8_F	GCGTAAGCGGGGCACATTTCATT
	8_R	CCGAAGGCAAGAGCAGAATGTGTG
	F_{RTseq}	CCACGTGGGCCACACCATCC
	R_{RTseq}	GGGCCAATGTTGATGTTGACTGAGC
	F_{cnTrap}	CGCAGCTTCCCAGAAGTTAGAG
	R_{cnTrap}	CCGCAAACTCCTATTTCTGAGAAAGA
Jmjd3.Venus	VENfw01	AGTCTGCCATGCCTGAGGGCT
	VENrv01	GGGAGCAGCACAGGGCCATC

3.1 Validation of the XB814 mouse strain as suitable loss-of-function model for Jmjd3 in the developing cortex

To study the role of Jmjd3 in neocortical development, we took advantage of a constitutive Jmjd3 loss-of-function mouse strain (XB814) that has been previously developed by our lab (Burgold et al., 2012). XB814 Jmjd3-/- mice die of respiratory failure shortly after birth: it has been demonstrated by our lab that the lack of Jmjd3 hinders the formation of a functional pre-Bötzinger complex (PBC), a neuronal circuit located in the embryonic brainstem that dictates the respiratory rhythm, together with the retrotrapezoid nucleus/parafacial respiratory group (RTN/pFRG) (Fortin and Thoby-Brisson, 2009).

In the XB814 mouse strain, Jmjd3 has been inactivated by inserting a splice acceptor-based knockout cassette in the first intron of the Jmjd3 gene, resulting in trapping of the first noncoding exon of the transcript. Gene expression and western blot analysis revealed that the trap cassette was not completely efficient and allowed for a small residual level of gene expression, around 10% of the WT levels (Burgold et al., 2012). Hence, since this strain is hypomorphic rather than a complete knockout, we wanted to confirm that this mouse strain is a bona fide knockout in the developing brain. To do so, we first assessed the mRNA level of Jmjd3 in the neocortex of developing mouse embryos at different days of embryonic development. TaqMan qPCR analysis shows more than 90% reduction of the Jmjd3 transcript at embryonic (E) days E13.5, E16.5 and E18.5 (fig. 7A). Moreover, RNA in situ hybridization confirms that the Jmjd3 mRNA is virtually absent in the E18.5 developing cortex of XB814 mice (fig. 7B).

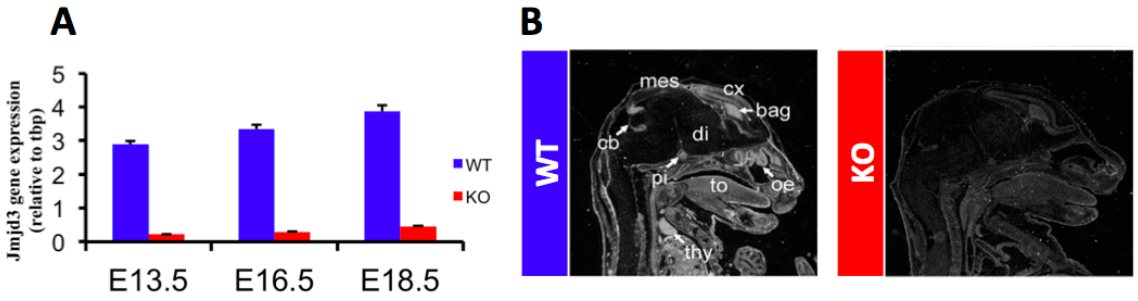

Figure 7. The XB814 mouse strain displays reduced level of Jmjd3 transcript in the telencephalon. (A) qRT-PCR on RNA extracted from WT or KO telencephali at E13.5, E16.5, E18.5. Tbp is used as reference gene. Mean ±SD of three biological replicates is shown. (B) RNA *in situ* hybridization on WT or Jmjd3 KO mouse embryos at day E16.5. Regions of specific signal are indicated by the following abbreviations: bag: basal ganglia, cb: cerebellum, cx: cortex, Di: diencephalon, Mes: mesencephalon, oe: olfactory epithelium, pi: pineal gland, thy: thymus, to: tongue (from Burgold et al., 2012).

We next assessed the reduction of Jmjd3 at the protein level, by western blot on lysates from cortical tissue and immunofluorescence on brain sections. To this end, we tested several commercially available antibodies but we were not able to obtain reliable and reproducible results for any of these applications with any of the tested antibodies. Based on these results and on the necessity of effectively detecting the Jmjd3 protein, we developed, in collaboration with the CNIO institute in Madrid, several monoclonal antibodies, in order to choose the best one for several downstream applications.

Mice were immunized with a peptide comprising aminoacids 89-246 of the mouse protein. This portion of the Jmjd3 protein shows a high degree of homology (98%) between the human and mouse orthologs, and we chose it since it would most likely raise antibodies that would work both in human and in mouse. 8 hybridomas were generated and after testing them by WB against several human cells lines, we chose the two best performing (clones C6 and G2) for high-scale antibody production and purification. After further testing, we chose clone G2 as the best performing of the two clones.

Using this antibody, we were able to demonstrate by western blot (fig. 8A) and by immunohistochemistry (fig. 8B) that the Jmjd3 protein, despite a low level of remaining transcript, is virtually absent in the E13.5 XB814 developing cortex.

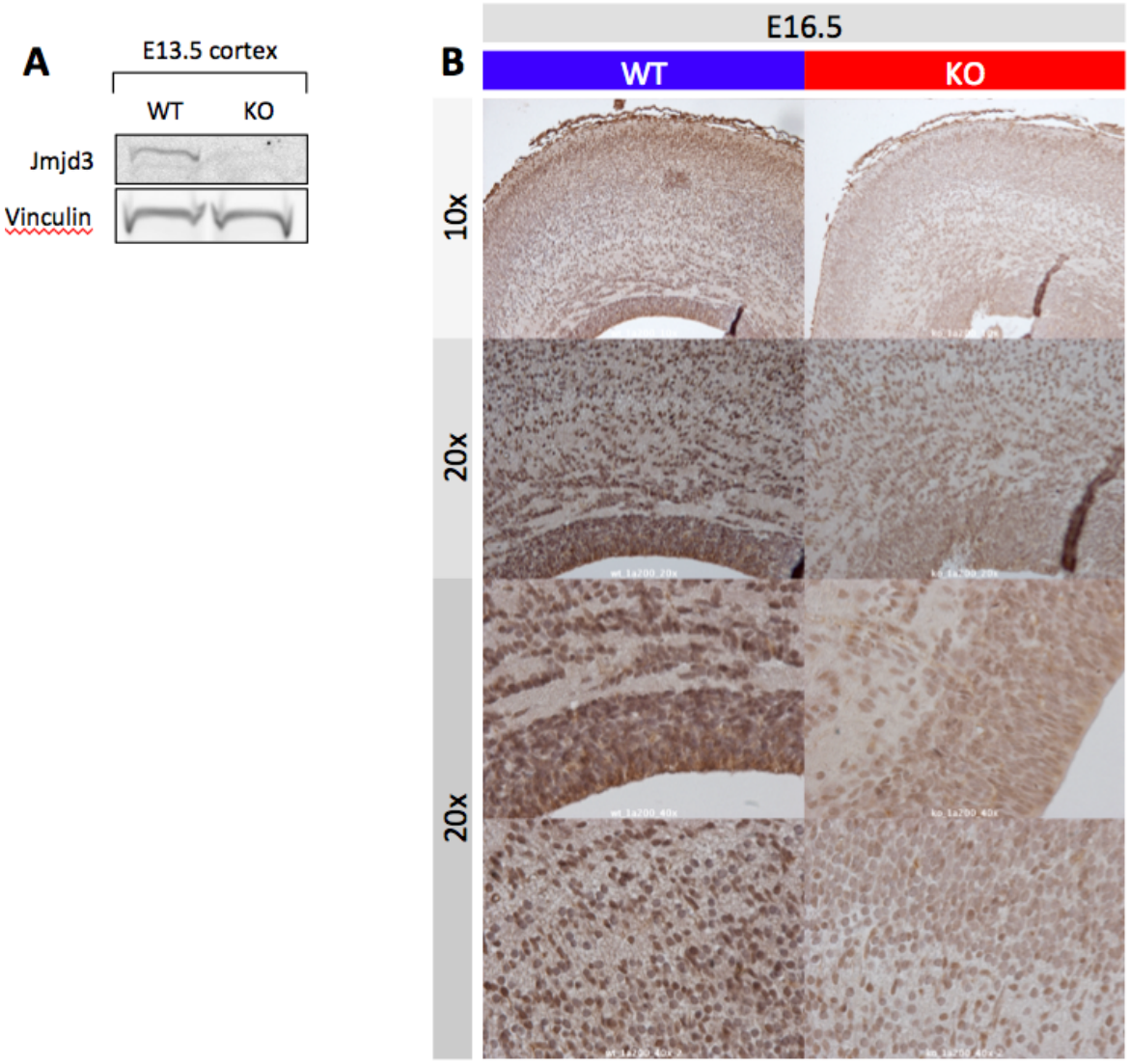

Figure 8. The XB814 mouse strain displays reduced level of Jmjd3 protein in the telencephalon. (A) Western blot on E13.5 telencephalic lysates using in-house developed anti-Jmjd3 antibody and anti-Vinculin antibody as loading control. (B) Immunohistochemistry on coronal sections of muouse necortex from WT or Jmjd3 KO embryos. The antibody used is the in-house developed anti-Jmjd3 antibody.

Taken together, these data allowed us to consider the XB814 mouse a bona-fide Jmjd3 KO in the developing cortex, supporting our initial idea of using it as a model to characterize the role of Jmjd3 in neocortical development.

3.2 Loss of Jmjd3 causes a late-onset expansion of NPCs in the developing mouse brain

To investigate the effect of Jmjd3 loss on neocortical development, we analyzed coronal sections of KO embryonic brains at different developmental stages using markers for neural stem cells and differentiated neurons. As the earliest time point, we chose day E13.5: at this time, deep-layer (Tbr1+) excitatory projection neurons have already colonized the cortical plate and constituted layer VI, and layer V Ctip2+ neurons are being produced by VZ NPCs (Kriegstein and Álvarez-Buylla, 2009). As the latest time point, we chose day E18.5, when neurogenesis is essentially over and the NPC population is reduced in numbers and has mainly switched to astrogenesis. By analyzing the developing brain at these different time points, and also at day E16.5, we were able to assess whether the loss of Jmjd3 impacts the generation of specific subtypes.

We started our analysis by assessing how the loss of Jmjd3 impacts the VZ stem cell compartment. To do so, we chose to quantify the number of Pax6+ cells at differential developmental stages: Pax6 is a transcription factor that is central to embryonic brain development and that specifically marks cortical neural stem cells, which give rise to excitatory glutamatergic neurons. Immunofluorescence analysis of coronal sections of brains at different stages of embryonic development shows an increase in the number of Pax6+ NPCs in the ventricular zone of Jmjd3 KO mice with respect to WT littermates (fig. 9A). Such a difference becomes apparent starting from E16.5 and is maintained up to the late phases of development (E18.5), whereas it is not detectable at early phases of neocortical development (E13.5). In order to further confirm the expansion of the NPC compartment following loss of Jmjd3, we also assessed the expression of Sox2, a transcription factor that is present in NPCs of both the dorsal (cortical) and ventral (ganglionic eminence) telencephalon. As shown in figure 9B, the

Sox2+ population is expanded in Jmjd3 KO mice starting at E16.5, mirroring and thus confirming the finding obtained with the Pax6 staining.

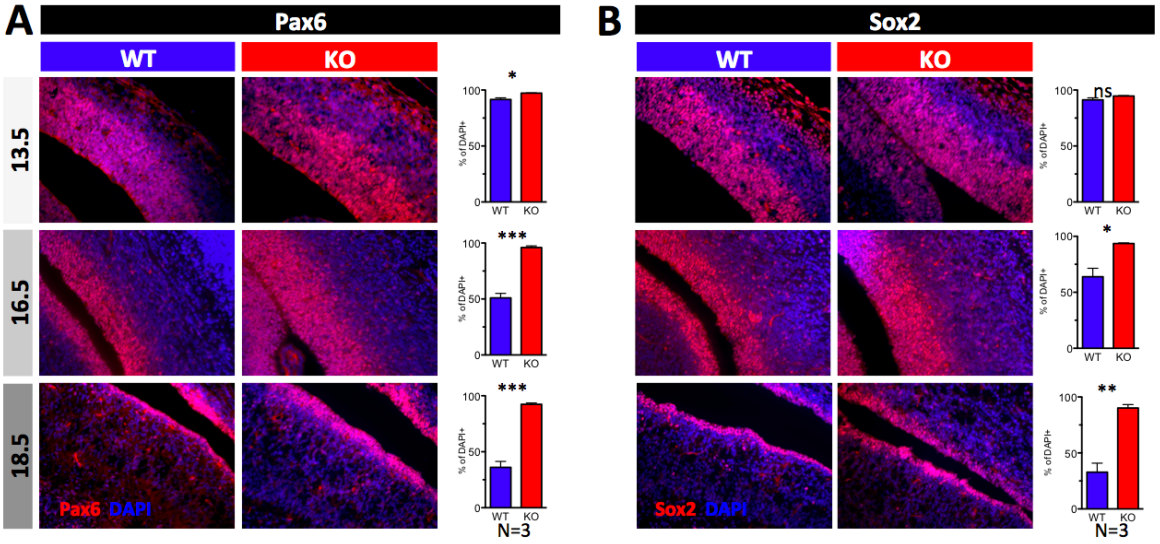

Figure 9. Immunofluorescence stainings for NPC markers in the VZ of WT and Jmjd3 KO mice. (A-B) Representative immunofluorescence stainings and graphs for Pax6, Sox2 in coronal sections of WT or KO brains at days E13.5, E16.5, E18.5. Graphs show percentage of positive cells over DAPI, in a window of constant width and height set based on the thickness of VZ in KO brains. Graphs show mean ±SD of three biological replicates. (ns = P>0.05, * = P≤0.05, ** = P≤0.01, *** = P≤0.001)

3.2.1 The expansion of the stem population in Jmjd3 KO brains is not restricted to cortical NPCs

In addition to the cortical phenotype, we decided to investigate the effect of Jmjd3 loss on other telencephalic regions. Based on a previous report that Jmjd3 activates Mash1 (Dai et al., 2010), a marker of ventral telencephalic stem cells that generate GABAergic neurons, we probed Mash1 expression in the ventricular portion of the lateral ganglionic eminence (LGE). In contrast with such report, but coherently with the NPC expansion that we see in the cortical VZ, immunostaining shows increased number of Mash1+ progenitor cells in the LGE of Jmjd3 KO at E16.5 (fig. 10A). Consistently, Hematoxylin and Eosin (HE) staining demonstrate that loss of Jmjd3 causes a thickening of the LGE (fig. 10B), suggesting that the function of Jmjd3 in embryonic NPCs is not restricted to the cortical, glutamatergic progenitors.

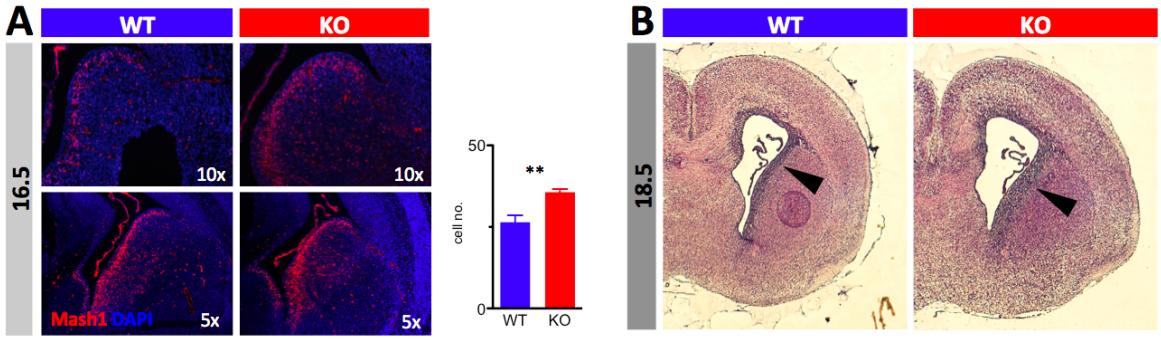

Figure 10. Jmjd3 KO mouse embryonic brains show increase in the proliferating zone of the lateral ganglionic eminence (LGE). (A) Representative immunofluorescence stainings and graphs for Mash1 in coronal sections of WT or KO brains at day E16.5. (B) Representative HE stainings of E18.5 WT or KO brains. Black arrowheads indicate the LGE. Graphs show total numbers of positive cells in a 100x50 um area. Graphs show mean ±SD of three biological replicates. (ns = P>0.05, * = P≤0.05, ** = P≤0.01, *** = P≤0.001)

3.3 Loss of Jmjd3 causes a late-onset reduction in the neuronal production in the developing mouse neocortex

In the developing brain, cortical NPCs produce the different subtypes of glutamatergic neurons following a timed sequence, and the newly generated neurons populate and form the cortical plate in an inside-out fashion: the early-born neurons contribute to the innermost layers and the late-born end up constituting the more superficial layers (Kriegstein and Álvarez-Buylla, 2009).

After determining that loss of Jmjd3 causes a generalized expansion of the NPC population in the developing neocortex, we proceeded to assess whether the cortical post-mitotic neuronal populations were also affected.

To do so, we performed multiple staining for markers of neuronal subtypes and we found that, in Jmjd3 KO brains, the early-born Tbr1+ (layer 6) and Ctip2+ (layer 5) neurons are reduced starting from E16.5 whereas the late-born Brn2+ (layer 2-4) neurons show no apparent defect at any time point of development (fig. 11A-B).

The fact that production of late-born neurons is not affected by Jmjd3 loss might seem in contrast with the reduced numbers of early-born neurons. We reasoned that this might be explained by the fact that Brn2+ neurons are produced at a time in which

the pool of NPCs is already expanded: the higher number of NPCs might thus compensate for their lower efficiency in neuronal production.

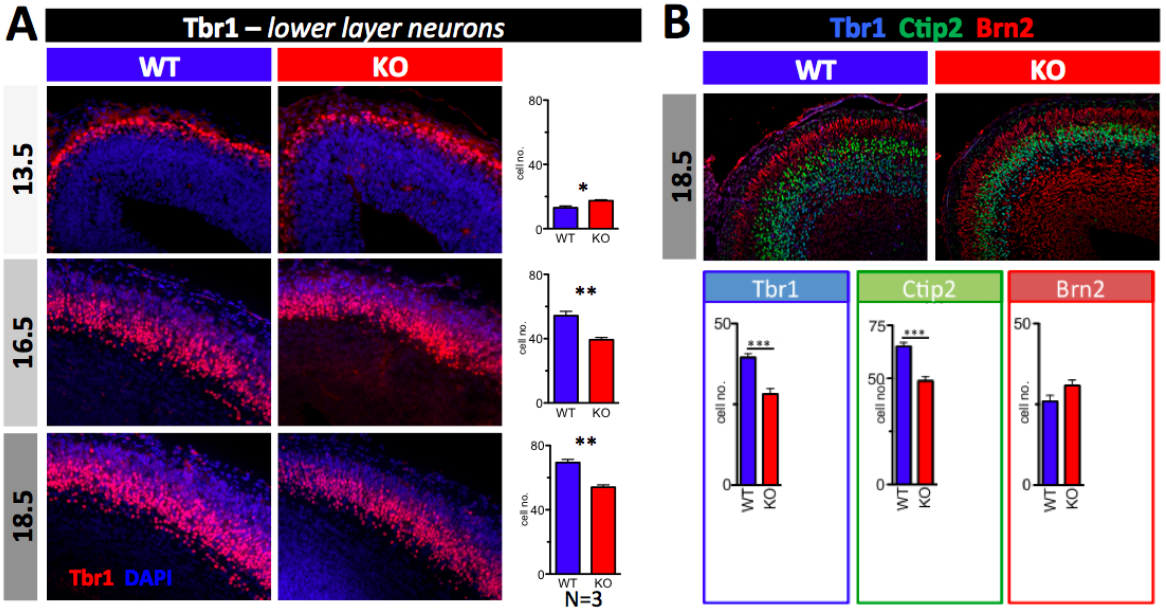

Figure 11. Loss of Jmjd3 causes a late-onset reduction in the neuronal production in the developing mouse neocortex. (A) Representative immunofluorescence stainings for Tbr1 in coronal sections of WT or KO brains at days E13.5, E16.5, E18.5. Graphs show percentage of positive cells over DAPI, in a window of constant width and height set based on the thickness of VZ in KO brains. Graphs show mean ±SD of three biological replicates. (B) Representative immunofluorescence stainings and graph for Tbr1, Ctip2, Brn2 in coronal sections of WT or KO brains at day E18.5. Graphs show total numbers of positive cells in a window spanning the entire cortex and 50 um wide. Graphs show mean ±SD of three biological replicates. (ns = P>0.05, * = P≤0.05, ** = P≤0.01, *** = P≤0.001)

3.3.1 The Tbr2+ population of cortical intermediate progenitors is not affected by the loss of Jmjd3 in the developing neocortex

In the developing neocortex, neurons can derive from Pax6+ NPCs either directly, in a process known as direct neurogenesis, or indirectly, through an intermediate cell state known that is characterized by the presence of the Tbr2 T-box transcription factor: such cells are known as intermediate progenitors or transit-amplifying cells. In this second case, Pax6+ NPCs first differentiate into Tbr2+ cells, which can in turn self-replicate by symmetric division or generate neurons via both asymmetric and symmetric divisions. Given the observed imbalance between the stem and the differentiated compartment of the Jmjd3 KO embryonic brain, we reasoned that also the intermediate compartment could be affected by the loss of Jmjd3. However,

immunofluorescence analysis revealed that the number of Tbr2+ intermediate progenitors is comparable in WT and KO brains at all the observed stages of development (E13.5, E16.5, E18.5, fig. 12A): this result could imply that the loss of Jmjd3 preferentially impairs the direct route of neurogenesis.

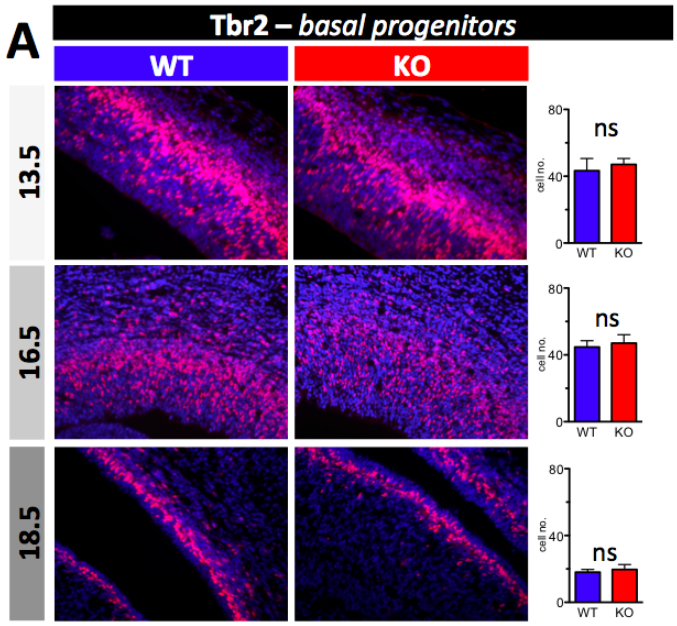

Figure 12. The Tbr2+ population of intermediate progenitors is not affected by the loss of Jmjd3. Representative immunofluorescence stainings for Tbr2 in coronal sections of WT or KO brains at days E13.5, E16.5, E18.5. Graphs show total numbers of positive cells in a window spanning the entire cortex and 50 um wide. Graphs show .mean ±SD of three biological replicates. (ns = P>0.05, * = P≤0.05, ** = P≤0.01, *** = P≤0.001)

To summarize these findings, we showed that lack of Jmjd3 in the developing brain causes an expansion of the cortical stem population at the expense of the production of mature neurons, and that this defects start to be apparent at day E16.5. We hypothesize that the phenotype starts to be apparent only late in development because the increase in the NPC population needs to accumulate over time before becoming detectable and statistically relevant. This hypothesis could also provide an alternative explanation to the observation that the Tbr2+ intermediate precursors are not reduced in Jmjd3 KO brains. Indeed, since the Tbr2-positive is only a transient rather than a terminal compartment and thus does no allow to accumulate abundance difference over time, and since we assume that, when analyzed in a short time frame,

the neuronal output of Jmjd3 KO NPCs is not significantly lower than their WT counterpart, the very nature of the Tbr2+ compartment would not allow scoring a statistically significant difference.

3.4 The demethylase activity of Jmjd3 is necessary for proper development of the mouse neocortex

Recent reports, which show that Jmjd3 is able to regulate expression of target genes in a demethylation-independent manner (Chen et al., 2012; De Santa et al., 2009; Miller et al., 2010), prompted us to investigate the contribution of the catalytic activity of Jmjd3 to the phenotype. Moreover, since our lab previously demonstrated that the enzymatic activity of Jmjd3 is required to rescue the correct formation of the pre-Bötzinger complex in the brainstem of XB814 mice, we wished to clarify whether the cortical phenotype of enlarged VZ and reduced cortical plate was dependent on the enzymatic activity of Jmjd3 (Burgold et al., 2012).

To do so, we took advantage of our unique cohort of mouse strains and crossed them to XB814 mice to re-express WT or mutant Jmjd3 in KO embryos (fig. 13A-B).

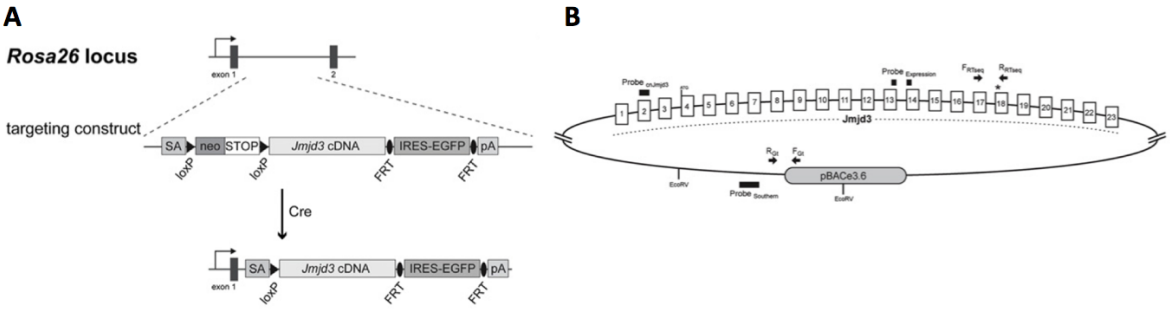

Figure 13. Mouse strains used for rescue experiments. The R26.Jmjd3 and BACmut strains are described in the methods section (§2.6) and have been previously published in Burgold et al., 2012.

When crossed with a mouse strain expressing a WT Jmjd3 cDNA from the Rosa26 locus, Jmjd3 KO embryos displayed numbers of Pax6+ NPCs and Tbr1+, Ctip2+ post-mitotic neurons comparable to their WT littermates. We then crossed Jmjd3 KO mice with a strain harboring a bacterial artificial chromosome (BAC) containing the whole

Jmjd3 genomic region, in which Jmjd3 has been modified with a point mutation that renders it catalytically inactive (His1388Ala) (Burgold et al., 2012). As shown in figure 14A-C, mutant Jmjd3 fails to rescue the phenotype as the numbers of both NPCs and differentiated neurons remain similar to those of Jmjd3 KO embryos. Taken together, these data demonstrate that the demethylase activity of Jmjd3 is necessary for the normal embryonic development of the mouse neocortex.

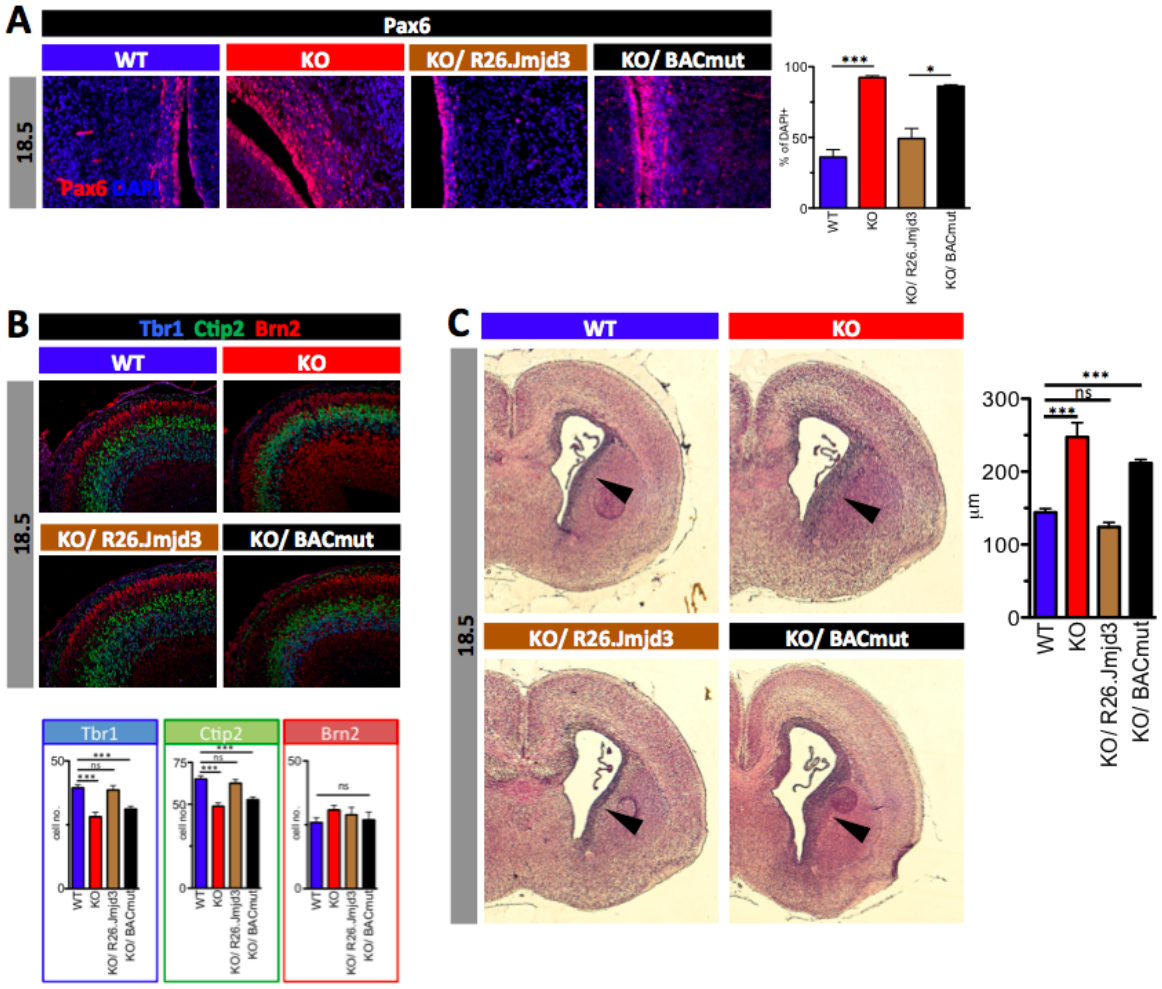

Figure 14. The demethylase activity of Jmjd3 is necessary for the correct development of the mouse neocortex. R26.Jmjd3: mouse strain harboring an allele overexpressing the WT Jmjd3 mouse cDNA from the Rosa26 locus. BACmut: mouse strain harboring a bacterial artificial chromosome (BAC) containing the whole Jmjd3 genomic region, in which Jmjd3 has been modified with a point mutation that renders it catalytically inactive (His1388Ala). (A) Representative immunofluorescence stainings and graph for Pax6 in coronal sections of WT or KO brains at day E18.5. Graphs show percentage of positive cells over DAPI, in a window of constant width (100um) and height set based on the thickness of VZ in KO brains. Graphs show mean ±SD of three biological replicates. (B) Representative immunofluorescence stainings and graph for Tbr1, Ctip2, Brn2 in coronal sections of WT or KO brains at day E18.5. Graphs show total numbers of positive cells in a window spanning the entire cortex and 50 um wide. Graphs show mean ±SD of three biological replicates. (C) Representative HE stainings of E18.5 WT or KO brains. Black arrowheads indicate the LGE. (A-C) ns = P>0.05, * = P≤0.05, ** = P≤0.01, *** = P≤0.001.

3.5 In vivo characterization of the Jmjd3 KO NPC population

Since the Pax6+ NPCs are the founding population of the mouse neocortex, it is safe to assume that alterations in their behavior might lead to the defects that we observed in the post-mitotic neurons of Jmjd3 KO brains, which are generated by Pax6+ NPCs via the direct or indirect route of neurogenesis. Based on this, in order to better understand the phenotype observed in Jmjd3 KO brains, we decided to characterize in depth the Pax6+ VZ population.

3.5.1 Jmjd3 KO NPCs proliferate actively and have a higher rate of cell cycle re-entry after completing mitosis

We reasoned that the expansion of the VZ in Jmjd3 KO brains might be related to alterations in the proliferation rate of NPCs, and we thus sought to investigate *in vivo* the cell cycle behavior of the expanded NPC population.

To assess the proliferation rate of VZ NPCs, we pulse-labeled embryos with the thymidine analogue EdU and detected its distribution 24 hours later together with the cell proliferation marker Ki67. The ratio of cell cycle exit can be calculated as the number of EdU+/Ki67- postmitotic cells among the total EdU+ cells. As shown in figure 15A-B, the exiting fraction is lower in Jmjd3 KO embryonic brains, implying that lack of Jmjd3 negatively affects the ability of NPCs to exit the cell cycle after mitosis.

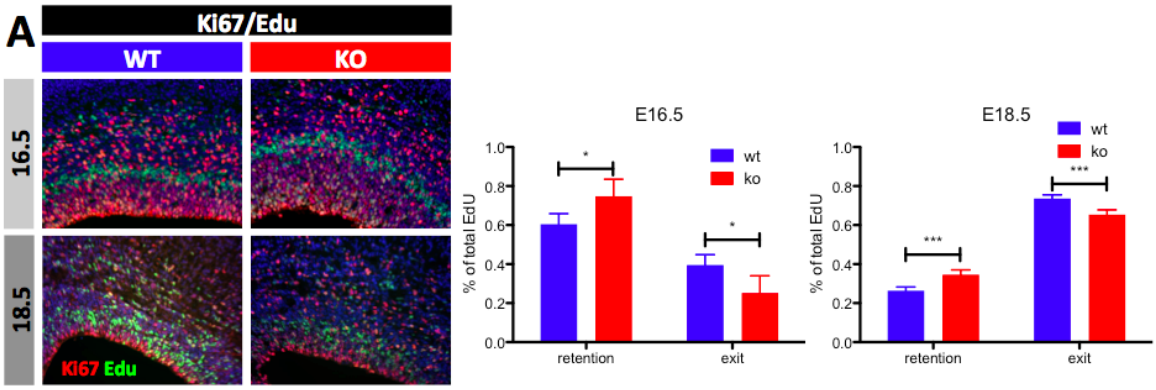

Figure 15. Loss of Jmjd3 enhances cell cycle reentry in VZ NPCs. (A) Representative immunofluorescence stainings for EdU and Ki67 in coronal sections of WT or KO brains at days E16.5 and E18.5. Graphs show ratios of EdU+Ki67+/ total EdU+ (retention) or Edu+Ki67-/ total EdU+ (exit) counted in windows of constant width (100um) and height set based on the thickness of VZ in KO brains. Graphs show mean ±SD of five biological replicates.

3.5.2 Jmjd3 KO NPCs do not display aberrantly-localized mitoses

In the developing neocortex, the nuclei of the NPCs in the VZ undergo a characteristic periodic movement between the ventricular surface and the VZ-SVZ boundary, in phase with cell cycle progression, known as interkinetic nuclear migration (INM) (Kriegstein and Álvarez-Buylla, 2009). Specifically, DNA replication occurs towards the VZ-SVZ boundary, whereas phospho-histone H3 (pH3) –positive mitotic figures are restricted to the ventricular surface in physiologic conditions.

A mechanism of overcrowd-induced mitosis delamination has been proposed almost 50 years ago (Smart, 1965) and recently demonstrated in drosophila and mouse (Marinari et al., 2012; Okamoto et al., 2013). According to this mechanism, when cell abundance at the ventricular surface rises to an intolerable level, some NPCs may leave the ventricular, apical surface to undergo mitosis at a more basal position.

We reasoned that the cellular overabundance in the VZ of brains lacking Jmjd3 might thus in turn cause defects in the localization of mitoses and in the neural differentiation process. We determined the ratio of apical versus non-apical mitoses by pH3 staining, and found that this ratio is similar in WT and Jmjd3 KO mice, at both

early and late stages of brain development, suggesting that the degree of VZ expansion in KO mice is not high enough to influence INM (fig. 16A).

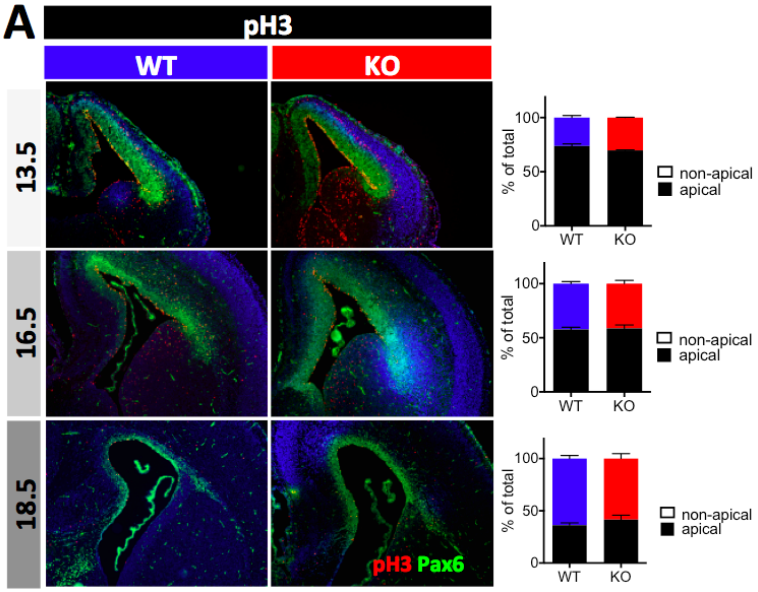

Figure 16. Loss of Jmjd3 does not affect the localization of NPC mitoses. (A) Representative immunofluorescence stainings for Pax6 and pH3 in coronal sections of WT or KO brains at days E13.5, E16.5 and E18.5. Graphs show percentages of apical and non-apical mitoses over the total number of pH3+ cells, counted in a whole section of a single hemisphere.

3.5.3 The timing of neuronal subtype production is not altered by loss of Jmjd3

During the progression of neocortical development, NPCs sequentially generate different neuronal subtypes, which migrate radially and constitute the different layers of the mature cortex, with the late-born neurons contributing to the outermost layer (Greig et al., 2013). It has been previously shown that KO of the H3K27 demetyhlase EzH2 affects the timing of neuronal production due to its function in repressing target genes that regulate neurogenesis (Hirabayashi et al., 2009; Pereira et al., 2010), and as outlined in the introduction, fine-tuning of H3K27 methylation is required for the proper sequence of neuron and astrocyte production (Testa, 2011). We reasoned that the alterations that we observed in the numbers of cortical neurons in Jmjd3 KO mice might be as well linked to changes in the timing of neuronal subtype production.

To assess whether the timing of neuronal production is altered, we performed a neuronal birthdating experiment by injecting E13.5 pregnant mice with EdU, and collecting embryos five days later (E18.5) to check the distribution of EdU-labeled post-mitotic neurons (fig. 17A). EdU is incorporated in actively-dividing VZ stem cells at the moment of administration, and is passed to the daughter cells upon mitosis. By studying the co-localization of EdU and layer-specific nuclear markers in the cortical plate it is possible to understand which neuronal subtype was being generated at the time of EdU administration.

Co-staining of EdU with Tbr1 and Ctip2 showed that both WT and Jmjd3 KO NPCs produce mainly Ctip2+ neurons at day E13.5, pointing out that the loss of Jmjd3 does not impact on the timing of neuronal production (fig 17B-C).

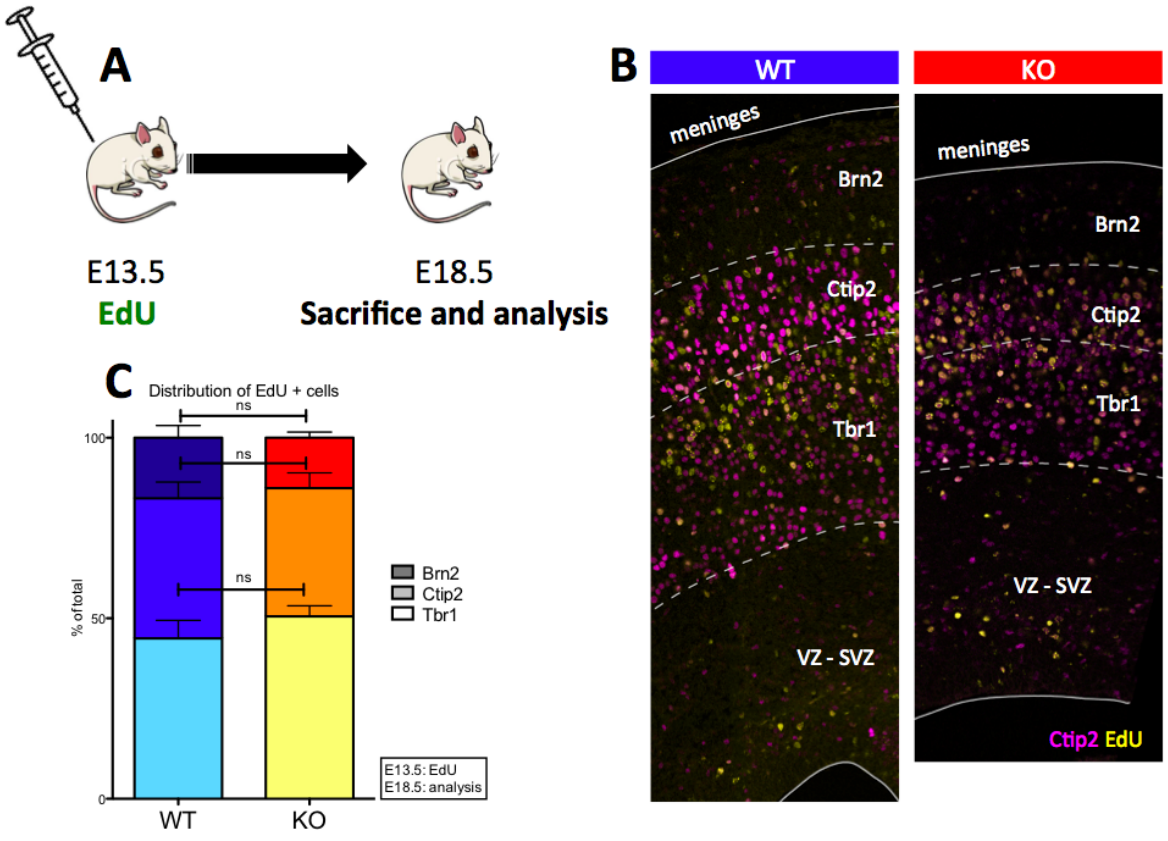

Figure 17. Loss of Jmjd3 does not affect the timing of neuronal production. (A) Pregnant mice were injected with EdU (50mg/kg of total weight) in PBS at day E13.5. Five days later (E18.5), mice were sacrificed and embryos collected. (B) Representative immunofluorescence stainings for Ctip2 and EdU in coronal sections of WT or KO brains at day E18.5. Tbr1 staining was also performed to define cell layers but is not shown. (C) Graph showing distribution of EdU+ cells in three neuronal layers defined by Tbr1 and Ctip2 staining. Mean ±SD of 5 WT and 3 KO biological replicates is shown. ns = P>0.05, * = P≤0.05, ** = P≤0.01, *** = P≤0.001.

Taken together, these data suggest that, in absence of Jmjd3, the modality of cell division of VZ NPCs is skewed towards self-renewal rather than differentiation. Interestingly, contrary to what has been shown for the Ezh2 methyl-transferase (Hirabayashi et al., 2009; Pereira et al., 2010), KO of the Jmjd3 demethylase does not alter the timing of neuronal production. This suggests that the functions of Jmjd3 in brain development go beyond counteracting the action of Ezh2 on H3K27, and hints at a possibly different mechanism of action of these two proteins despite their opposing role in regulating the dynamics of H3K27 methylation.

3.6 In vitro characterization of Jmjd3 KO brain-derived NPCs

To investigate the consequences of Jmjd3 ablation on NPCs at single-cell resolution, we resorted to *in vitro* cultures of primary embryonic NPCs. To isolate NPCs, we dissected, disaggregated and put in culture E13.5 cortices, and then selectively expanded nestin-positive NPCs by daily addition of the mitogen bFGF. It has been previously demonstrated that cells cultured in these conditions can be expanded for several passages while keeping a self-renewing behavior, allowing to study their cell cycle dynamics (Ravin et al., 2008). Also, when pushed to differentiate by change of culture conditions (see materials and methods §2.1.2 and fig. 18C for details), they are able to generate neurons and glia through complex lineages that can be tracked via high-resolution time-lapse video-microscopy. This analysis allows to track a high number of neural stem cells for days in culture and to gain information at the single cell level on different aspects of their behavior, such as their differentiation potential and cell cycle time.

3.6.1 In vitro-cultured Jmjd3 KO VZ NPCs can differentiate in the three neural lineages

In order to parallel the *in vivo* observation of reduced neuronal output, we first wanted to assess the differentiation potential of Jmjd3 KO NPCs. To do so, we adopted a previously described differentiation protocol (Ravin et al., 2008) that allows cortical NPCs to generate the three neural lineages: Tuj1+ neurons, O4+ oligodendrocytes and GFAP+ astrocytes. As assessed by qRT-PCR (Fig. 18D), Jmjd3 expression is upregulated during neural differentiation and peaks after 2 days of bFGF withdrawal, whereas the expression level remains stably low in KO samples. However, at the end of the differentiation process, both WT and Jmjd3 KO samples displayed similar proportions of the three cell types (Fig. 18A-B). This suggests that loss of Jmjd3 does not impact the intrinsic capability of NPCs to start a differentiation program: these data are in agreement with the observation that, albeit at lower efficiency, NPCs *in vivo* are indeed able to differentiate into neurons. However, it could be expected that Jmjd3 KO NPCs would display also *in vitro* a reduced capability to generate neurons. This apparent discrepancy might be caused by the strict culture conditions, which entail the presence of a high concentration of bFGF until its total withdrawal and substitution with differentiating factors. These culture conditions might be constraining enough on the NPC population to shroud subtle mechanisms that on the other hand allow for a fine-tuning of the differentiation process *in vivo*.

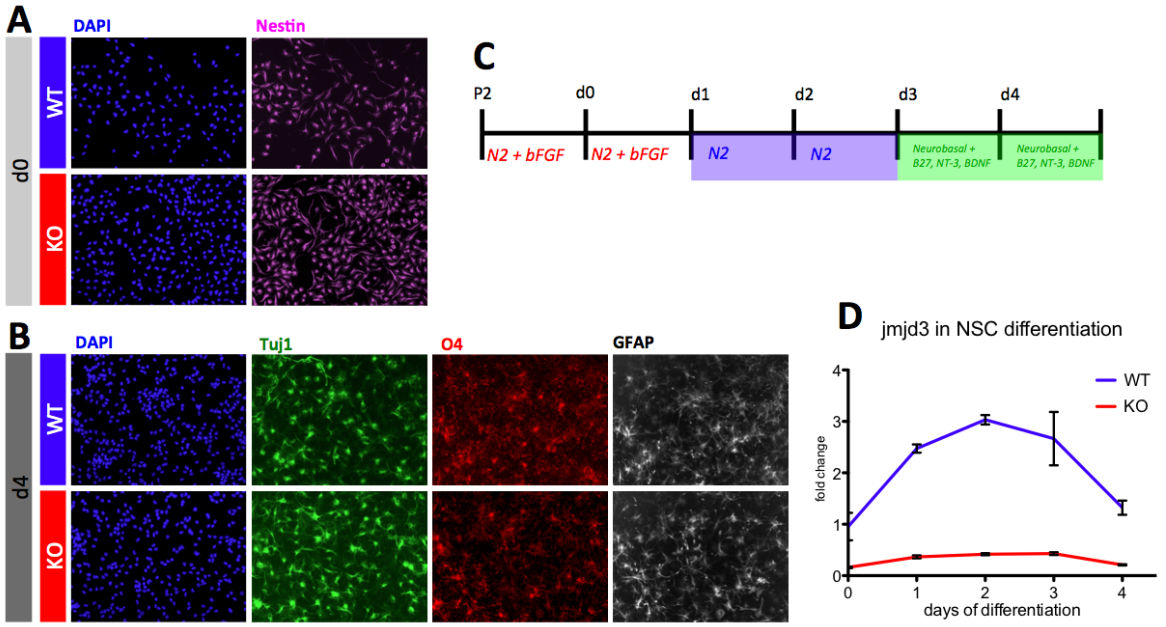

Figure 18. In vitro-cultured Jmjd3 KO VZ fail to upregulate Jmjd3 but can differentiate in the three neural lineages. (A-B) Representative immunofluorescence stainings for Nestin (NPC), Tuj1 (neurons), O4 (oligodendrocytes), GFAP (astrocytes), DAPI, of undifferentiated (d0) and differentiated (d4) WT and KO NPCs. (C) Differentiation protocol of cortical NPCs, which entails NPC expansion in medium with bFGF, 2 days of bFGF withdrawal, 2 days of differentiation in Neurobasal medium with B27 supplement, neurotrophin-3 and BDNF. (D) The graph shows qRT-PCR data of Jmjd3 expression in differentiating NPCs, days of differentiation correspond to figure 4 C. Data are plotted as mean ±SD of three independent biological replicates.

3.6.2 Jmjd3 KO NPCs show a lower proliferation rate upon serial passaging

We then sought to investigate the proliferative capacity of Jmjd3 KO NPCs. To do so, we plated 1x10^6 WT or KO NPCs at passage 1 after culture establishment, kept them in proliferative conditions by daily bFGF addition, and serially replated 1x10^6 cells after three days of culture, until passage 5 (fig. 19A). The resulting growth curves, performed in biological triplicates, revealed that Jmjd3 KO cells proliferate less than their WT counterpart (fig 19B). The lower cell numbers observed in KO NPCs at the end of the growth curve might be due to higher cell death, to the presence of cells that do not divide, or to a general lengthening of the cell cycle.

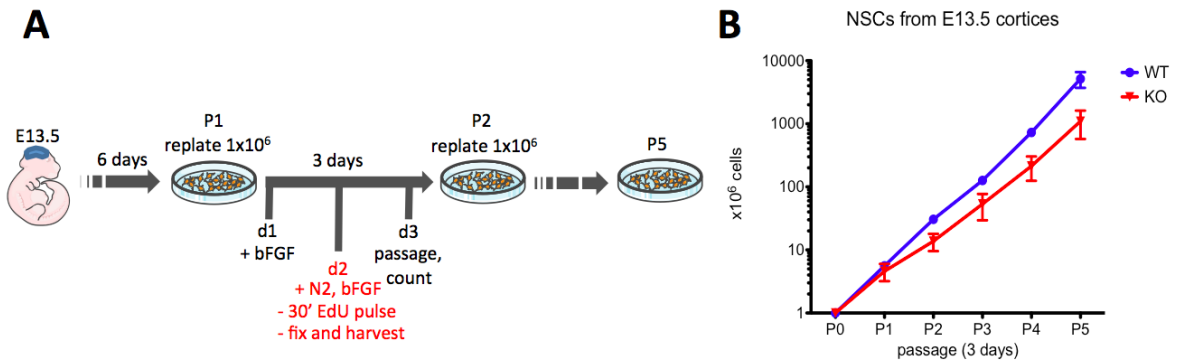

Figure 19. Loss of Jmjd3 causes reduced proliferation of *in vitro*-cultured NPCs derived from the embryonic brain. (A) Schematics of the protocol used to expand NPCs in order to obtain growth curves and cell cycle data. 1x10^6 WT or KO NPCs were plated at passage 1 after culture establishment, kept in proliferative conditions by daily bFGF addition, and 1x10^6 cells were serially replated after three days of culture, until passage 5. NPCs were exposed to 30' of EdU pulse, followed by EdU detection, PI staining and FACS analysis. Since *in vitro* cultured NPCs stop proliferating when they reach high confluence levels, the cells were pulsed with EdU 48 hours after replating, when they are still in exponential growth phase. (B) Log scale graph showing cumulative growth curves of WT and KO NPCs, kept in proliferative conditions by the method in Fig. 4 E.

3.6.3 In vitro-cultured Jmjd3 KO VZ NPCs have a longer cell cycle

To precisely pinpoint the cause of the lower proliferation rate observed upon serial passaging, we subjected cultures in proliferative conditions of WT and KO NPCs to time-lapse video-microscopy: such high-resolution analysis allowed us to track the progeny of single NPCs and assess their proliferative behavior. By measuring the interval between subsequent mitoses in a cell progeny, we observed that in the absence of Jmjd3, NPCs have a much longer cell cycle than their WT counterpart (Fig. 19A-C). This feature is even more evident when cell cycle times are stratified by cell generation, with cells belonging to the first generation (that is, cells deriving from the first mitosis to be scored) having the highest difference (KO 18.3±5.3 hrs, WT 13.6±2.2 hrs).

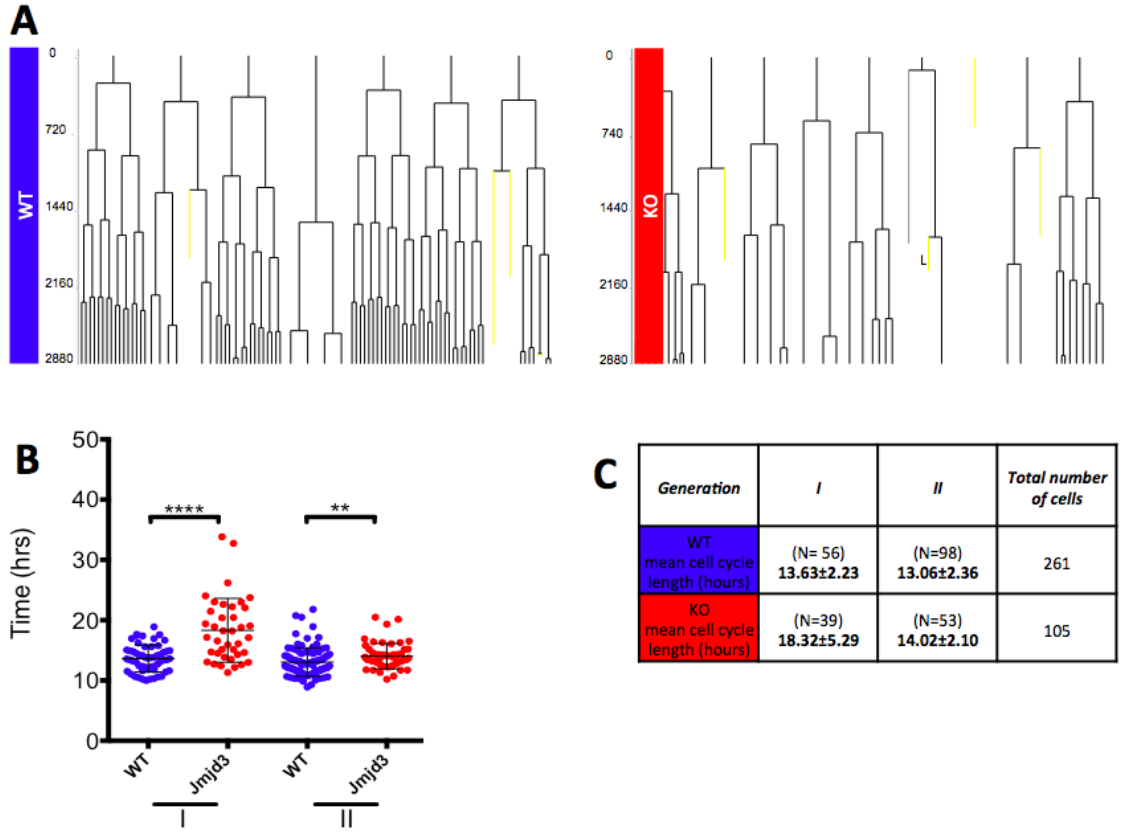

C

Generation	*I*	*II*	*Total number of cells*
WT mean cell cycle length (hours)	(N= 56) **13.63±2.23**	(N=98) **13.06±2.36**	261
KO mean cell cycle length (hours)	(N=39) **18.32±5.29**	(N=53) **14.02±2.10**	105

Figure 20. Loss of Jmjd3 causes a lengthening of the total cell cycle time in *in vitro*-cultured NPCs (A) Representative lineage dendrograms of WT and KO NPCs, imaged by time-lapse videomicroscopy while kept in differentiating conditions. The interval between two nodes (mitoses) is used to determine the cell cycle time. Time in minutes is shown on the left Y axis. (B) Aggregated cell cycle times of WT and KO NPCs, stratified by cell generation. The cell cycle length was measured as difference in time (ΔT) of two subsequent mitoses occurring in the time frame of 48 hours. (C) Mean ±SD of the cell cycle times for WT and KO samples is shown, aggregated by cell generation. ns = P>0.05, * = P≤0.05, ** = P≤0.01, *** = P≤0.001.

3.6.4 Loss of Jmjd3 causes a general lengthening of the cell cycle in in vitro-cultured, brain-derived NPCs

Some recent reports (Arai et al., 2011; Lange et al., 2009) demonstrated that the length of specific cell phases is associated with the choice between symmetric and asymmetric cell division in both apical and basal cortical progenitors. In particular, in apical progenitors (Pax6+ NPCs), cells that will perform a symmetric self-renewing division have a longer S phase (Arai et al., 2011). Based on these evidences, and since we observed that Jmjd3 KO NPCs have both a preference for self-renewal and a

overall longer cell cycle, we wondered whether lack of Jmjd3 would selectively impact the length of a specific phase of the cell cycle.

To do so, we exposed NPCs to 30' of EdU pulse, followed by EdU detection, PI staining and FACS analysis. Since *in vitro* cultured NPCs stop proliferating when they reach high confluence, the cells were pulsed with EdU 48 hours after replating, when they are still in exponential growth phase (fig. 20A). As indicated in figure 21A-B, the relative percentages of cells in G1, S and G2 phases in Jmjd3 KO NPCs were comparable to WT NPCs, suggesting that the overall longer cell cycle uncovered by the time-lapse video-microscopy analysis is due to a general lengthening of all the cell cycle phases, thus including S-phase. Thus, despite the lack of a proportional lengthening of S-phase at the expense of the other phases, these results show that Jmjd3 KO NPCs do anyway have a longer S-phase than their WT counterpart, which in turn can explain their bias towards self-renewing divisions.

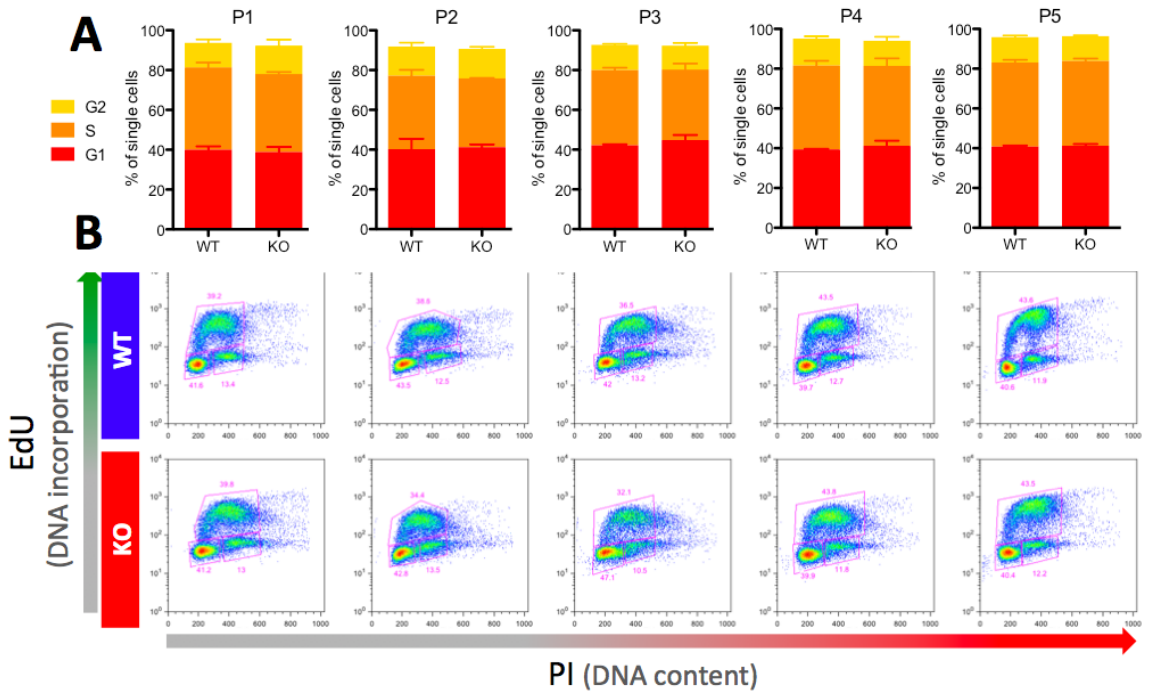

Figure 21. Loss of Jmjd3 causes a general lengthening of the all the cell cycle phases in *in vitro*-cultured NPCs. (A-B) Representative FACS plot and graphs showing percentages of WT and KO NPCs in G0/G1, S and G2/M phases, as determined by PI/ EdU detection. The graphs show mean ±SD of three independent biological replicates.

However, a careful evaluation of the cell cycle parameters *in vivo* is necessary before the *in vitro* observation can be linked to the selective expansion of NPCs that we observe in the VZ of Jmjd3 KO embryonic brains. To address this point, we resorted to *in vivo* cell cycle parameters analysis (§3.7), as described in methods (§2.5.2).

3.6.5 Cyclins and crucial cell cycle regulators are not affected at the protein level in in vitro-*cultured NPCs by the loss of Jmjd3*

As shown above, our FACS analysis on *in vitro*-cultured NPCs did not reveal neither a lengthening of a specific cell cycle phase nor a block at any cell cycle checkpoint. However, subtle defects in cell cycle progressions might escape FACS analysis: we thus decided to assess the abundance of critical cell cycle regulators at the protein level in Jmjd3 KO *in vitro*-cultured NPCs.

Cyclins regulate the progression of the eukaryotic cell cycle by interacting with cyclin-dependent kinases (CdKs) and alterations in their levels are associated to defects in the unwinding of the cell cycle. We thus probed the expression level of cyclins associated to different phases of the cell cycle: cyclin D1, linked to the G1/S transition, cyclin A, which is present during S-phase progression and G2/M-phase, and cyclin B1, which is necessary for the completion of mitosis. As shown in figure 22A, and consistently with the FACS results, western blot reveals that the protein level of these cyclins is not altered in Jmjd3 KO NPCs, strengthening our previous observation that the increase in cell cycle length is not specific of a given phase but rather a distributed phenomenon.

p16-Ink4a and p19-Arf are two proteins that are encoded by the Cdkn2a locus and play a crucial role in cell cycle regulation by inhibiting the G1/S phase transition. It has been reported (Agger et al., 2009) that Jmjd3 can activate the Cdkn2a locus, and that loss of Jmjd3 causes an acceleration of the cell cycle progression in MEFs via

reduced expression of p16 and p19 and faster G1/S transition. This effect of Jmjd3 loss in MEFs is diametrically opposed to the one we observe in our model of *in vitro*-cultured brain-derived NPCs. This apparent discrepancy is most likely due to the fact that p16 and p19 are not present in the developing telencephalon VZ, as reported in (Bruggeman et al., 2007; Molofsky et al., 2005; Nishino et al., 2008), and thus their expression cannot be further downregulated by the lack of Jmjd3. We anyway wished to assess the expression level of p16-Ink4a and p19-Arf in the E13.5 brain-derived NPCs: as shown in figure 22B, western blot analysis reveals that both proteins are not expressed in WT as well as in Jmjd3 KO NPC protein extract, supporting our idea of a Cdkn2a-independent function of Jmjd3 in regulating cell cycle progression.

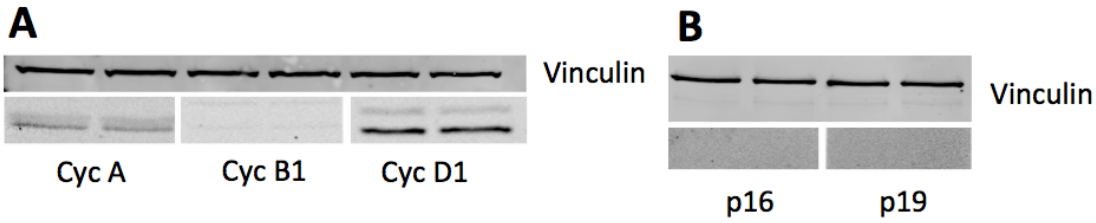

Figure 22. Western blot analysis shows that the level of cyclins and crucial cell cycle regulators are not altered in Jmjd3 KO brains. (A) Western blot for Cyclin A, Cyclin B1, Cyclin D1 on protein lysates prepared from E13.5 WT or Jmjd3 KO brains using RIPA buffer. Vinculin is used as a loading control. (A) Western blot for p16-Ink4a and p19-Arf on protein lysates prepared from E13.5 WT or Jmjd3 KO brains using RIPA buffer. Vinculin is used as a loading control.

3.6.6 Synchronization and release of WT and KO NPCs shows similar S-phase progression

In order to strengthen our understanding of the kinetics of S-phase in Jmjd3 KO NPCs, we chose to analyze the cell cycle progression in synchronized NPC populations after double thymidine block and release. Briefly, by providing high concentrations of thymidine, cultured cells can be blocked at the G1/S boundary and then released by the addition of normal growth medium: two such blocks performed in sequence allow to obtain a higher level of synchronization. However, the efficacy of this method is very dependent on the cell type being analyzed: it is indeed possible that some

particular cell types might be less responsive to the block and not get synchronized, other might exhibit cell death due to thymidine toxicity, and other could fail to be released upon thymidine withdrawal.

PI staining and FACS analysis of WT and KO NPCs after double thymidine block revealed that 95% of the cells could be synchronized, but 50% of the NPCs of both genotypes failed to be released upon thymidine withdrawal, as it is shown by the G1 peak present in all plots in figure 23A and highlighted in figure 23B. The other 50% of cells, which are indistinguishable by physical parameters from the stalled subpopulation (fig. 23C), proceeded through cell cycle with similar kinetics in both conditions, fully completing S-phase by 5 hours after the release.

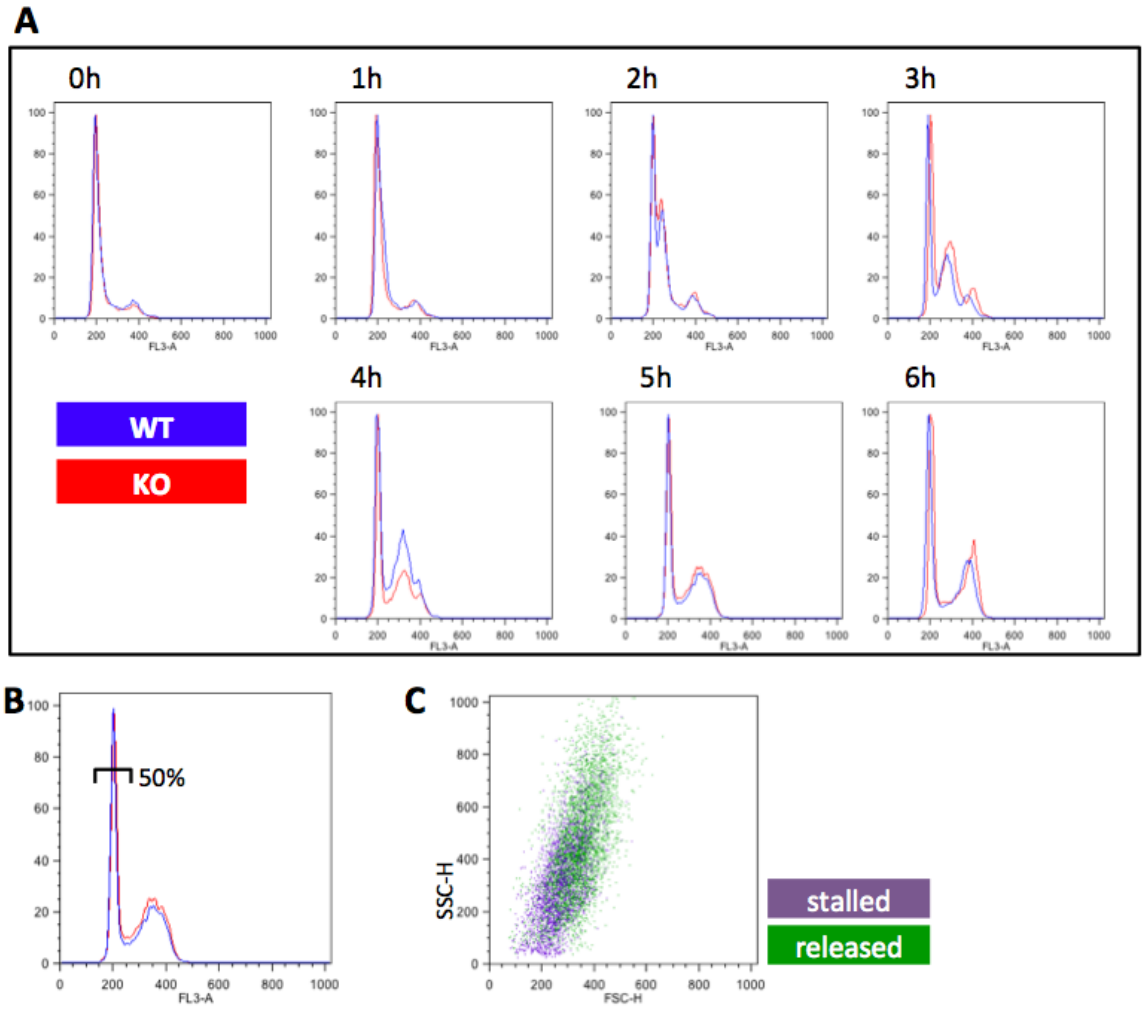

Figure 23. WT and Jmjd3 KO brain-derived NPCs show similar cell cycle progression upon release after double thymidine block. (A) FACS plots showing PI (FL3-A) staining of WT (blue) or Jmjd3 KO (red) *in vitro*-cultured NPCs. 0h indicates a sample analyzed without thymidine removal, 1-6h show progressive entry in S phase upon release. (B) Highlighted graph (5h). (C) FACS plot for physical parameters (FSC-H, SSC-H) of the 5h time point.

Taken together, these results show that the cell cycle progression of brain-derived NPCs is hampered by the thymidine treatment. For this reason, and since this lack of difference in S-phase length between WT and KO NPCs is also in stark contrast with the results shown previously on *in vitro*-cultured NPCs and also with the *in vivo* evidences that are shown in the following paragraphs, we consider this particular experimental system as not suitable to investigate differences in the cell cycle kinetics of this particular cell type.

3.7 VZ NPCs in the Jmjd3 KO developing brain display a generalized lengthening of the cell cycle, dependent on the loss of the catalytic activity of Jmjd3

In order to complement the observation that *in vitro*-cultured NPCs show a longer cell cycle upon Jmjd3 loss, we decided to assess the cell cycle parameters of VZ NPCs in the developing embryonic brain in vivo. Historically, cumulative BrdU labeling has been the method of choice to perform such analysis. This method entails sequential intraperitoneal administration of BrdU to the pregnant mouse at fixed intervals of time, tipically 1.5 hrs, and analysis of the BrdU incorporation levels in the VZ cells of the embryonic brains: a BrdU saturation curve can then be plotted that yields the desired cell cycle parameters (Nowakowski et al., 1989). However, this method entails the use of a high number of animals, since for each time point (tipically 6-8 per experiment) several mice need to be sacrificed in order to obtain enough embryos to perform a meaningful statistical analysis.

Recently, more advanced methods that make use of different thymidine analogues while allowing a dramatic reduction of the number of animals needed have been developed (Martynoga et al., 2005). We took advantage of one such method that is based on the sequential administration of BrdU and IdU to the same pregnant mouse. As described in detail in methods (§2.5.2), the differential incorporation of the two

analogs can be used to mathematically reconstruct the S phase length and, based on the warranted assumption that the 100% of the VZ population is actively proliferating, the total cell cycle length.

We sequentially administered E13.5 pregnant mice with IdU and BrdU, and by analyzing their incorporation in Jmjd3 WT or KO embryonic brains, we found that the length of both S phase and total cell cycle is proportionately increased in the absence of Jmjd3 in VZ NPCs. Importantly, we were able to rescue the phenotype by crossing XB814 mice with a strain expressing a wild type Jmjd3 cDNA from the Rosa26 locus, paralleling the observation that the enzymatic activity of Jmjd3 is necessary to rescue the expansion of Pax6+ cells in the VZ (fig 24A-B).

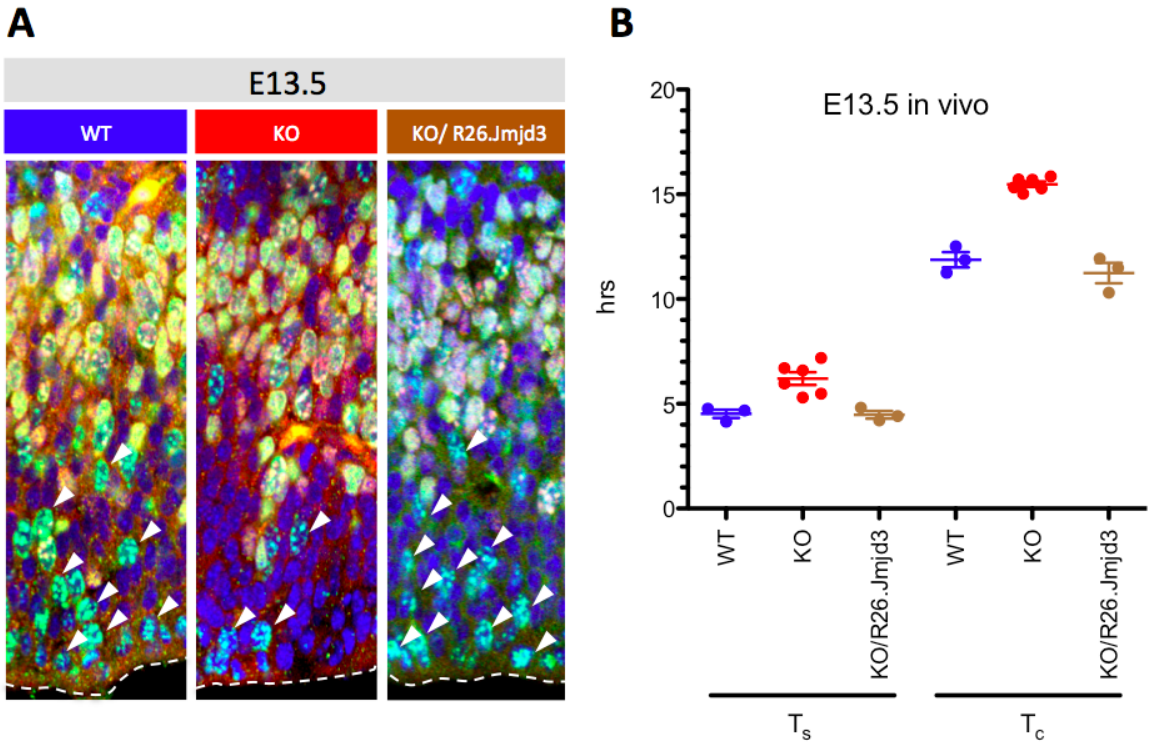

Figure 24. Loss of Jmjd3 causes lengthening of S phase and total cell cycle *in vivo*. (A) Representative immunofluorescences of IdU (green), BrdU (red), DAPI (blue) of E13.5 VZ in cortical sections from WT, Jmjd3 KO or Jmjd3 KO/R26.Jmjd3 (rescued) mice. White arrowheads indicate IdU+/BrdU- nuclei, which have exited the S phase between the administration of IdU and BrdU. (B) Graph showing individual T_s and T_c for all the analyzed embryos. Images from at least four distinct sections were acquired for each embryo, and were averaged before plotting and analysis. Each dot represents a single embryo. Mean ±SD for each genotype is also included in the graph.

In order to assess whether the *in vitro* NPC experimental system faithfully recapitulates the *in vivo* finding, we compared the total and relative length of the total

cell cycle and of the S phase that we obtained from E13.5-derived, *in vitro* cultured NPCs and from the E13.5 *in vivo* experiments. As shown in figure 25A, the overall ratio between S-phase and total cell cycle is conserved in the two conditions, and the lengthening deriving from the loss of Jmjd3 is similar in both systems. This confirms that our *in vitro* model offers a suitable recapitulation of the VZ NPC features to study alterations of the cell cycle dynamics.

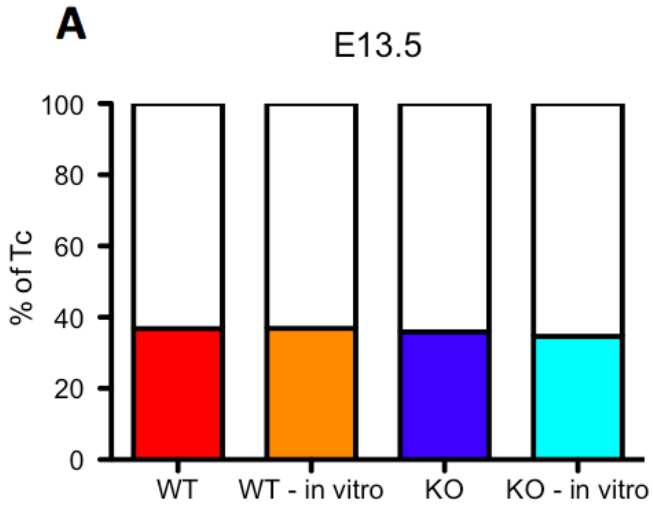

Figure 25. The ratio between S phase and total cell cycle length is conserved among *in vitro* and *in vivo* conditions and between WT and Jmjd3 KO mice. The length of S phase is shown as a percentage of the total cell cycle length. The ratio for the *in vitro* experiments is extrapolated from the data presented in figure 15, whereas the ratio for the *in vivo* experiments is extrapolated from the data presented in figure 18.

We also noted that both S phase and total cell cycle length show a slight increase in the *in vitro* condition over the *in vivo*, an observation that probably reflects the time that the cells were kept in culture. It has indeed been reported that the NPC cell cycle becomes longer as embryonic corticogenesis proceeds and that this phenomenon can be mirrored *in vitro,* by serial passaging of NPCs sourced from cortical tissue (Hirabayashi et al., 2009).

The fact that the lengthening of the cell cycle is already detectable at E13.5 is of particular interest. Indeed, we previously demonstrated that the phenotype of VZ expansion is absent at day E13.5 and only visible starting at day E16.5, and hypothesized that this might be due to the fact that the VZ expansion needs to be

accumulated over time in order to be statistically detectable. The fact that the cell cycle lengthening, which might be causing the VZ expansion, is indeed present before the appearance of the VZ expansion supports our initial hypothesis, despite we are not able to provide a formal causative link between the two phenomena at this point.

3.8 Generation of a conditional Jmjd3 KO strain

In order to better understand the function of Jmjd3 *in vivo*, we developed a mouse carrying a conditional (floxed) Jmjd3 allele (Jmjd3.fl). In this mouse line, loxP sites flank exons 2-4, which contain the first ATG of the Jmjd3 gene (fig. 26A) (see methods §2.6.6 for details). This mouse was obtained using the 'knockout-first' targeting strategy (Testa et al., 2004a), that has been adopted by the EUCOMM consortium for the high-throughput generation of versatile conditional knockout mouse strains. Thanks to the presence of FRT sites surrounding a LacZ-neo selection cassette placed in an intronic region, followed by loxP sites flanking an exon, it is possible to flexibly generate constitutive or conditional mice that can then be bred with Cre-deleter strains that allow for time- or space-specific deletion of the gene of interest.

We first crossed the Jmjd3-KOfirst mice with an Flp deleter to get rid of the LacZ-neo selection cassette and thus obtained Jmjd3.fl mice. When crossed with the constitutive deleter strain PGK-Cre, homozygous mice die at birth, mirroring the perinatal lethality phenotype of the constitutive KO XB814 strain. To confirm the abrogation of protein expression *in vivo*, we analyzed the level of Jmdj3 by western blot on protein lysates taken from Jmjd3.fl/PGK.Cre embryos at developmental days E13.5 and E16.5, confirming that the protein is absent throughout neural development (fig. 26B).

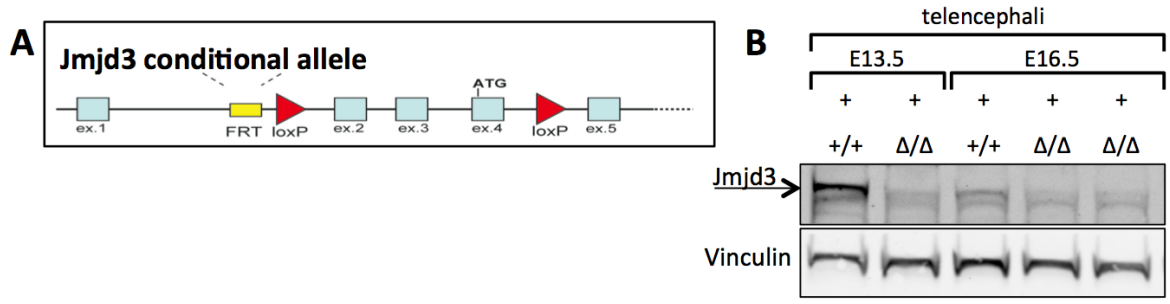

Figure 26. The Jmjd3 conditional KO allele. (A) Structure of the allele after Flp recombination, and prior to Cre recombination. (B) Western blot showing reduced levels of Jmjd3 protein in Jmjd3.fl/PGK.Cre embryonic telencephali, at days E13.5 and E16.5. Jmjd3 is detected using our in house-developed MAb (black arrow), Vinclin is used as a loading control.

3.8.1 Constitutive deletion of Jmjd3.fl upon crossing with PGK.Cre strain recapitulates the cortical phenotype of XB814 mice but to a slightly lesser degree of severity

After confirming that constitutive deletion in our Jmjd3.fl conditional mouse strain, by crossing it with the PGK.Cre deleter strain, recapitulates the phenotype of perinatal death of the XB814 constitutive Jmjd3 KO, we proceeded to assess whether the cortical phenotype of NPC expansion was reproduced as well. To do so, we analyzed the numbers of Pax6+ NPCs at days E16.5 and E18.5 of development in cortical sections of WT and KO brains. Surprisingly we were not able to detect any increase in the Pax6+ NPC compartment at day E16.5 at any level along the rostrocaudal axis (fig. 27A). E18.5 Jmjd3 brains, however, displayed as expected the expansion of the Pax6+ NPC compartment, albeit at a lower level than what we could observe at the same day of development in the XB814 mouse model (fig. 27B).

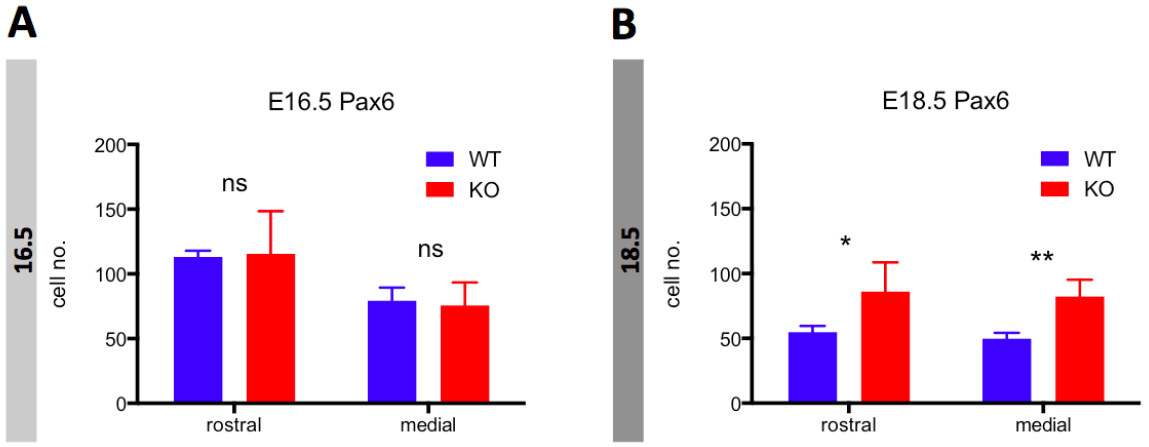

Figure 27. Jmjd3.fl/PGK.Cre embryos show a milder phenotype than XB814 embryos. (A-B) Graphs show total numbers of positive cells in a window spanning the entire cortex and 50 um wide. Graphs show mean ±SD of three biological replicates. (ns = P>0.05, * = P≤0.05, ** = P≤0.01, *** = P≤0.001)

We believe that this discrepancy is due to a different genetic background in the two mouse strains XB814 and Jmjd3.fl. The initial XB814 gene trapping was done in the e14tg2a cell line (129/Ola background) and has been completely backcrossed in C57BL/6 background; on the other hand, the Jmjd3.fl mice were also initially 129/Ola but had not been completely backcrossed in C57/BL6 at the time that the experiments were done. It is indeed known that a different genetic background can influence phenotype variability in mouse models (Montagutelli, 2000; Nadeau, 2005; Tanabe et al., 2012).

Taken together, these evidences suggest that lack of Jmjd3 is able to cause expansion of the NPC compartment regardless of the different genetic background of the mouse strains we used. However, the fact that the phenotype is significantly stronger in the XB814 constitutive KO suggests that better mechanistic insights might be gained by focusing our study on this particular strain.

3.9 Transcriptomic analysis shows differences between WT and Jmjd3 KO mRNA extracted from in vitro-cultured NPCs

It has been extensively demonstrated that the demethylase activity of Jmjd3, which we showed to be responsible for the *in vivo* phenotype and for the *in vitro* cell cycle lengthening, is mainly directed at regulating the dynamics of H3K27 methylation, eventually impacting on gene expression levels (Agger et al., 2007; Burgold et al., 2008; Burgold et al., 2012; De Santa et al., 2009; De Santa et al., 2007), even though the gene expression deregulation is usually restricted to small subsets of genes that are context-specific. In order to investigate the mechanisms that underlie the NPC cell cycle lengthening and VZ population expansion in the absence of Jmjd3, we resorted to transcriptomic analysis.

To do so, we extracted mRNA from WT and Jmjd3 KO *in vitro*-cultured NPCs, 4 samples from each condition (fig. 28A), and subjected it to Illumina sequencing. We chose RNAseq over microarray technology since RNAseq allows for the discovery of uncharacterized transcripts, and we wished to keep an explorative approach in our transcriptional analysis rather than focusing on the limited number of targets that microarray technology allows. RNAseq has also the advantage of delivering a low background signal while allowing for the quantification of transcripts over a high dynamic range, thus facilitating the discovery of subtle differences in gene expression between conditions.

We decided to prepare "stranded" libraries, which retain strand-of-origin information with high accuracy and avoid confusion during sequence analysis and data alignment deriving from the presence of both direct and reverse reads.

We obtained an average of 55 million reads from each of the 4 WT and 4 Jmjd3 KO samples (fig. 28A), and aligned them to the mouse transcriptome (mm9) using TopHat, as detailed in methods §2.3.1. We then quantified the reads and estimated

differential gene expression using Cufflinks. Thanks to this approach, we were able to identify 117 genes that are differentially expressed between WT and KO samples, as shown in figure 28B.

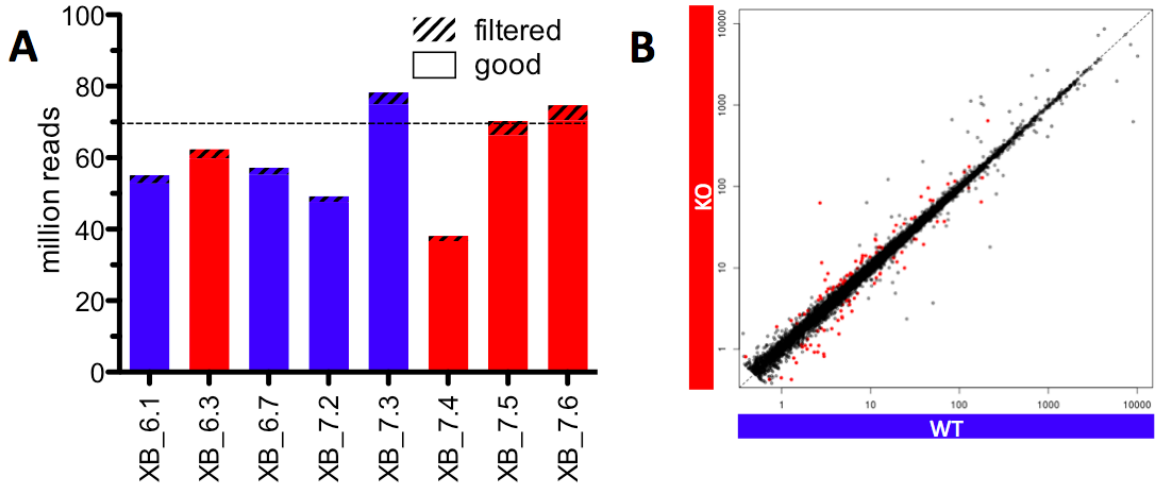

Figure 28. Transcriptomic analysis of WT or Jmjd3 KO *in vitro*-cultured NPCs identifies 117 differentially expressed genes (DEG). (A) 4 WT and 4 KO samples were analyzed, the histogram shows the total number of reads obtained for each sample. 70 million reads (dashed lines) were expected based on flow cell loading. (B) Scatterplot showing the averaged expression level of all read mapped to a RefSeq annotated gene. Red dots represent DEGs.

3.9.1 Bioinformatics analysis highlights enrichment of DEGs among pathways relevant to the phenotype of NPC expansion and cell cycle lengthening

We then took advantage of the IPA software package to understand whether there was an enrichment of the differentially expressed genes among particular pathways or gene functions, and we found several interesting candidate pathways that are relevant to the phenotype of NPC expansion (fig. 29A-B): TR-RXR (retinoic acid receptor) activation, Wnt/B-catenin, Glycolysis, Axon Guidance, ES pluripotency and Notch signaling. It is of particular interest that we found upregulation in genes belonging to the Wnt/B-catenin and the Notch pathways, which are involved in defining the symmetry of NPC cell division in the VZ. It has indeed been shown that high levels of Notch signaling inhibit neural differentiation (Lui et al., 2011) and Wnt

signaling has also been shown to increase the self-renewal potential of neural stem cells (Kalani et al., 2008; Pei et al., 2012; Piccin and Morshead, 2011).

Thus, we hypothesize that the *in vivo* expansion of the NPC population observed in Jmjd3 KO embryonic cortices might be linked to the alterations in the expression level of genes belonging to these two pathways, which causes the NPCs to preferentially undergo self-renewal rather than neural differentiation. We also found an enrichment of downregulated genes in the "Axon Guidance" pathway, whose upregulation is usually associated with the process of neurogenic differentiation. We reasoned that the fact that genes involved in the definition of neuronal identity are less expressed in absence of Jmjd3 already in the NPC state might reflect a reduced proneness of the Jmjd3 KO NPCs to differentiate into neurons. This speculation parallels the *in vivo* observation that the neuronal production is reduced in the absence of Jmjd3 during the early stages of corticogenesis.

A

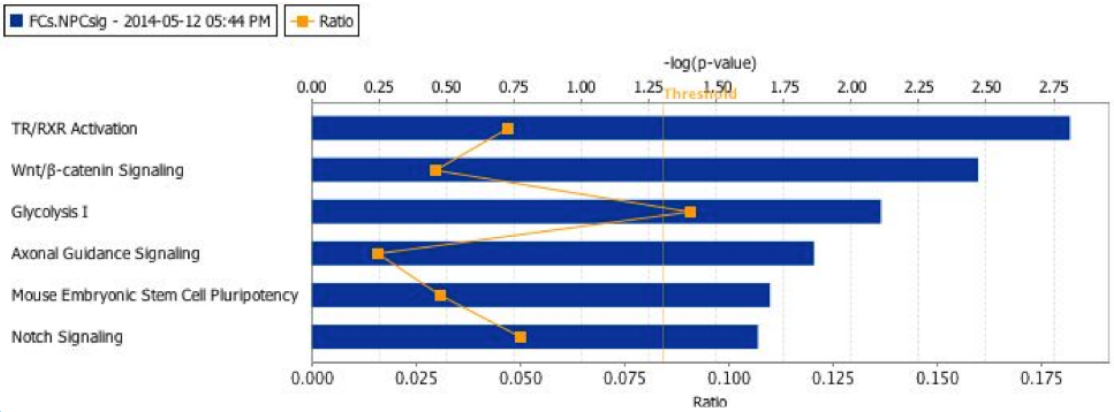

B

Wnt/B-catenin	
Gene Symbol	Log Ratio
Dvl3	0.587
Fzd1	-0.77
Ppp2r2a	0.885
Sox9	0.54
Tcf7l2	0.606

Notch	
Gene Symbol	Log Ratio
Maml2	0.392
Notch3	0.479

TR/RXR	
Gene Symbol	Log Ratio
Gm5506	1.106
Ncor2	0.671
Ppargc1a	0.595
Slc16a3	1.824

Glycolysis	
Gene Symbol	Log Ratio
Gm5506	1.106
Pfkl	0.406

Axon Guidance	
Gene Symbol	Log Ratio
Adamts1	-0.433
Fzd1	-0.77
Itga4	-0.888
Nfat5	0.502
Nrp2	-0.443
Ntng1	-0.804
Plxnb3	0.56

Figure 29. Ingenuity Pathway Analysis highlights enrichment of DEGs among pathways relevant to the phenotype of NPC expansion and cell cycle lengthening. (A) Histogram showing pathways selected among the most enriched ones, -log(p-value) is indicated. (B) Genes belonging to the most enriched pathways are shown for each pathway, together with the degree of upregulation (red) or downregulation (green).

Surprisingly, despite the abundance of *in* vivo and *in vitro* evidences corroborating the observation that lack of Jmjd3 causes a general lengthening of the cell cycle, we were not able to detect an enrichment of DEGs in pathways relevant to the cell cycle progression. However, we found an upregulation in genes involved in the glycolysis pathway, together with a pronounced downregulation of Atp5g1 (-1.44 Log_2FC), a gene encoding for a subunit of the mitochondrial ATP synthase machinery. Taken together, these data might suggest that there is a reduction in the phosphorylative oxidation capacity of Jmjd3 KO cells followed by an upregulation of the anaerobic glycolysis pathway. In turn, this general metabolic alteration might be causatively linked to the general lengthening of the cell cycle that we observed *in vivo* and *in vitro* in the absence of Jmjd3.

3.9.2 Integration of RNAseq data with publicly available Jmjd3 and H3K27 ChIPseq profiles identifies a subset of putative direct Jmjd3 targets

RNAseq analysis has helped us in defining the molecular consequences of the loss of Jmjd3, and in generating mechanistic hypotheses on how they underlie the cortical phenotype that I described in the previous paragraphs. However, the direct targets of Jmjd3 are most likely only a subset of all the genes that show differential expression, while the others represent secondary targets. In order to precisely pinpoint the mechanism of action of Jmjd3 in our system and to discern the direct targets of Jmjd3, we complemented our RNAseq analysis with publicly available datasets of Jmjd3 binding (Estarás et al., 2012) and H3K27me3 distribution (Burney et al., 2013), obtained from WT mouse NPCs. We reasoned that a gene, in order to be considered a direct target of Jmjd3, should display: a) reduced mRNA expression in Jmjd3 KO NPCs, b) Jmjd3 binding in WT NPCs, c) no or reduced H3K27me3 levels in WT NPCs. Based

on these criteria, we were able to identify a subset of 13 genes which might be direct targets of Jmjd3 in NPCs (fig. 30).

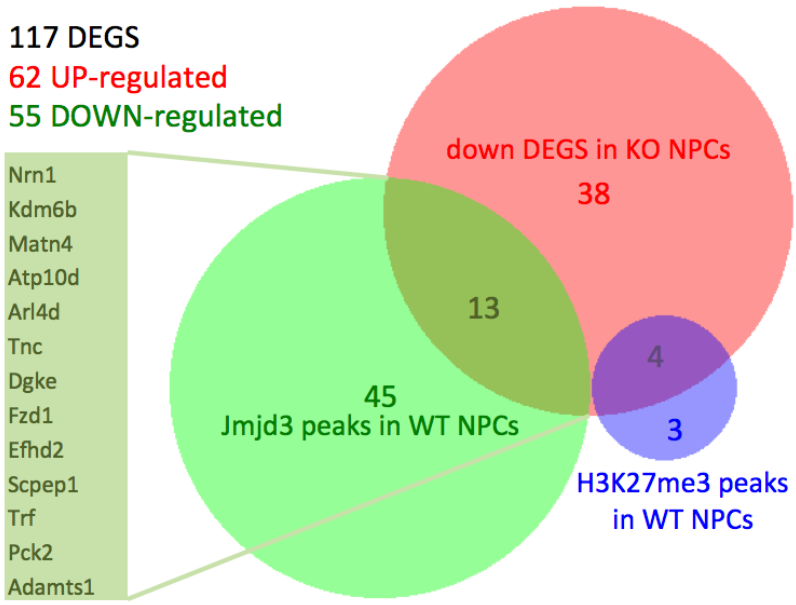

Figure 30. Identification of putative Jmjd3 targets. Venn diagram showing the subset of genes, among those found downregulated in Jmdj3 KO NPCs (red), that were found bound by Jmjd3 in a published study (green) (REF). Genes that displayed high levels of H3K27 (ref) are shown in blue, and do not overlap with the possible targets of Jmjd3.

3.9.3 Transcriptomic analysis of E16.5 cortical tissue reveals minor overlap with in vitro-cultured NPCs

We next wanted to assess the transcriptional effects of loss of Jmjd3 on the developing neocortex. To do so, we extracted mRNA from whole forebrains of WT and Jmjd3 KO E16.5 embryos, and subjected them to RNA sequencing. We decided to extract mRNA from whole forebrains in order to obtain high yields of material in a streamlined manner, and to avoid more selective techniques like laser-capture microdissection and FACS sorting, which can worsen RNA quality and yield. After bioinformatics analysis we were able to detect differential expression for 19 genes, 4 of which are shared between the *in vivo* and the *in vitro* samples (Lars2, Rsad1, Atp5g1, and Jmjd3).

Two of these targets, Lars2 and Rsad1, are poorly characterized nuclear-encoded, mitochondrial proteins with a role in aminoacylation of mitochondrial $tRNA^{Leu}$ (Li

and Guan, 2010) and an uncharacterized role, respectively. As stated above, Atp5g1 encodes for a subunit of the mitochondrial ATP synthase machinery: the fact that mitochondrial genes are significantly enriched among the common DEGs found in *in vitro* and *in vivo* samples reinforces our previous hypothesis that a general disregulation of mitochondrial function might be linked to the observed general lengthening of the cell cycle in Jmjd3 KO NPCs.

This degree of correlation could be explained by the relative low abundance of NPCs with respect to the whole telencephalon at day E16.5, which might cause differences in gene expression levels to be diluted to the point of becoming undetectable. In order to address this issue, we are trying to isolate NPCs from embryonic brains using fluorescent antibodies against Pax6 coupled to FACS sorting. This method has the drawback that cells need to be fixed and permeabilized for the antibody to access the antigen in the nucleus, causing reduction in yield and quality of the resulting RNA. Nonetheless, we were able to set up an intracellular staining protocol to consistently isolate NPCs from other cell types, and to obtain total RNA that, despite its low integrity (RIN 3±0.42 as measured by Agilent Bioanalyzer), can be used to create RNAseq libraries using an adapted protocol (fig. 31A-B).

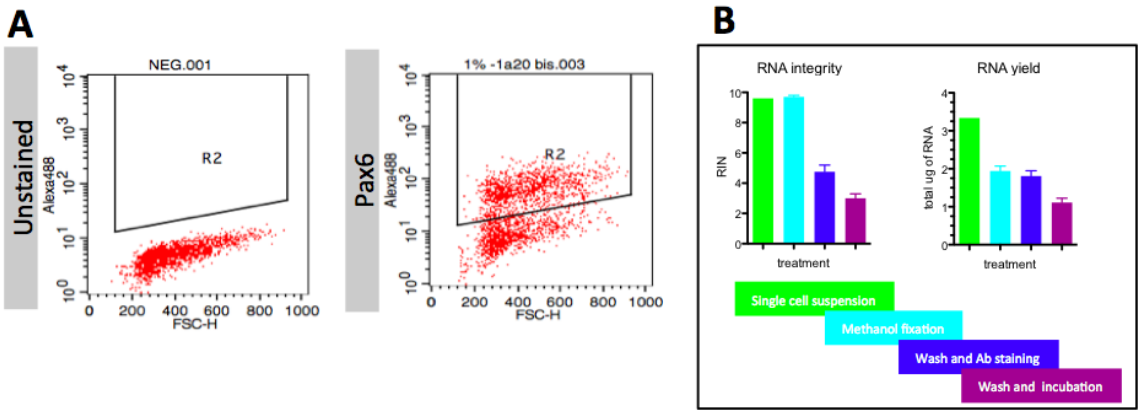

Figure 31. FACS-based strategy to isolate RNA from freshly-derived cortical NPCs. (A) FACS plots showing specific staining using a Pax6-488 primary conjugated antibody on single-cell suspension derived from E15.5 cortical tissue. (B) Histograms showing the RNA integrity number (RIN) as determined by the Agilent Bioanalyzer (left) and the total yield of RNA in µg (right) for each step of the protocol. Protocol steps: green = fresh single cell suspension; light blue = after methanol fixation; dark blue = after antibody staining; purple = after a long incubation mimicking FACS processing.

As a more suitable alternative, we are currently testing a fluorescent small molecule, CDr3 (Yun et al., 2012), which is able to selectively stain live NPCs without the need for fixation and permeabilization, in virtue of its ability to bind BLBP, a protein that is characteristic of embryonic NPCs.

3.10 Generation of a mouse strain harboring a Jmjd3-Venus fusion protein

ChIP approaches to evaluate chromatin binding of transcription can be heavily influenced by the quality of the antibodies used. All the commercial anti-Jmjd3 antibodies that we tested perform poorly in IP, and also our in house-developed monoclonal antibodies did not yield reliable results when tested in simple IP applications. The use of tagged constructs to transfect or transduce the target cell population can solve the need for an antigen-specific antibody, as anti-tag antibodies are optimized for these applications: however, the abundance of the fused protein cannot be easily controlled by transduction of transfection, leading to situations of over- or under-abundance of the tagged protein with respect to its wild type counterpart. In these cases, false positive or false negatives can be easily generated in high-throughput applications such as ChIPseq, and the targets need anyway to be validated using an anti-antigen antibody.

In order to circumvent these limitations, we generated a mouse line harboring a BAC containing the whole genomic region of Jmjd3, and a Venus fluorescent protein tag at the C-terminal of Jmjd3 (see methods §2.6.7) (fig. 32A) (Choo et al., 2011; Ciotta et al., 2011). The presence of the whole genomic region allows for a physiological control of gene expression, such that the level of the fused protein should always mirror that of the wild type protein. The Venus tag represents a suitable substrate for IP applications (Ciotta et al., 2011; Hofemeister et al., 2011), and it moreover allows

detecting the distribution of the protein in fluorescence microscopy applications, both live through direct fluorescence and on fixed tissues by indirect fluorescence.

After several rounds of nuclear microinjection, we were able to obtain a single founder female (fig. 32B), which has recently given birth to generation F_1. Once the colony has been established, we will derive NPCs from E13.5 telencephali and will perform ChIPseq analysis to complement the RNAseq data.

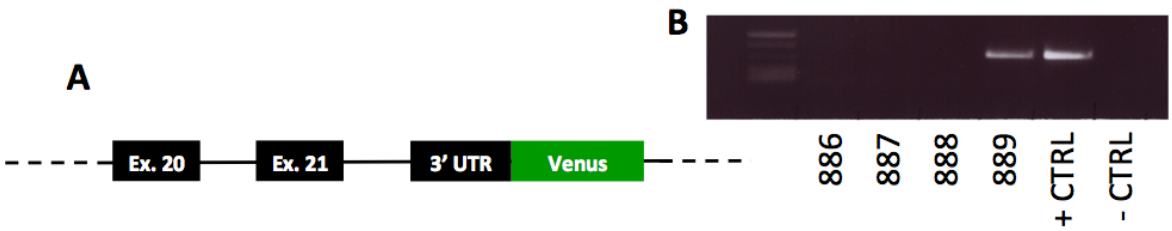

Figure 32. Generation of the Jmjd3.Venus mouse strain. (A) Diagram showing the structure of the fusion protein harbored in the modified BAC that was used to generate the mouse strain. (B) PCR showing the presence of the band corresponding to the Venus CDS (obtained with the primers VENfw01, VENrv01) in mouse #889. Diluted purified BAC is used as a positive control.

3.10.1 Derivation of NPCs from mouse ES cells harboring a human Jmjd3-Venus fusion protein

Furthermore, we obtained from a collaborating group mouse ES cells that have been engineered to express a human Jmjd3-Venus fusion protein from a BAC containing the whole locus control region. The absence of a murine genomic context, with the proper enhancer and promoter sequences, does not guarantee that physiologically dynamic expression levels are reached during differentiation processes, but the mouse and the human Jmjd3 orthologs share 98% aminoacid identity, suggesting that the binding preferences should anyway be comparable.

We first assessed the cellular distribution of the Jmjd3.Venus fusion protein by immunofluorescence in ES cell cultures. As shown in figure, Jmjd3.Venus displays a nuclear localization and is excluded from nucleoli. Some cells show low to undetectable levels of fluorescence, suggesting heterogeneous expression of the

fusion protein in the ES cell population (fig. 33A). Moreover, by the use of a dual color fluorescence western blotting system we were able to confirm that the fusion protein is indeed reactive to both anti-Jmjd3 and anti-Venus antibody (fig. 33B).

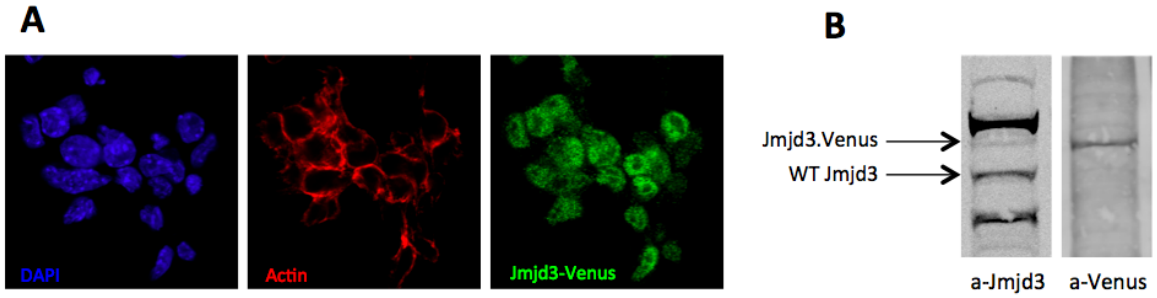

Figure 33. Detection of the hJmjd3.Venus fusion protein in mouse ESCs. (A) Confocal immunofluorescence image showing indirect detection (via an anti C-YFP antibody) of the hJmjd3.Venus fusion protein (green). DAPI (blue) and Phalloidin-TRITC (red) are used as nuclear and cytoplasmic counterstain, respectively. (B) Dual-color immunofluorescence WB showing co-occurrence of the Jmjd3 and Venus signal in ESC lysate. The two images are shown in black and white for clarity.

We differentiated the Jmjd3.Venus ES cells into Pax6+ NPCs by taking advantage of a previously published protocol(Bibel et al., 2007), and we are currently performing ChIP using an anti-Venus antibody in order to gain information about the chromatin distribution of Jmjd3 in NPCs.

3.11 Jmjd3 binds to the Dlx2 promoter in an in vitro model of adult neurogenesis

The H3K4 methyltransferase Mixed-lineage leukemia 1 (Mll1) has been shown to be necessary for adult neurogenesis, in virtue of its role in the activation of genes necessary for the unwinding of the neurogenic program (Lim et al., 2009). Dlx2 is a key regulator of adult SVZ neurogenesis: in the undifferentiated state, the Dlx2 promoter is bivalently marked by both H3K4me3 and H3K27me3, and is hence transcriptionally silent but poised for activation. Lim and coworkers have observed in in vitro-cultured SVZ RGCs that Dlx2 shows high levels of H3K4me3 and low H3K27me3 on the promoter region upon differentiation, and that lack of Mll1 prevents the expression of Dlx2, hampering neuronal production. Interestingly, the

loss of Mll1 does not affect the levels of H3K4 but rather prevents demethylation of H3K27, and the authors hypothesize that Mll1 recruits a H3K27 demethylase during the differentiation process to allow activation of the Dlx2 locus.

We established a collaboration with the lab of Daniel Lim in order to provide proof that Jmjd3 is selectively recruited on the Dlx2 locus upon differentiation of adult SVZ RGCs, and to demonstrate that Jmjd3 is indeed recruited by Mll1 to allow transcriptional activation of Dlx2. Using the same system of adult SVZ RGC differentiation, we analyzed by ChIP-qPCR the dynamics of the binding of Jmjd3 at the Dlx2 promoter upon differentiation, and compared it to the Hoxa2 and Olig2 promoters as a control: we found that Jmjd3 is selectively increased at the Dlx2 promoter with respect to the controls, supporting a role for Jmjd3 in the process of adult neurogenesis (fig. 34).

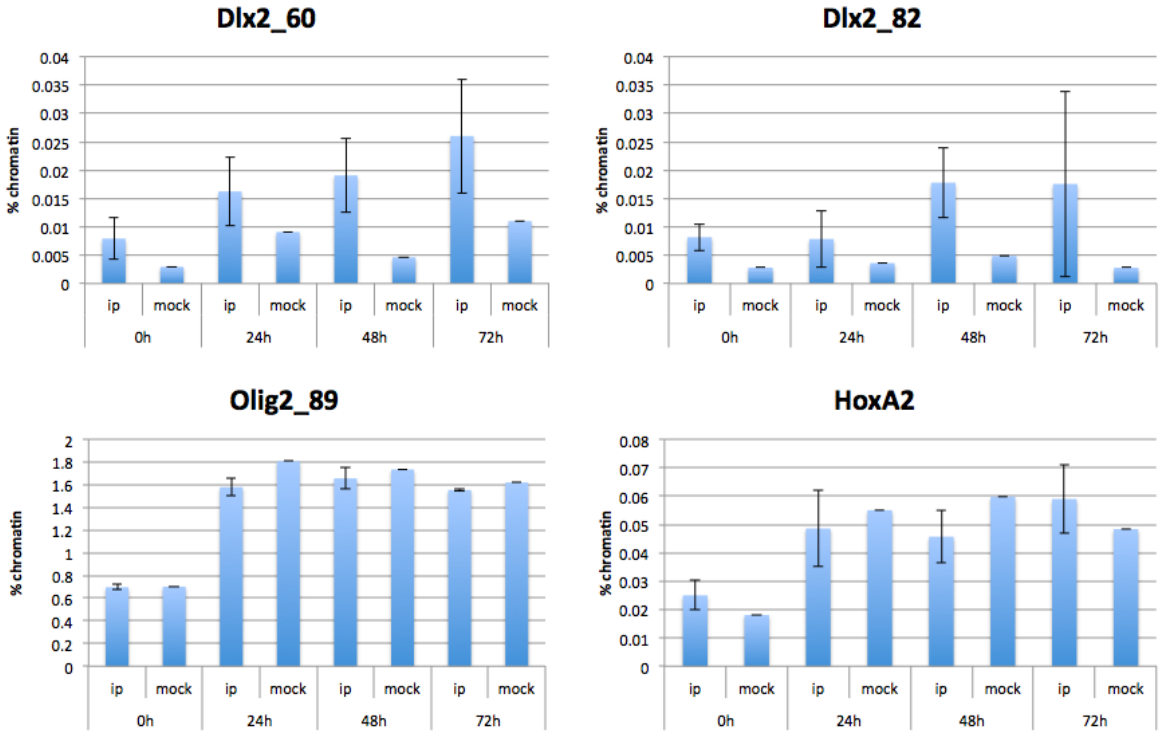

Figure 34. Jmjd3 is enriched at the Dlx2 promoter in an *in vitro* model of adult SVZ neurogenesis. Histograms show that Jmjd3 is enriched at the Dlx2 promoter (Dlx2_60, Dlx2_82) but not at the Olig2 and HoxA2 promoters. IPs were performed in triplicates per each time point, and a single mock IP is used as a control.

Our experiments have then contributed to a paper by the Lim lab that has been recently published in Cell Reports (Park et al., 2014).

In this thesis, I define a role for Jmjd3 in regulating cell cycle progression and the rate of self-renewing versus differentiating divisions in the ventricular zone neural progenitor cells of the developing mouse neocortex. Loss of Jmjd3 causes VZ NPCs to lengthen their cell cycle and preferentially undergo self-renewing cell divisions, resulting in an aberrantly expanded ventricular zone and a reduced number of differentiated neurons in the cortical plate. I propose that this phenotype is linked to the supraphysiological activation of the Wnt/B-catenin and Notch pathways, two known regulators of the choice between self-renewal and differentiation in the VZ NPCs of the developing brains, whose hyperactivation has been demonstrated to be associated with an increased proliferative potential.

Histone-modifying proteins, including histone methyltransferases and histone demethylases, have been demonstrated to play a role in cell state transitions and developmental processes, in virtue of their ability to participate in the activation or repression of lineage-specific genes. Jmjd3, in particular, has been shown by us and by others to have a role in enabling cellular differentiation along the neural lineage, beyond other roles in osteoblast differentiation, macrophage activation, Hox genes activation and transcriptional regulation of the Cdkn2a locus.

Based on these lines of evidence, the initial aim of our work was to investigate the specific role of Jmjd3 in the cell state transitions that allow the stem cells of the developing neocortex, or radial glial cells, to give rise to the different subtypes of neurons. By taking advantage of the XB814 loss-of-function mouse strain, previously published by our lab (Burgold et al., 2012), we were able to score abnormalities in the developing neocortex of mouse embryos lacking Jmjd3. In particular, we noted that

Jmjd3 KO embryos showed a higher number of VZ NPCs and a reduced number of differentiated neurons, and that this phenotype was detectable only at late time points in development, at day E16.5 or later. This observation can easily be reconciled with our initial hypothesis that Jmjd3 is necessary for the differentiation of NPCs to neurons. When we characterized specifically the NPC population of Jmdj3 KO embryos *in vivo* by EdU/Ki67 staining, we found that these cells are more prone to undergo self-renewing rather than differentiating divisions, suggesting that the neural differentiation program is indeed affected by the loss of Jmjd3. Our model so far would thus entail that the *differentiation* of NPCs is specifically hampered by the loss of Jmjd3, but the *stem cell state* in itself should not be affected.

The observation of *in vivo* systems allows to analyze biological processes as a whole, and to assess the role of a specific factor in its physiological environment, without the potential artifacts that derive from the use of *in vitro* models. However, the use of cellular *in vitro* models, which are inherently reductionist, can help in dissecting the role of a target factor in a specific cellular context whose boundaries would appear blurred when analyzed *in vivo*.

To characterize in detail the NPC population, we resorted to *in vitro* time-lapse videomicroscopy. This technique allowed us to analyze the behavior of a pure population of NPCs derived from the E13.5 embryonic brain, and to track their mitotic choices at the single-cell level over a period of several days. We were also able, by modulating the availability of the mitotic factor bFGF, to selectively grow them in self-renewing (high bFGF) or differentiative (no bFGF) conditions, and to assess the effect of the role of Jmjd3 specific to each of these two conditions.

Intriguingly, we found that loss of Jmdj3 specifically affects the cell cycle behavior of NPCs when they are kept in strict proliferative conditions. Indeed, repeated experiments showed Jmjd3 KO NPCs have a significantly longer cell cycle time than

their WT counterpart, and that this is caused by a generalized lengthening of all the cell cycle phases. We then sought to parallel this observation *in vivo*, and by the use of multiple thymidine analogues to mark cells in S-phase in the VZ, we were able to confirm that loss of Jmdj3 caused cell cycle lengthening also in an *in vivo* context. This observation moved the focus of our analysis from the cell state *transition* between NPCs and neurons, to the maintenance of the neural stem cell state *itself.*

The fact that Jmjd3 KO NPCs show both a longer cell cycle together and an increased propensity to undergo self-renewal is of particular interest. It has indeed been shown that self-renewing and differentiating VZ NPC populations show differential length in specific cell cycle phases. No detailed mechanistic explanations have been provided for these phenomena: however, the "cell-cycle length hypothesis" suggests that in general, a longer cell cycle is associated to a differentiating behavior, and that the length of a specific cell cycle phase might influence the overall availability and hence activity of a cell fate determinant that is typically present during that phase.

Evidences supporting this hypothesis show that a longer G1 phase is causally linked with differentiation, since forced modulation of the length of G1 phase can influence the cell division choice (Lange et al., 2009). On the other hand, it has also been shown that self-renewing VZ NPCs generally show a longer S phase than their differentiating counterpart (Arai et al., 2011).

Our observations are in apparent contradiction with the "cell cycle length hypothesis" recounted above: in Jmjd3 KO NPCs, a longer cell cycle is associated with an increased propensity for self-renewal. However, differently from what has been shown in other instances, the lengthening of the cell cycle in our case is generalized and not restricted to a specific cell cycle phase. In fact, we observe *both* a longer G1 *and* a longer S phase in the preferentially self-renewing Jmjd3 KO NPC population.

We were not able to clarify whether the increased cell cycle length is causally linked to the preference for self-renewal, or whether the two phenomena are both caused by the lack of Jmjd3 but do not bear a causal impact on each other. However, we confirmed the correlation between the two phenomena in different *in vitro* and *in vivo* settings, and we furthermore showed that re-expression of Jmjd3 can rescue both the phenotypes. We therefore believe that these solid observations can contribute to the growing body of evidences that conflate into the "cell-cycle length hypothesis", and provide advancement to the field.

Jmjd3 is a lysine-specific demethylase that can influence the level of expression of target genes based on its ability to demethylate H3K27 and counteract the effects of the PRC2 repressive complex. In order to link the absence of Jmjd3 to the phenotype of cell cycle lengthening and increased self-renewal of VZ NPCs, we sought to characterize the transcriptional effects that the loss of Jmjd3 is able to cause in such cell types. RNAseq analysis on *in vitro*-cultured NPCs revealed a molecular signature deriving from the loss of Jmjd3 that is consistent with the phenotype that we observed *in vivo* and *in vitro.* Indeed, the Notch and Wnt pathways, which are involved in defining the symmetry of NPC cell division in the VZ, were among the top enriched pathways according to our analysis: hyperactivation of both these pathways has been associated with increased self-renewal of neural stem cells and a reduced propensity to undergo neural differentiation. Intriguingly, genes or pathways linked to cellular proliferation or cell cycle progression were not significantly altered in Jmjd3 KO NPCs. However, we found that genes involved in the glycolysis pathway were significantly upregulated, together with a pronounced downregulation of a gene encoding for a subunit of the mitochondrial ATP synthase machinery (Atp5g1). These data might suggest that there is a reduction in the phosphorylative oxidation capacity

of Jmjd3 KO cells followed by an upregulation of the anaerobic glycolysis pathway. In turn, this general metabolic alteration might be causatively linked to the lengthening of the cell cycle that we observed *in vivo* and *in vitro* in the absence of Jmjd3.

Capitalizing on our extensive *in vivo* screening of the developing mouse brain, on the detailed characterization of the brain stem cell compartment both *in vivo* and *in vitro*, and on the molecular analysis of the expression level of the whole transcriptome, we propose that loss of Jmjd3 causes upregulation of the Notch and Wnt pathways and a reduced mitochondrial activity, resulting in an increased self-renewal and a longer cell cycle in the VZ NPCs. This, in turn, leads to aberrant expansion of the stem compartment and a reduction in the neuronal output.

Hypothesizing that Jmjd3 exerts these effects through its activity as a H3K27 demethylase, and hence through transcriptional dysregulation of direct target genes, we sought to investigate the binding of Jmjd3 to chromatin in proliferating VZ NPCs. Unfortunately, despite our efforts to develop monoclonal antibodies suitable for ChIP and IP applications, we were not able to setup a reliable ChIPseq protocol for Jmjd3, and we thus complemented our analysis with publicly-available data on Jmjd3 binding in neural stem cells generated by other labs, that we re-analyzed in-house. We identified a subset of 13 genes that might be direct targets of Jmjd3, but we were not able to pinpoint a target that would explain the downstream dysregulation of the Wnt, Notch and Glycolysis pathways and the brain phenotype. We speculate that this is due to the fact that the publicly available dataset has been generated on neural stem cells that have been obtained and cultured using a protocol different from ours, thus resulting in a chromatin state that cannot be faithfully compared with the one that we obtained using our protocol.

In order to overcome this setback and to gain detailed mechanistic insights on the action of Jmjd3 in embryonic NPCs, we seek to generate our own Jmjd3 ChIPseq binding profiles in NPCs and to correlate them with the transcriptomic data that we obtained from the same cell type. To do so without having to use anti-Jmjd3 antibodies, which have proven unreliable for ChIP applications in our hands, we generated a mouse strain that harbors a BAC containing a Venus-tagged version of Jmjd3. The presence of the whole genomic region allows for a physiological control of gene expression, such that the level of the fused protein should hence mirror that of the wild type protein, and the Venus tag represents a suitable substrate for IP applications. We are currently in the process of obtaining offspring from the founder mouse of this colony: we are confident that we will be able to identify a subset of direct targets of Jmjd3 in a short time frame, and to provide a detailed mechanistic explanation of the role of Jmjd3 in regulating cell cycle progression and self-renewal in NPCs of the developing brain.

Aaku-Saraste, E., Oback, B., Hellwig, A., and Huttner, W. B. (1997). Neuroepithelial cells downregulate their plasma membrane polarity prior to neural tube closure and neurogenesis. Mech Develop *69*, 71-81.

Agger, K., Cloos, P. A. C., Christensen, J., Pasini, D., Rose, S., Rappsilber, J., Issaeva, I., Canaani, E., Salcini, A. E., and Helin, K. (2007). UTX and JMJD3 are histone H3K27 demethylases involved in HOX gene regulation and development. In Nature, pp. 731-734.

Agger, K., Cloos, P. A. C., Rudkjaer, L., Williams, K., Andersen, G., Christensen, J., and Helin, K. (2009). The H3K27me3 demethylase JMJD3 contributes to the activation of the INK4A-ARF locus in response to oncogene- and stress-induced senescence. In Genes & Development, pp. 1171-1176.

Arai, Y., and Pierani, A. (2014). Development and evolution of cortical fields. In Neuroscience Research, (Elsevier Ireland Ltd and Japan Neuroscience Society), pp. 1-11.

Arai, Y., Pulvers, J. N., Haffner, C., Schilling, B., Nüsslein, I., Calegari, F., and Huttner, W. B. (2011). Neural stem and progenitor cells shorten S-phase on commitment to neuron production. In Nature Communications, p. 154.

Barradas, M., Anderton, E., Acosta, J. C., Li, S., Banito, A., Rodriguez-Niedenfuhr, M., Maertens, G., Banck, M., Zhou, M. M., Walsh, M. J.*, et al.* (2009). Histone demethylase JMJD3 contributes to epigenetic control of INK4a/ARF by oncogenic RAS. In Genes & Development, pp. 1177-1182.

Berger, S. L., Kouzarides, T., Shiekhattar, R., and Shilatifard, A. (2009). An operational definition of epigenetics. In Genes & Development, pp. 781-783.

Bernstein, B. E., Mikkelsen, T. S., Xie, X., Kamal, M., Huebert, D. J., Cuff, J., Fry, B., Meissner, A., Wernig, M., Plath, K.*, et al.* (2006). A Bivalent Chromatin Structure Marks Key Developmental Genes in Embryonic Stem Cells. In Cell, pp. 315-326.

Betizeau, M., Cortay, V., Patti, D., Pfister, S., Gautier, E., Bellemin-Menard, A., Afanassieff, M., Huissoud, C., Douglas, R. J., Kennedy, H., and Dehay, C. (2013). Precursor diversity and complexity of lineage relationships in the outer subventricular zone of the primate. Neuron *80*, 442-457.

Bibel, M., Richter, J., Lacroix, E., and Barde, Y.-A. (2007). Generation of a defined and uniform population of CNS progenitors and neurons from mouse embryonic stem cells. In Nature Protocols, pp. 1034-1043.

Blackledge, N. P., Farcas, A. M., Kondo, T., King, H. W., McGouran, J. F., Hanssen, L. L., Ito, S., Cooper, S., Kondo, K., Koseki, Y.*, et al.* (2014). Variant PRC1 complex-dependent H2A ubiquitylation drives PRC2 recruitment and polycomb domain formation. Cell *157*, 1445-1459.

Boniolo, G., and Testa, G. (2012). The Identity of Living Beings, Epigenetics, and the Modesty of Philosophy. Erkenntnis *76*, 279-298.

Bruggeman, S. W., Hulsman, D., Tanger, E., Buckle, T., Blom, M., Zevenhoven, J., van Tellingen, O., and van Lohuizen, M. (2007). Bmi1 controls tumor development in an Ink4a/Arf-independent manner in a mouse model for glioma. Cancer cell *12*, 328-341.

Burgold, T., Spreafico, F., De Santa, F., Totaro, M. G., Prosperini, E., Natoli, G., and Testa, G. (2008). The Histone H3 Lysine 27-Specific Demethylase Jmjd3 Is Required for Neural Commitment. In PLoS ONE, p. e3034.

Burgold, T., Voituron, N., Caganova, M., Tripathi, P. P., Menuet, C., Tusi, B. K., Spreafico, F., Bévengut, M., Gestreau, C., Buontempo, S.*, et al.* (2012). The H3K27 demethylase JMJD3 is required for maintenance of the embryonic respiratory neuronal network, neonatal breathing, and survival. In Cell Reports, pp. 1244-1258.

Burney, M. J., Johnston, C., Wong, K. Y., Teng, S. W., Beglopoulos, V., Stanton, L. W., Williams, B. P., Bithell, A., and Buckley, N. J. (2013). An epigenetic signature of developmental potential in neural stem cells and early neurons. Stem cells *31*, 1868-1880.

Byrd, K. N., and Shearn, A. (2003). ASH1, a Drosophila trithorax group protein, is required for methylation of lysine 4 residues on histone H3. Proceedings of the National Academy of Sciences of the United States of America *100*, 11535-11540.

Calegari, F., Haubensak, W., Haffner, C., and Huttner, W. B. (2005). Selective Lengthening of the Cell Cycle in the Neurogenic Subpopulation of Neural Progenitor Cells during Mouse Brain Development. In Journal of Neuroscience, pp. 6533-6538.

Cao, R., and Zhang, Y. (2004). SUZ12 is required for both the histone methyltransferase activity and the silencing function of the EED-EZH2 complex. Molecular cell *15*, 57-67.

Casola, S. (2004). Conditional gene mutagenesis in B-lineage cells. Methods in molecular biology *271*, 91-109.

Caviness, V. S., Jr., Takahashi, T., and Nowakowski, R. S. (1995). Numbers, time and neocortical neuronogenesis: a general developmental and evolutionary model. Trends in neurosciences *18*, 379-383.

Chen, S., Ma, J., Wu, F., Xiong, L. j., Ma, H., Xu, W., Lv, R., Li, X., Villen, J., Gygi, S. P.*, et al.* (2012). The histone H3 Lys 27 demethylase JMJD3 regulates gene expression by impacting transcriptional elongation. In Genes & Development, pp. 1364-1375.

Choo, S. W., White, R., and Russell, S. (2011). Genome-wide analysis of the binding of the Hox protein Ultrabithorax and the Hox cofactor Homothorax in Drosophila. PloS one *6*, e14778.

Ciotta, G., Hofemeister, H., Maresca, M., Fu, J., Sarov, M., Anastassiadis, K., and Stewart, A. F. (2011). Recombineering BAC transgenes for protein tagging. Methods *53*, 113-119.

Dai, J.-p., Lu, J.-y., Zhang, Y., and Shen, Y.-f. (2010). Jmjd3 activates Mash1 gene in RA-induced neuronal differentiation of P19 cells. In Journal of Cellular Biochemistry, pp. 1457-1463.

De Santa, F., Narang, V., Yap, Z. H., Tusi, B. K., Burgold, T., Austenaa, L., Bucci, G., Caganova, M., Notarbartolo, S., Casola, S*., et al.* (2009). Jmjd3 contributes to the control of gene expression in LPS-activated macrophages. In The EMBO Journal, (Nature Publishing Group), pp. 3341-3352.

De Santa, F., Totaro, M. G., Prosperini, E., Notarbartolo, S., Testa, G., and Natoli, G. (2007). The Histone H3 Lysine-27 Demethylase Jmjd3 Links Inflammation to Inhibition of Polycomb-Mediated Gene Silencing. In Cell, pp. 1083-1094.

Deaton, A. M., and Bird, A. (2011). CpG islands and the regulation of transcription. Genes & development *25*, 1010-1022.

Dehay, C., and Kennedy, H. (2007). Cell-cycle control and cortical development. In Nature Reviews Neuroscience, pp. 438-450.

Desai, A. R., and McConnell, S. K. (2000). Progressive restriction in fate potential by neural progenitors during cerebral cortical development. In Development, pp. 2863-2872.

Ene, C. I., Edwards, L., Riddick, G., Baysan, M., Woolard, K., Kotliarova, S., Lai, C., Belova, G., Cam, M., Walling, J*., et al.* (2012). Histone Demethylase Jumonji D3 (JMJD3) as a Tumor Suppressor by Regulating p53 Protein Nuclear Stabilization. In PLoS ONE, p. e51407.

Estarás, C., Akizu, N., García, A., Beltrán, S., de la Cruz, X., and Martínez-Balbás, M. A. (2012). Genome-wide analysis reveals that Smad3 and JMJD3 HDM co-activate the neural developmental program. In Development, pp. 2681-2691.

Estivill-Torrus, G., Pearson, H., van Heyningen, V., Price, D. J., and Rashbass, P. (2002). Pax6 is required to regulate the cell cycle and the rate of progression from symmetrical to asymmetrical division in mammalian cortical progenitors. In Development, pp. 455-466.

Fonseca, M. B., Nunes, A. F., Morgado, A. L., Solá, S., and Rodrigues, C. M. P. (2012). TAp63γ demethylation regulates protein stability and cellular distribution during neural stem cell differentiation. In PLoS ONE, p. e52417.

Fortin, G., and Thoby-Brisson, M. (2009). Embryonic emergence of the respiratory rhythm generator. Respiratory physiology & neurobiology *168*, 86-91.

Franco, S. J., Gil-Sanz, C., Martinez-Garay, I., Espinosa, A., Harkins-Perry, S. R., Ramos, C., and Muller, U. (2012). Fate-Restricted Neural Progenitors in the Mammalian Cerebral Cortex. In Science, pp. 746-749.

Fujita, S. (1962). Kinetics of cellular proliferation. Experimental cell research *28*, 52-60.

Gorisch, S. M., Wachsmuth, M., Toth, K. F., Lichter, P., and Rippe, K. (2005). Histone acetylation increases chromatin accessibility. Journal of cell science *118*, 5825-5834.

Götz, M., and Huttner, W. B. (2005). The cell biology of neurogenesis. In Nature Reviews Molecular Cell Biology, pp. 777-788.

Greig, L. C., Woodworth, M. B., Galazo, M. J., Padmanabhan, H., and Macklis, J. D. (2013). Molecular logic of neocortical projection neuron specification, development and diversity. Nature Reviews Neuroscience *14*, 755-769.

Groth, A., Corpet, A., Cook, A. J. L., Roche, D., Bartek, J., Lukas, J., and Almouzni, G. (2007). Regulation of Replication Fork Progression Through Histone Supply and Demand. In Science, pp. 1928-1931.

Guo, C., Eckler, M. J., McKenna, W. L., McKinsey, G. L., Rubenstein, J. L. R., and Chen, B. (2013). Fezf2 Expression Identifies a Multipotent Progenitor for Neocortical Projection Neurons, Astrocytes, and Oligodendrocytes. In Neuron, pp. 1167-1174.

Hansen, K. H., Bracken, A. P., Pasini, D., Dietrich, N., Gehani, S. S., Monrad, A., Rappsilber, J., Lerdrup, M., and Helin, K. (2008). A model for transmission of the H3K27me3 epigenetic mark. Nature Cell Biololgy *10*, 1291-1300.

Hawkins, R. D., Hon, G. C., Lee, L. K., Ngo, Q., Lister, R., Pelizzola, M., Edsall, L. E., Kuan, S., Luu, Y., Klugman, S.*, et al.* (2010). Distinct epigenomic landscapes of pluripotent and lineage-committed human cells. Cell stem cell *6*, 479-491.

Hirabayashi, Y., Suzki, N., Tsuboi, M., Endo, T. A., Toyoda, T., Shinga, J., Koseki, H., Vidal, M., and Gotoh, Y. (2009). Polycomb Limits the Neurogenic Competence of Neural Precursor Cells to Promote Astrogenic Fate Transition. In Neuron, pp. 600-613.

Hofemeister, H., Ciotta, G., Fu, J., Seibert, P. M., Schulz, A., Maresca, M., Sarov, M., Anastassiadis, K., and Stewart, A. F. (2011). Recombineering, transfection, Western, IP and ChIP methods for protein tagging via gene targeting or BAC transgenesis. Methods *53*, 437-452.

Holliday, R. (1990). Mechanisms for the control of gene activity during development. Biological reviews of the Cambridge Philosophical Society *65*, 431-471.

Hong, S., Cho, Y. W., Yu, L. R., Yu, H., Veenstra, T. D., and Ge, K. (2007). Identification of JmjC domain-containing UTX and JMJD3 as histone H3 lysine 27 demethylases. Proceedings of the National Academy of Sciences of the United States of America *104*, 18439-18444.

Huang, J., Sengupta, R., Espejo, A. B., Lee, M. G., Dorsey, J. A., Richter, M., Opravil, S., Shiekhattar, R., Bedford, M. T., Jenuwein, T., and Berger, S. L. (2007). p53 is regulated by the lysine demethylase LSD1. Nature *449*, 105-108.

Ingham, P. W. (1985). A clonal analysis of the requirement for the trithorax gene in the diversification of segments in Drosophila. Journal of Embryology & Experimental Morphology *89*, 349-365.

Jepsen, K., Solum, D., Zhou, T., McEvilly, R. J., Kim, H.-J., Glass, C. K., Hermanson, O., and Rosenfeld, M. G. (2007). SMRT-mediated repression of an H3K27 demethylase in progression from neural stem cell to neuron. In Nature, pp. 415-419.

Kalani, M. Y., Cheshier, S. H., Cord, B. J., Bababeygy, S. R., Vogel, H., Weissman, I. L., Palmer, T. D., and Nusse, R. (2008). Wnt-mediated self-renewal of neural stem/progenitor cells. Proceedings of the National Academy of Sciences of the United States of America *105*, 16970-16975.

Kooistra, S. M., and Helin, K. (2012). Molecular mechanisms and potential functions of histone demethylases. In Nature Reviews Molecular Cell Biology, (Nature Publishing Group), pp. 297-311.

Kouzarides, T. (2007). Chromatin modifications and their function. Cell *128*, 693-705.

Kriaucionis, S., and Heintz, N. (2009). The nuclear DNA base 5-hydroxymethylcytosine is present in Purkinje neurons and the brain. Science *324*, 929-930.

Kriegstein, A., and Álvarez-Buylla, A. (2009). The Glial Nature of Embryonic and Adult Neural Stem Cells. In Annual Review of Neuroscience, pp. 149-184.

Lallemand, Y., Luria, V., Haffner-Krausz, R., and Lonai, P. (1998). Maternally expressed PGK-Cre transgene as a tool for early and uniform activation of the Cre site-specific recombinase. Transgenic research *7*, 105-112.

Lan, F., Bayliss, P. E., Rinn, J. L., Whetstine, J. R., Wang, J. K., Chen, S., Iwase, S., Alpatov, R., Issaeva, I., Canaani, E.*, et al.* (2007). A histone H3 lysine 27 demethylase regulates animal posterior development. In Nature, pp. 689-694.

Lange, C., Huttner, W. B., and Calegari, F. (2009). Cdk4/CyclinD1 Overexpression in Neural Stem Cells Shortens G1, Delays Neurogenesis, and Promotes the Generation and Expansion of Basal Progenitors. In Stem Cell, (Elsevier Ltd), pp. 320-331.

Laugesen, A., and Helin, K. (2014). Chromatin repressive complexes in stem cells, development, and cancer. Cell stem cell *14*, 735-751.

Lee, M. G., Wynder, C., Cooch, N., and Shiekhattar, R. (2005). An essential role for CoREST in nucleosomal histone 3 lysine 4 demethylation. Nature *437*, 432-435.

Lee, T. I., Jenner, R. G., Boyer, L. A., Guenther, M. G., Levine, S. S., Kumar, R. M., Chevalier, B., Johnstone, S. E., Cole, M. F., Isono, K.*, et al.* (2006). Control of developmental regulators by Polycomb in human embryonic stem cells. Cell *125*, 301-313.

Lewis, E. B. (1978). A gene complex controlling segmentation in Drosophila. Nature *276*, 565-570.

Li, E., Bestor, T. H., and Jaenisch, R. (1992). Targeted mutation of the DNA methyltransferase gene results in embryonic lethality. Cell *69*, 915-926.

Li, R., and Guan, M. X. (2010). Human mitochondrial leucyl-tRNA synthetase corrects mitochondrial dysfunctions due to the tRNALeu(UUR) A3243G mutation, associated with mitochondrial encephalomyopathy, lactic acidosis, and stroke-like symptoms and diabetes. Molecular and cellular biology *30*, 2147-2154.

Lim, D. A., Huang, Y.-C., Swigut, T., Mirick, A. L., Garcia-Verdugo, J. M., Wysocka, J., Ernst, P., and Álvarez-Buylla, A. (2009). Chromatin remodelling factor Mll1 is essential for neurogenesis from postnatal neural stem cells. In Nature, (Nature Publishing Group), pp. 529-533.

Lui, J. H., Hansen, D. V., and Kriegstein, A. R. (2011). Development and Evolution of the Human Neocortex. In Cell, (Elsevier Inc.), pp. 18-36.

Margueron, R., Justin, N., Ohno, K., Sharpe, M. L., Son, J., Drury, W. J., 3rd, Voigt, P., Martin, S. R., Taylor, W. R., De Marco, V.*, et al.* (2009). Role of the polycomb protein EED in the propagation of repressive histone marks. Nature *461*, 762-767.

Marinari, E., Mehonic, A., Curran, S., Gale, J., Duke, T., and Baum, B. (2012). Live-cell delamination counterbalances epithelial growth to limit tissue overcrowding. Nature *484*, 542-545.

Martynoga, B., Morrison, H., Price, D. J., and Mason, J. O. (2005). Foxg1 is required for specification of ventral telencephalon and region-specific regulation of dorsal telencephalic precursor proliferation and apoptosis. In Developmental Biology, pp. 113-127.

Mcconnell, S. K., and Kaznowski, C. E. (1991). Cell-Cycle Dependence of Laminar Determination in Developing Neocortex. Science *254*, 282-285.

Meloni, M., and Testa, G. (2014). Scrutinizing the epigenetics revolution. BioSocieties.

Mikkelsen, T. S., Hanna, J., Zhang, X., Ku, M., Wernig, M., Schorderet, P., Bernstein, B. E., Jaenisch, R., Lander, E. S., and Meissner, A. (2008). Dissecting direct reprogramming through integrative genomic analysis. In Nature, pp. 49-55.

Miller, S. A., Mohn, S. E., and Weinmann, A. S. (2010). Jmjd3 and UTX Play a Demethylase-Independent Role in Chromatin Remodeling to Regulate T-Box Family Member-Dependent Gene Expression. In Molecular Cell, (Elsevier Inc.), pp. 594-605.

Mohn, F., Weber, M., Rebhan, M., Roloff, T. C., Richter, J., Stadler, M. B., Bibel, M., and Schübeler, D. (2008). Lineage-Specific Polycomb Targets and De Novo DNA Methylation Define Restriction and Potential of Neuronal Progenitors. In Molecular Cell, pp. 755-766.

Molofsky, A. V., He, S., Bydon, M., Morrison, S. J., and Pardal, R. (2005). Bmi-1 promotes neural stem cell self-renewal and neural development but not mouse growth and survival by repressing the p16Ink4a and p19Arf senescence pathways. Genes & development *19*, 1432-1437.

Montagutelli, X. (2000). Effect of the genetic background on the phenotype of mouse mutations. Journal of the American Society of Nephrology *11 Suppl 16*, S101-105.

Morey, L., and Helin, K. (2010). Polycomb group protein-mediated repression of transcription. Trends in biochemical sciences *35*, 323-332.

Muyrers, J. P., Zhang, Y., Benes, V., Testa, G., Rientjes, J. M., and Stewart, A. F. (2004). ET recombination: DNA engineering using homologous recombination in E. coli. Methods in molecular biology *256*, 107-121.

Nadeau, J. H. (2005). Listening to genetic background noise. New England Journal of Medicine *352*, 1598-1599.

Nishino, J., Kim, I., Chada, K., and Morrison, S. J. (2008). Hmga2 promotes neural stem cell self-renewal in young but not old mice by reducing p16Ink4a and p19Arf Expression. Cell *135*, 227-239.

Nowakowski, R. S., Lewin, S. B., and Miller, M. W. (1989). Bromodeoxyuridine immunohistochemical determination of the lengths of the cell cycle and the DNA-synthetic phase for an anatomically defined population. In Journal of Neurocytology, pp. 311-318.

Okamoto, M., Namba, T., Shinoda, T., Kondo, T., Watanabe, T., Inoue, Y., Takeuchi, K., Enomoto, Y., Ota, K., Oda, K.*, et al.* (2013). TAG-1-assisted progenitor elongation streamlines nuclear migration to optimize subapical crowding. Nature neuroscience *16*, 1556-1566.

Okano, M., Bell, D. W., Haber, D. A., and Li, E. (1999). DNA methyltransferases Dnmt3a and Dnmt3b are essential for de novo methylation and mammalian development. Cell *99*, 247-257.

Park, D. H., Hong, S. J., Salinas, R. D., Liu, S. J., Sun, S. W., Sgualdino, J., Testa, G., Matzuk, M. M., Iwamori, N., and Lim, D. A. (2014). Activation of Neuronal Gene Expression by the JMJD3 Demethylase Is Required for Postnatal and Adult Brain Neurogenesis. Cell reports.

Pei, Y., Brun, S. N., Markant, S. L., Lento, W., Gibson, P., Taketo, M. M., Giovannini, M., Gilbertson, R. J., and Wechsler-Reya, R. J. (2012). WNT signaling increases proliferation and impairs differentiation of stem cells in the developing cerebellum. Development *139*, 1724-1733.

Pereira, J. D., Sansom, S. N., Smith, J., Dobenecker, M.-W., Tarakhovsky, A., and Livesey, F. J. (2010). Ezh2, the histone methyltransferase of PRC2, regulates the balance between self-renewal and differentiation in the cerebral cortex. In Proc Natl Acad Sci U S A, pp. 15957-15962.

Piccin, D., and Morshead, C. M. (2011). Wnt signaling regulates symmetry of division of neural stem cells in the adult brain and in response to injury. Stem cells *29*, 528-538.

Pilz, G. A., Shitamukai, A., Reillo, I., Pacary, E., Schwausch, J., Stahl, R., Ninkovic, J., Snippert, H. J., Clevers, H., Godinho, L.*, et al.* (2013). Amplification of progenitors in the mammalian telencephalon includes a new radial glial cell type. Nature communications *4*, 2125.

Ravin, R., Hoeppner, D. J., Munno, D. M., Carmel, L., Sullivan, J., Levitt, D. L., Miller, J. L., Athaide, C., Panchision, D. M., and McKay, R. D. G. (2008). Potency and Fate Specification in CNS Stem Cell Populations In Vitro. In Cell Stem Cell, pp. 670-680.

Riggs, A. D., Martienssen, R. A., and Russo, V. E. A. (1996). Introduction. Epigenetic mechanisms of gene regulation, 1.

Salomoni, P., and Calegari, F. (2010). Cell cycle control of mammalian neural stem cells: putting a speed limit on G1. In Trends in Cell Biology, (Elsevier Ltd), pp. 233-243.

Schoeftner, S., Sengupta, A. K., Kubicek, S., Mechtler, K., Spahn, L., Koseki, H., Jenuwein, T., and Wutz, A. (2006). Recruitment of PRC1 function at the initiation of X inactivation independent of PRC2 and silencing. The EMBO journal *25*, 3110-3122.

Schuettengruber, B., Chourrout, D., Vervoort, M., Leblanc, B., and Cavalli, G. (2007). Genome regulation by polycomb and trithorax proteins. Cell *128*, 735-745.

Schuurmans, C., Armant, O., Nieto, M., Stenman, J. M., Britz, O., Klenin, N., Brown, C., Langevin, L.-M., Seibt, J., Tang, H.*, et al.* (2004). Sequential phases of cortical specification involve Neurogenin-dependent and -independent pathways. In The EMBO Journal, pp. 2892-2902.

Seibler, J., Zevnik, B., Kuter-Luks, B., Andreas, S., Kern, H., Hennek, T., Rode, A., Heimann, C., Faust, N., Kauselmann, G.*, et al.* (2003). Rapid generation of inducible mouse mutants. Nucleic acids research *31*, e12.

Shang, Y., Hu, X., DiRenzo, J., Lazar, M. A., and Brown, M. (2000). Cofactor dynamics and sufficiency in estrogen receptor-regulated transcription. Cell *103*, 843-852.

Shen, Q., Wang, Y., Dimos, J. T., Fasano, C. A., Phoenix, T. N., Lemischka, I. R., Ivanova, N. B., Stifani, S., Morrisey, E. E., and Temple, S. (2006). The timing of cortical neurogenesis is encoded within lineages of individual progenitor cells. In Nature Neuroscience, pp. 743-751.

Shi, Y., Lan, F., Matson, C., Mulligan, P., Whetstine, J. R., Cole, P. A., Casero, R. A., and Shi, Y. (2004). Histone demethylation mediated by the nuclear amine oxidase homolog LSD1. Cell *119*, 941-953.

Siegenthaler, J. A., Ashique, A. M., Zarbalis, K., Patterson, K. P., Hecht, J. H., Kane, M. A., Folias, A. E., Choe, Y., May, S. R., Kume, T.*, et al.* (2009). Retinoic Acid from the Meninges Regulates Cortical Neuron Generation. In Cell, pp. 597-609.

Sing, A., Pannell, D., Karaiskakis, A., Sturgeon, K., Djabali, M., Ellis, J., Lipshitz, H. D., and Cordes, S. P. (2009). A vertebrate Polycomb response element governs segmentation of the posterior hindbrain. Cell *138*, 885-897.

Smart, I. H. (1965). The operation of ependymal 'choke' in neurogenesis. Journal of Anatomy, 941-943.

Solá, S., Xavier, J. M., Santos, D. M., Aranha, M. M., Morgado, A. L., Jepsen, K., and Rodrigues, C. M. P. (2011). p53 Interaction with JMJD3 Results in Its Nuclear Distribution during Mouse Neural Stem Cell Differentiation. In PLoS ONE, p. e18421.

Solomon, M. J., Larsen, P. L., and Varshavsky, A. (1988). Mapping protein-DNA interactions in vivo with formaldehyde: evidence that histone H4 is retained on a highly transcribed gene. Cell *53*, 937-947.

Steffen, P. A., and Ringrose, L. (2014). What are memories made of? How Polycomb and Trithorax proteins mediate epigenetic memory. Nature Reviews Molecular Cell Biololgy *15*, 340-356.

Stryke, D., Kawamoto, M., Huang, C. C., Johns, S. J., King, L. A., Harper, C. A., Meng, E. C., Lee, R. E., Yee, A., L'Italien, L.*, et al.* (2003). BayGenomics: a resource of insertional mutations in mouse embryonic stem cells. Nucleic acids research *31*, 278-281.

Suzuki, M. M., and Bird, A. (2008). DNA methylation landscapes: provocative insights from epigenomics. Nature Reviews Genetics *9*, 465-476.

Tahiliani, M., Koh, K. P., Shen, Y., Pastor, W. A., Bandukwala, H., Brudno, Y., Agarwal, S., Iyer, L. M., Liu, D. R., Aravind, L., and Rao, A. (2009). Conversion of 5-methylcytosine to 5-hydroxymethylcytosine in mammalian DNA by MLL partner TET1. Science *324*, 930-935.

Takahashi, T., Nowakowski, R. S., and Caviness, V. S., Jr. (1993). Cell cycle parameters and patterns of nuclear movement in the neocortical proliferative zone of the fetal mouse. Journal of Neuroscience *13*, 820-833.

Takahashi, T., Nowakowski, R. S., and Caviness, V. S., Jr. (1995). The cell cycle of the pseudostratified ventricular epithelium of the embryonic murine cerebral wall. Journal of Neuroscience *15*, 6046-6057.

Tanabe, L. M., Martin, C., and Dauer, W. T. (2012). Genetic background modulates the phenotype of a mouse model of DYT1 dystonia. PloS one *7*, e32245.

Testa, G. (2011). The time of timing: How Polycomb proteins regulate neurogenesis. In Bioessays, pp. 519-528.

Testa, G., Schaft, J., van der Hoeven, F., Glaser, S., Anastassiadis, K., Zhang, Y., Lobo, M. K., Stremmel, W., and Stewart, A. F. (2004a). A reliable lacZ expression reporter cassette for multipurpose, knockout-first alleles. In Genesis, pp. 151-158.

Testa, G., Vintersten, K., Zhang, Y., Benes, V., Muyrers, J. P., and Stewart, A. F. (2004b). BAC engineering for the generation of ES cell-targeting constructs and mouse transgenes. Methods in molecular biology *256*, 123-139.

Tsukada, Y.-i., Fang, J., Erdjument-Bromage, H., Warren, M. E., Borchers, C. H., Tempst, P., and Zhang, Y. (2005). Histone demethylation by a family of JmjC domain-containing proteins. In Nature, pp. 811-816.

Van Keuren, M. L., Gavrilina, G. B., Filipiak, W. E., Zeidler, M. G., and Saunders, T. L. (2009). Generating transgenic mice from bacterial artificial chromosomes: transgenesis efficiency, integration and expression outcomes. Transgenic research *18*, 769-785.

Vintersten, K., Testa, G., Naumann, R., Anastassiadis, K., and Stewart, A. F. (2008). Bacterial artificial chromosome transgenesis through pronuclear injection of fertilized mouse oocytes. Methods in molecular biology *415*, 83-100.

Vintersten, K., Testa, G., and Stewart, A. F. (2004). Microinjection of BAC DNA into the pronuclei of fertilized mouse oocytes. Methods in molecular biology *256*, 141-158.

Waddington, C. H. (1942). Endeavour *1*, 18-20.

Wei, Y., Yu, L., Bowen, J., Gorovsky, M. A., and Allis, C. D. (1999). Phosphorylation of histone H3 is required for proper chromosome condensation and segregation. Cell *97*, 99-109.

Wen, B., Wu, H., Shinkai, Y., Irizarry, R. A., and Feinberg, A. P. (2009). Large histone H3 lysine 9 dimethylated chromatin blocks distinguish differentiated from embryonic stem cells. Nature genetics *41*, 246-250.

Ying, Q.-L., Wray, J., Nichols, J., Batlle-Morera, L., Doble, B., Woodgett, J., Cohen, P., and Smith, A. (2008). The ground state of embryonic stem cell self-renewal. In Nature, pp. 519-523.

Yun, S.-W., Leong, C., Zhai, D., Tan, Y. L., Lim, L., Bi, X., Lee, J.-J., Kim, H. J., Kang, N.-Y., Ng, S. H.*, et al.* (2012). Neural stem cell specific fluorescent chemical probe binding to FABP7. In Proc Natl Acad Sci U S A, pp. 10214-10217.

Zhao, W., Li, Q., Ayers, S., Gu, Y., Shi, Z., Zhu, Q., Chen, Y., Wang, H. Y., and Wang, R.-F. (2013). Jmjd3 Inhibits Reprogramming by Upregulating Expression of INK4a/Arf and Targeting PHF20 for Ubiquitination. In Cell, (Elsevier Inc.), pp. 1037-1050.

Zhou, V. W., Goren, A., and Bernstein, B. E. (2011). Charting histone modifications and the functional organization of mammalian genomes. Nature Reviews Genetics *12*, 7-18.